

# THE VIRTUAL INSECT BRAIN PROTOCOL

Development and application of software for  
the standardization of neuroanatomy

Dissertation zur Erlangung des  
naturwissenschaftlichen Doktorgrades der  
Julius-Maximilians-Universität Würzburg

vorgelegt von

Arnim Jenett

Münster

Würzburg, 2006

Eingereicht am: 08.01. 2007

1. Gutachter: Prof. Dr. Martin Heisenberg

2. Gutachter: Prof. Dr. Thomas Dandekar

Vorsitzender: Prof. Dr. Martin Müller, vertreten durch Prof. Dr. Erich Buchner  
der Dissertation

Tag der mündlichen Prüfung: 21.03.2007

Doktorurkunde ausgehändigt am:

## ERKLÄRUNG

Erklärung gemäß § 4 Absatz 3 der Promotionsordnung der Fakultät für Biologie der Julius-Maximilians-Universität zu Würzburg vom 15. März 1999.

Hiermit erkläre ich, die vorliegende Dissertation selbständig angefertigt zu haben und keine anderen als die von mir angegebenen Quellen und Hilfsmittel verwendet zu haben. Alle aus der Literatur entnommenen Stellen sind als solche kenntlich gemacht. Des Weiteren erkläre ich, dass die vorliegende Arbeit weder in gleicher noch in ähnlicher Form bereits in einem anderen Prüfungsverfahren vorgelegen hat. Zuvor habe ich keine akademischen Grade erworben oder zu erwerben versucht.

Würzburg, den 08.01.2007

Arnim Jenett

## ABSTRACT

Since the fruit fly *Drosophila melanogaster* entered the laboratories as a model organism, new genetic, physiological, molecular and behavioral techniques for the functional analysis of the brain rapidly accumulated. Nowadays this concerted assault obtains its main thrust from Gal4 expression patterns that can be visualized and provide the means for manipulating -in unrestrained animals- groups of neurons of the brain. To take advantage of these patterns one needs to know their anatomy.

This thesis describes the Virtual Insect Brain (VIB) protocol, a software package for the quantitative assessment, comparison, and presentation of neuroanatomical data. It is based on the 3D-reconstruction and visualization software Amira (Mercury Inc.). Its main part is a standardization procedure which aligns individual 3D images (series of virtual sections obtained by confocal microscopy) to a common coordinate system and computes average intensities for each voxel (volume pixel). The VIB protocol facilitates direct comparison of gene expression patterns and describes their interindividual variability. It provides volumetry of brain regions and helps to characterize the phenotypes of brain structure mutants. Using the VIB protocol does not require any programming skills since all operations are carried out at a (near to) self-explanatory graphical user interface. Although the VIB protocol has been developed for the standardization of *Drosophila* neuroanatomy, the program structure can be used for the standardization of other 3D structures as well.

Standardizing brains and gene expression patterns is a new approach to biological shape and its variability. Using the VIB protocol consequently may help to integrate knowledge on the correlation of form and function of the insect brain. The VIB protocol provides a first set of tools supporting this endeavor in *Drosophila*. The software is freely available at <http://www.neurofly.de>.

## ZUSAMMENFASSUNG

Seitdem die Taufliege *Drosophila melanogaster* als Modellorganismus Einzug in die Forschung erhalten hat, sammeln sich mehr und mehr genetische, physiologische und molekulare Techniken für die Funktionsanalyse des Gehirns an. Diese beruhen heutzutage meist auf Gal4 Expressionsmustern, die sichtbar gemacht werden können und eine gezielte Manipulierung von definierten Zellgruppen ermöglichen. Um Ergebnisse verschiedener Untersuchungen miteinander in Beziehung setzen zu können, muss man jedoch die typische Anatomie der zugrunde liegenden Expressionsmuster kennen.

Diese Arbeit beschreibt das Virtual Insect Brain (VIB) Protokoll, eine Software für die Darstellung, die quantitative Einschätzung und den Vergleich von neuroanatomischen Daten, sowie einige exemplarische Anwendungen des VIB Protokolls. Die Software basiert auf der 3D-Rekonstruktions- und der Visualisierungs-Software Amira (Mercury Inc.). Sein Hauptbestandteil ist ein Normierungsverfahren, das 3D-Bild-Stapel (Folgen virtueller Schnittbilder, erhalten durch konfokale Mikroskopie) auf ein gemeinsames Koordinatensystem abbildet und für jedes Voxel (dreidimensionaler Bildpunkt) die durchschnittliche Intensität berechnet. Das VIB Protokoll erleichtert dadurch den direkten Vergleich von Expressionsmustern und beschreibt ihre interindividuelle Variabilität. Es liefert volumetrische Messungen zu definierten Gehirnregionen und hilft, die durch Mutation entstehenden Veränderungen der Gehirnstruktur zu erkennen. Das Verwenden des VIB Protokolls erfordert keinerlei Programmierkenntnisse, da alle Vorgänge auf einer selbsterklärenden graphischen Benutzeroberfläche ausgeführt werden können. Obgleich das VIB Protokoll für die Normierung der Neuroanatomy von Taufliegen entwickelt worden ist, kann die Programmstruktur auch für die Normierung anderer 3D-Strukturen benutzt werden.

Gehirne und Expressionsmuster zu standardisieren ist ein neuer Ansatz die Variabilität der Neuroanatomie zu hinterfragen. Bei konsequenter Verwendung kann das VIB Protokoll helfen Wissen über Form und Funktion des Insektengehirns zu miteinander zu vernetzen. Das VIB Protokoll liefert einen ersten Satz Werkzeuge, die diese Bemühung in der Taufliege ermöglichen. Die Software kann kostenfrei von <http://www.neurofly.de> herunter geladen werden.



## TABLE OF CONTENT

## TABLE OF CONTENT

1	The development of the VIB protocol	1
1.1	Background	1
1.2	<i>Drosophila</i> as a model organism	1
1.3	The Gal4-UAS system	2
1.4	The history of standardized insect neuroanatomy	3
2	Definition of terms	5
3	Data import and export	6
3.1	Supported image file formats	6
3.2	Results	7
3.3	Statistics	7
3.4	Naming conventions	7
3.5	Space requirements	8
4	Implementation	10
4.1	Configuration of the Amira VIB protocol	11
4.1.1	Extension:	11
4.1.2	File group:	11
4.1.3	Show Group:	12
4.1.4	Template	12
4.1.5	Number of channels:	13
4.1.6	Channel of reference staining (nc82):	14
4.1.7	Use resampling:	14
4.1.8	Expert options:	15
4.1.9	Transform by:	15
4.1.9.1	VIBregistrationTransformation (RT)	15
4.1.9.2	VIBlabelSurfaceTransformation (LST)	15
4.1.9.3	VIBcenterTransformation (CT)	15
4.1.9.4	VIBlabelDiffusion (DT)	16
4.1.10	Cluster computing:	16
4.1.11	Batch run all groups:	17
4.1.12	Batch run:	17
4.1.13	Debug level:	17
4.1.14	Navigate:	17
4.2	The VIB protocol	18
4.2.1	Flowchart	19
4.2.1.1	Preprocessing (PREP)	19
4.2.1.2	Labeling (LAB)	20
4.2.1.3	Quality Control (QC)	20
4.2.1.4	Registrations (RT, LST, CT, LDT)	21
4.2.1.5	Averaging (AV)	21
4.2.2	The modules	21
4.2.2.1	Common elements of the VIB script modules	22
4.2.2.2	VIBspiltChannels.hx	22
4.2.2.3	VIBscissors.hx	23
4.2.2.4	VIBlabelWizard	23

## TABLE OF CONTENT

4.2.2.5	VIBresample.hx	24
4.2.2.6	VIBresampleLabels.hx	25
4.2.2.7	VIBtissueStatistics.hx	25
4.2.2.8	VIBvolumetry.hx	25
4.2.2.9	VIBgreyTransformation.hx	25
4.2.2.10	VIBlabelSurfaceTransformation.hx	26
4.2.2.11	VIBcenterTransformation.hx	26
4.2.2.12	VIBlabelDiffusionTransformation.hx	26
4.2.2.13	VIBdiffusion.hx	27
4.2.2.14	VIBaverageGrey.hx	27
4.2.2.15	VIBaverageLabels.hx	28
4.2.2.16	VIBmergeAverageLabels.hx	28
5	The choice of templates	29
5.1	Iterative approach for Template selection	29
5.2	Bias-free approach	29
5.2.1	Overall mean distance of centers of gravity	30
5.2.2	Core-to-seam-ratio	32
5.2.3	Core-to-seam ratio after non-rigid transformation (non-rigid c2s)	33
5.2.4	Core-to-seam ratio after rigid transformation (rigid c2s)	34
5.3	Template data sets for <i>Drosophila melanogaster</i>	35
6	Towards a nomenclature for neuropil areas	37
7	Material and Methods	43
7.1	Flies	43
7.2	Immunochemistry	46
7.2.1	nc82/anti-GFP standard double staining protocol	46
7.2.2	Antibodies:	47
7.2.3	Chemicals:	47
7.2.3.1	Mounting:	47
7.3	Confocal microscopy	47
8	Applications of the VIB protocol	49
8.1	Reporter-test-scans	49
8.1.1	Gal4-201y	49
8.1.2	Gal4-ok107	52
8.1.3	Gal4-mb247	53
8.1.4	The UAS-reporters	54
8.1.4.1	Nuclear marker expression for the standardization of cell body position	54
8.1.4.2	Presynaptic marker expression for the standardization of synapses	57
8.1.4.3	Cytoplasmatic and membrane bound marker expression for the standardization of arborization patterns	59
8.1.5	Conclusion	64
8.2	Comparison of Gal4 expression patterns in the central complex	64

## TABLE OF CONTENT

8.2.1	Image processing for the comparison of expression patterns	67
8.2.2	Analysis of standardized Gal4 expression patterns interfering with the memory for 'elevation'	71
8.2.3	Expression in the pars intercerebralis (PI) and the ventral brain with subesophageal ganglion (SOG) and antennal nerves (AN)	74
8.2.4	Expression in the optic lobes (OL),	75
8.2.5	Expression in the dorsal brain region	75
8.2.6	Expression in the fan shaped body (FB)	76
8.2.7	Analysis of standardized Gal4 expression patterns which do not interfere with the memory for 'elevation'.	86
8.2.8	Conclusion	87
8.3	Standardization of expression patterns specific for olfactory projection neurons	88
8.3.1	Gal4-GH146	89
8.3.2	Gal4-NP225	90
8.3.3	Results	92
8.3.4	Conclusion	94
8.4	Alignment of individual neurons	94
8.4.1	3D reconstruction and alignment of individual visual projection neurons.	95
8.4.2	Conclusion	97
9	Discussion and outlook	98
9.1	The VIB protocol	98
9.2	The standard brain atlas	99



## **1 The development of the VIB protocol**

### **1.1 Background**

The structure of the brain and the localization of its functions have been of consistent interest throughout history. In the early 16th century Leonardo da Vinci performed remarkable studies on the gross morphology of the human brain relating the structure of the brain to mental functions [1]. Outstanding studies of the fine structure of the human brain were presented in the late 19th century by Santiago Ramón y Cajal using Golgi's silver stain method. His sketches of stainings of limited numbers of neurons in the brain and the spinal cord contributed significantly to the understanding of the wiring of the human brain.

In 1909 Korbinian Brodman published an atlas of the human brain cortex assigning names to areas of functional identity. Soon ongoing progress in neurosurgery demanded a common coordinate system for the communication of the correlation of form and function which was developed by J. Talairach and P. Tournoux in 1988 [2]. This common coordinate system enables neurologists to compare neuroanatomical investigations from patient to patient. However, the strong variability in human brain anatomy and in the localization of (measured) functional activity does not allow to transfer results from one subject to the other.

Basic studies on the neuronal processing of information therefore have to be conducted in smaller and simpler systems.

### **1.2 *Drosophila* as a model organism**

With a size of about 200.000 neurons the brain of *Drosophila melanogaster* is about six orders of magnitude smaller than the human brain (which is about  $10^{10}$ - $10^{11}$  neurons) and one order of magnitude larger than the brain of the sea slug *Aplysia californica* (18.000 -20.000 neurons) which is another popular model organism for the study of learning and memory [3].

The flies are conveniently small, inexpensive to breed, clean, harmless (except for occasional allergies), and easy to cultivate. Their generation time is only about 10 days at 25°C, and the life cycle includes easily identifiable phases [4].

Despite the small brain *Drosophila* spontaneously shows considerably complex behaviors including positive phototaxis, negative geotaxis, and courtship. The flies are also able to link certain cues of their environment and establish a memory for such associations [5-10]. They show clear behavioral phenotypes in

experiments on the plasticity of behavior [11-14] like visual orientated walking [15, 16] or flying [17-20] or olfactory associative learning [14, 21-23].

But it is the possibility of interfering with the genetics of *Drosophila* that has made the real progress in behavioral neuroscience. Beside its sequenced genome [24] the enormous expansion of genetic tools defined the fly as a model organism throughout its scientific history.

*Drosophila* was introduced into the laboratory in 1901 by C.W. Woodworth and W.E. Castle at Harvard who studied the effect of inbreeding and isolated the first mutants. From 1910 on T.H. Morgan and colleagues used *Drosophila* to extend Mendel's work by describing X-linked inheritance and by showing that genes located on the same chromosome do not show independent assortment. H.J. Muller 1927 discovered a technique for artificially inducing mutations by means of X rays that has since had broad application. From that time on *Drosophila* gained more and more popularity in the field of genetics and neurobiology. J. Hirsch performed broad studies in experimental behavior genetics [25-28] screening mutagenized populations in various behavioral paradigms. In the 1960s chemically induced mutations of the *Drosophila* genome became available by application of ethyl methanesulfonate (EMS) [29-33]. With the proceeding understanding of the regulatory sequences in the *Drosophila* genome more directed mutagenesis by translocation of transposable elements, so called P-elements that mutate the fly genome by jumping from one position to an other, became possible [34]. Based on the technique of P-element insertion the Gal4-UAS system was published in 1993 by A. Brand and N. Perrimon [35] enabling the functional modification of predefined populations of cells.

### **1.3 The Gal4-UAS system**

The Gal4-UAS system [35] is a 2-component system for targeted gene expression that allows the selective activation of any cloned gene in a wide variety of tissue- and cell-specific patterns. GAL4 encodes a protein that activates transcription in the yeast *Saccharomyces cerevisiae* which normally is induced by galactose [36, 37]. It directly binds to DNA at an Upstream Activating Sequence (UAS) starting the transcription of the adjacent (downstream) genes. For the Gal4-UAS system two P-elements are created, one carrying the information for Gal4 coupled to a very weak promoter (driver), the other the UAS-sequence connected to the transgene of interest (effector). These P-elements are inserted into the genomes of different flies creating a Gal4 driver line and a UAS effector line. The weak promoter of the Gal4 P-

element comes under the influence of endogenous enhancers specific for its insertion site. Therefore, the expression of Gal4 is confined to the fraction of cells specified by enhancers at the insertion site of the Gal4 P-element. In the UAS effector line due to the missing Gal4 the respective transgene is not expressed. In both fly lines, therefore, the insertion of the P-element should not have much of an effect, unless the GAL4 is toxic or the insertion interrupts an essential sequence. Only after the two lines are crossed to each other the two components come together. In the cells with active Gal4 expression the transcription factor binds to the UAS-sequence inducing the transcription of the effector transgene. The mayor advantage of the Gal4-UAS system is based on its bipartite nature because a given Gal4-driver line can drive the expression of any UAS-effector transgenes in a defined population of cells. Using this technique and its derivates a vast amount of data on the function of the fly brain and its correlation to behavior could be gathered.

#### **1.4 The history of standardized insect neuroanatomy**

The concept of standardization arose in the 1990s for the human brain. New imaging techniques, namely the magnetic resonance imaging (MRI), shed light on the morphology of the subjects' brains easily and at low risk. Advancing the idea of a common coordinate system like that of Talairach [2] the group around J. Ashburner and K.J. Friston developed a whole set of tools for the standardization of human neuroanatomy including automatic segmentation of the 3D images [38-47]. A great collection of advances and applications of standardized human brain morphology and function was compiled by A. Toga and his coworkers over the last couple of decades [48-78]. The same technique also was applied to the morphology of the rat brain [79-81], and mouse brain [82-84]. Working with vertebrate brains the major advantage is the clear and contrasted separation of grey matter and white matter, significantly facilitating automatic segmentation of areas. A drawback of these approaches - especially in working with human brains - is the enormous interindividual variability which has to be normalized during the process of standardization. This normalization may occlude morphological details of functional importance. Therefore the standardization of large brains (mouse and bigger) can not answer questions on brain function on the cellular or even sub-cellular level.

In contrast to the human brain the gross morphology of the insect brain is rather stereotypic. Therefore the constancy and variability of biological shapes can be quantitatively assessed by standardization more easily. This approach has been introduced to the study of the *Drosophila* brain by Rein et al. [85], [86] using a prototype of the VIB protocol with limited functionality. Since in

the last years large collections of GAL4 driver lines have been made available and are being used, improved tools for their anatomical investigation are at high demand. In the last years we advanced the prototype to an easily usable software, the Virtual Insect Brain (VIB) protocol (chapter 1 on page 10), serving a variety of applications in invertebrate neuroanatomy. For instance, and most significant in *Drosophila*, the biological variability of gene expression patterns can now be measured and evaluated by standardization (chapter 8.1 on page 49). Standardized expression patterns can be directly superimposed and compared. By arithmetical analysis of standardized structures mutual or different structures can be emphasized (see chapter 8.2 on page 64). By this approach congruous parts of expression patterns of different Gal4 lines can easily be detected. The algorithms used for the standardization proved even precise enough for the alignment of single cells (chapter 8.4 on page 94).

An independent approach to standardize the brain of the honey bee *Apis mellifera* was taken in the laboratory of R. Menzel [87]. Addressing a different set of questions this approach uses a different procedures [88, 89] for the transformation of individual data sets into the standard coordinate system. In the future, a closer cooperation would be desirable.

## **2 Definition of terms**

### **Voxel**

A voxel (a combination of the words *volumetric* and *pixel*) is a volume element, representing a value on a regular grid in 3D space. This is analogous to a pixel, which represents 2D image data.

### **Template**

The Template data set consists of a 3D image and the corresponding LabelField (see next paragraph). It provides the coordinate system to which the selected brains get registered. For *Drosophila melanogaster* (wildtype Canton S) a Template for each gender is provided. The Template needs to display the most normal brain morphology, which is selected in a process described below (chapter 0 on page 29).

### **LabelField, Regions, Materials**

A LabelField is a regular cubic grid with the same dimensions as the underlying 3D image. The LabelField is divided into regions.

For each voxel it contains a label indicating the region the voxel belongs to [90]. In the VIB protocol the LabelFields are created automatically by the VIBLabelWizard (see chapter 4.2.2.4 on page 23) and saved with the name of the corresponding 3D images in the labels folder (VIB-root/labels). With respect to their contents, the labeled neuropil regions are called Materials. Their volumes, surfaces and centers of gravity are used to compute rigid and non-rigid transformations of the Samples (chapter 4.2.1.4 on page 21)

### **Samples, 3D images, file group**

The Samples are the raw data (images, 3D images, image files) of individual brains. For standardization several Samples are assembled as a file group (see chapter 4.1.2 on page 11). The Samples can directly be used for standardization if the VIBregistrationTransformation (RT) is applied. For all other transformations, LabelFields are first generated (chapter 4.2.1.2 on page 20)

### 3 Data import and export

The VIB protocol is installed in an arbitrarily chosen folder. This becomes the root folder of the VIB protocol. In this folder the VIB protocol creates its own folder structure during installation. The raw 3D images to be standardized have to be introduced to the protocol by placing them to the images folder ('VIB-root'/images). An alternative to copying those to 'VIB-root'/images is on UNIX systems the creation of symbolic links pointing to the actual storing position of the images. Windows systems do not support symbolic links. Therefore in these systems the 3D images really have to be copied to 'VIB-root'/images.

#### 3.1 Supported image file formats

Using the import algorithms of Amira the VIB protocol principally can work on all image file formats supported by Amira.

**Table 1: Alphabetic index of image file formats supported by Amira (extracted from Amira user's guide)**

ACR-NEMA	predecessor of the DICOM format for medical images (r)
AVS Field	stores data defined on regular grid (rw)
AVS UCD Format	stores unstructured cell data (rw)
AmiraMesh Format	Amira's native general purpose format (rw)
Analyze 7.5	3D image data with separate header file (r)
AnalyzeAVW	contains 2D and 3D medical image data (rw)
BMP Image Format	uncompressed Windows bitmap format (rw)
Bio-Rad Confocal Format	simple uncompressed format for 3D image stacks (r)
DICOM	standard file format for medical images (rw)
Encapsulated Postscript	for 2D raster images only (w)
JPEG Image Format	2D image format with lossy compression (rw)
Leica 3D TIFF	contains 3D image data with voxel sizes (r)
Leica Binary Format (.lei)	3D image stacks, time series, and meta information (r)
Leica Slice Series (.info)	contains list of 2D TIFF files and meta information (r)
Metamorph STK Format	special TIFF variant for 3D image stacks (r)
PNG Image Format	portable network graphics format for 2D images (rw)
PNM Image Format	simple uncompressed 2D image format (rw)
Raw Data	reads binary data as a 3D uniform field (rw)
SGI-RGB Image Format	2D image format with run-length encoding (rw)
Stacked-Slices	info file grouping together 2D images (r)
TIFF Image Format	standard format for 2D and 3D image data (rw)

The VIB protocol was developed and extensively tested on stacked tagged image files (tif) created by a Leica-SP1 confocal microscope with a resolution of 8 bits. This file format was chosen because it is a common format most confocal microscopes are able to produce. Nevertheless proprietary image file formats like .pic (BioRad) or .lei (Leica) were tested successfully.

## 3.2 Results

Results of the standardization are saved in the output folders (VIB-root/output), sorted by type

non-rigidly transformed images → VIB/output/warped

average images → VIB/output/average

Main probability maps → VIB/output/Mainprop

Material's probability maps → VIB/output/prop

## 3.3 Statistics

Besides the image data and their derivatives statistical data are saved in the statistics folder (VIB/statistics). Together with the internal statistics files in proprietary Amira file format (AmiraMesh Format (.statistics)) all statistics are exported as comma separated values (.csv) for further analysis in any spreadsheet software (VIB/statistics/csv). The VIB protocol creates a table of statistical data for each image file respectively its LabelField (see chapter 4.2.2.8 on page 25) and two additional tables containing basic statistical analysis for each file group's LabelFields.

## 3.4 Naming conventions

Due to the usage of up to 3 different programming languages (tcl, C++, Java) during standardization some naming conventions should be followed. The most important is to avoid white space character in the file names. In the process of the VIB protocol lots of lists are created on the fly. As in most programming languages the arguments of these lists are separated from each other by white space characters. If a file name contains white space characters it will be read only partially and by this jam up the process of standardization mainly resulting in a crash of Amira and an error message.

File names should be as descriptive as possible.

Example: 030401\_f1\_201y\_GFP\_nc82.tif

This is the name of the raw image file (in Tagged Image File Format (\*.tif)) of the first female (f1) of a cross of the Gal4 driver line 201y with a UAS:GFP reporter line which is stained with the neuropil marker nc82 and has been scanned/prepared at first of April 2003 (030401).

Example scheme: <date>\_<gender><successive number>\_<Gal4 driver>\_<reporter>\_<additional staining>.<file extension>

Considering a scheme like this during the data acquisition enables to select a subgroup by typing in the common pattern of choice using wildcards (\* or ?) in the file group editor. The pattern "\*f\*" calls in the example scheme all females, "030401\*" all scans of this day and "\*GFP\*" all scans in which the Gal4-line was crossed with this the UAS:GFP-reporter. Of course common patterns can be combined ("\*201y\*nc82\*" = all nc82-stained crosses of the Gal4 line 201y).

### 3.5 Space requirements

Depending on the operation system, the kind of 3D images and the chosen transformation method (RT, LST, CT, DT) the VIB protocol may need a considerable amount of hard drive space:

**Table 2: List of data volumes used and created by the VIB protocol running on a 32-bit system including resampling. (f: number of file groups, n: number of channels in the 3D images of the Samples, N: overall data volume, S: number of Samples, v: volume of a Sample, vTemplate: volume of the Template)**

Data type	VIB folder	Size
VIB scripts	VIB-root/scripts	~2 MB
VIB <i>Drosophila</i> Templates	div. folders	~ 1GB
Original images	VIB-root/images	$s*v=N$
Split images	VIB-root/images-(1...n)	$s*(n*(v/n))=N$
Resampled images	VIB-root/images-small	$s*(v/4)=N/4$
Resampled split images	VIB-root/images-(1...n)-small	$s*(n*((v/n)/4))=N/4$
LabelFields	VIB-root/labels	$s*\sim 2-5$ MB
Statistics files	VIB-root/statistics	$s*\sim 1$ KB
	VIB-root/statistics/csv	$s*\sim 1$ KB
Average	VIB-root/output/average/[name-of-Template]	$n*v_{\text{Template}}/4$
MainProbabilityMaps	VIB-root/output/Mainprob	$f*v_{\text{Template}}/4$
ProbabilityMaps	VIB-root/output/prob/[name-of-Template]	$f*s*m*\sim 150$ KB
Warped data	VIB-root/output/warped/[name-of-Template]	$s*n*v_{\text{Template}}/4 + s*\sim 1$ MB

**Table 3: Example of space requirements for one file group containing ten images with 100 slices each. (HR: high resolution data (1024x1024 voxel per slice = 100MB per channel), LR: low resolution data (512x512 voxel per slice = 25MB per channel)).**

Method	Number of channels	Space requirements (in MB)		Space requirements (relative to original volume N)	
		HR	LR	HR	LR
		1000	250	1.00	1.00
RT	1	2300	550	2.30	2.20
RT	2	3350	850	3.35	3.40
LST	1	2370	620	2.37	2.48
LST	2	3420	920	3.42	3.68
CT	1	2370	620	2.37	2.48
CT	2	3420	920	3.42	3.68
DT	1	2870	1120	2.87	4.48
DT	2	4420	1920	4.42	7.68

## 4 Implementation

The VIB protocol is developed for the standardization and comparison of shapes of *Drosophila* brains and the gene expression patterns within these, but it can also be used for the standardization of any other biological shapes. In the case of *Drosophila* brains, the protocol uses data sets of 3D reconstructions obtained by confocal microscopy from immunostained wholemount preparations (Samples, 3D images, image files). The protocol is limited only by the size of the files. It can cope with this limitation by applying a user-defined step of resampling to generate the appropriate file sizes from the data sets.

Considering that some biologists would have difficulties using scripts from the command line, we introduced all functions of the VIB protocol as modules in the graphical user interface (GUI) of the 3d reconstruction software Amira and constructed a dynamic configuration module which enables the user to set up the parameters of the VIB protocol at the very beginning of the process. No further configuration is necessary during the process of standardization.

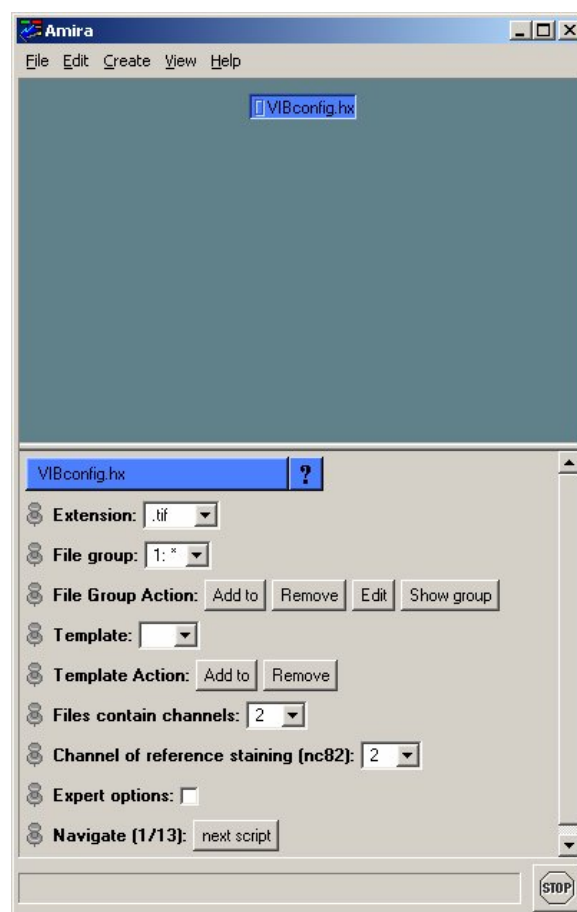


**Figure 1: The VIB protocol starts with the module VIBconfig.hx. This can be found in the folder VIB-root/scripts. The VIBconfig.hx configures all following modules and processes.**

## 4.1 Configuration of the Amira VIB protocol

The VIB protocol is solely configured in the configuration module VIBconfig.hx (Fig .1) which is called at the start of the protocol. It is recommended to fill in the form from top to bottom because the VIBconfig.hx is a dynamic module which changes its options according to earlier input. Before the configuration can be executed the confocal image data to be standardized have to be inserted in the images folder described above (VIB-root/images). In the following the VIBconfig.hx is described line by line.

### 4.1.1 Extension:

The function of the VIB protocol is restricted to data with identical file extension. In the folder VIB-root/images files may be located with several different file extensions. All these extensions are listed in the dropdown selector labeled 'Extension:'. Here the file format can be chosen that the VIB protocol will process.

### 4.1.2 File group:

As a statistical approach to neuroanatomy the VIB protocol works on groups of Samples representing the same type of brain. All of these files are supposed to be located in the images folder (VIB-root/images) and can be grouped using the 'File group Action' buttons. Multiple file groups can be set up to make batch runs more effective (see chapter 4.1.11 and chapter 4.1.12 on page 17). Building a file group can be done in two ways:

1. Defining a group by a common pattern in their file names (chapter 3.4 on page 7).
2. Combining individual file names to a file group by selecting them in the build-in browser.

Once a file group is defined it can easily be selected in the file group's dropdown selector.

In the next line which is labeled 'File Group Action' the buttons for interaction with the file groups are located:

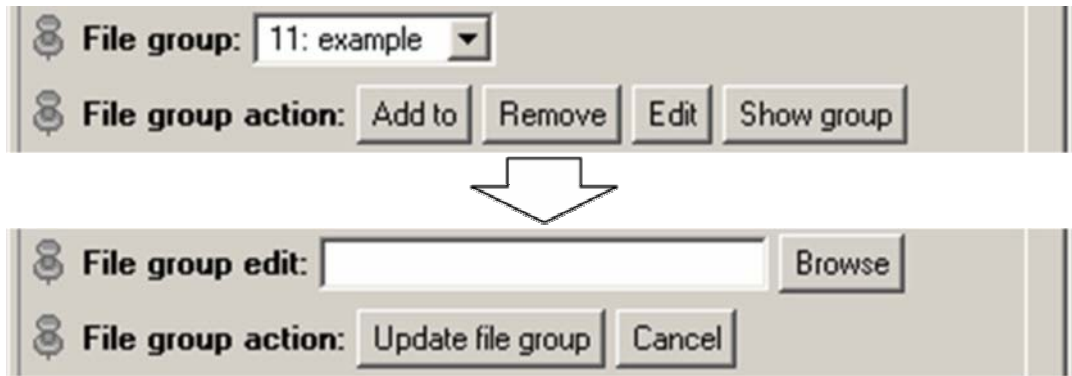


**Figure 2: File group editor: In the file group editor the files in VIB-root/images can be combined to meaningful groups.**

### **Add to:**

This button changes the line 'File group:' to the file group editor. In this field common patterns that are included in the file names to be grouped can be inserted. As a prerequisite for grouping by common file name patterns, a consistent and meaningful scheme of nomenclature has to be adopted (see chapter 3.4 on page 7).

If a group of files with arbitrary file names has to be combined to a file group these files can be selected using the button 'Browse' besides the editor's text line. This opens a window with a list whose content can be edited with the window's buttons 'Remove' and 'Add..'

### **Remove:**

This button removes the current file group from the list of file groups. By this misconfigured or old groups can be removed from the list of file groups.

### **Edit:**

This button opens the file group editor to edit the selected file group.

#### **4.1.3 Show Group:**

This button opens a SpreadSheet in which the files contained in the file group are listed.

#### **4.1.4 Template**

The Template provides the common coordinate system to which the other files of the current file group will be aligned. In the dropdown selector all predefined Templates are listed and can be chosen freely. A list of Templates was implemented to enable the quick change of the Template. This can be necessary while working on different genders or mutations at the same time. A meaningful standardization can only be accomplished if the Template specimen belongs to the same brain type (genetic identity; ontogenetic history; etc.) as

the data set to be standardized. For instance, standardizing the brain of a structural mutant such as 'sine oculis' to a wildtype Template would lead to misinterpretations of the standardized results.

The list of Templates is edited via the button 'Add to:' (see below).

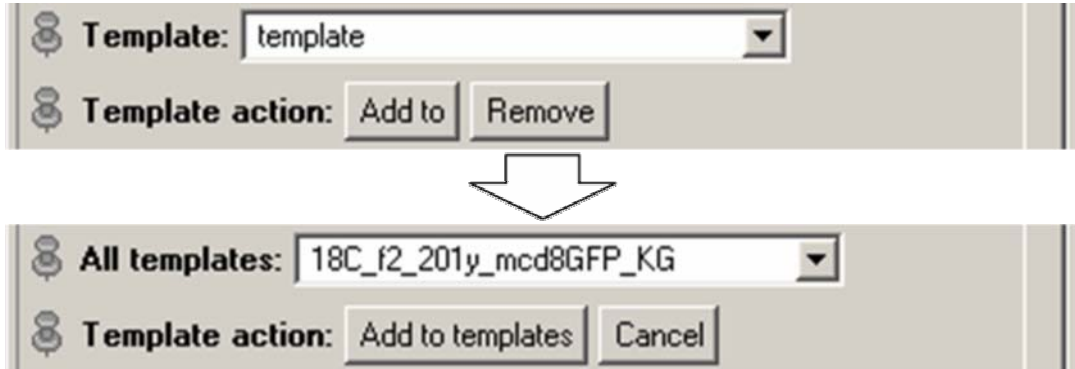


**Figure 3: Template selection. Using the buttons 'Add to' and 'Remove' Templates can be selected from a list of potential Templates.**

#### **Add to:**

This button replaces the preceding line ('Template:') with the Template editor. The dropdown selector in the Template editor lists all files which can be selected as Template. An image file can only be chosen as a template if a LabelField with the same name exists in the folder VIB-root/labels. At the very first call of the VIB protocol the template can not be chosen at this position, because there is no LabelField yet in the folder VIB-root/labels. In this case the template can be defined later on in the VIBlabelWizard (see below) and this setting can be skipped. Potential Templates (image files with a LabelField) can be added using the button 'Add to template'. 'Cancel' switches off the Template editor without any changes.

#### **Remove:**

Removes the currently selected Template from the list of Templates. By removing old or unused templates the list of templates can be kept short.

#### **4.1.5 Number of channels:**

The VIB protocol can work on single-channel as well as on multi-channel image data sets. For standardizing general brain anatomy (e.g. the brain structure phenotype of a mutant) working with only one channel is sufficient. Neuropil structures can be visualized using nc82 or anti-Synapsin antibody staining (see below). The process of standardization and the comparison of the overall neuroanatomy among e.g. genetic variants can be carried out on the basis of these stainings. Producing standardized Gal4 expression patterns requires the recording of multi-channel data sets at the confocal microscope. Besides the

actual expression pattern a reference staining like nc82 or anti-Synapsin is needed. The standardization of the expression pattern will be processed on the basis of the reference staining. Therefore the protocol has to be configured according to the content of the multi-channel image data sets imported from the confocal microscope. If the number of channels is set to  $>1$ , a new line appears in which the reference channel has to be defined.

#### **4.1.6 Channel of reference staining (nc82):**

This dropdown selector defines the channel number of the reference channel. The reference channel is the one, which contains the neuropil staining and which is the basis of the neuropil LabelFields. The channel number of the reference channel can easily be found out by loading a file of the raw data in Amira. It will appear as a number of data modules in the ObjectPool. The number of objects corresponds to the number of channels. Visualising the data modules one can easily find out which one contains the neuropil staining. The channel number corresponds to the successive number which is added to the name of the first module. This has to be entered in the dropdown selector of 'Channel of reference staining (nc82):'. A multi-channel file with three channels named 'somefile.tif' will appear in Amira as three modules: somefile.tif, somefile2.tif and somefile3.tif.

The expression pattern in the other channel will be standardized automatically according to the reference channel. The protocol can handle any number of channels.

#### **4.1.7 Use resampling:**

In neuroanatomy optical resolution and size of the object are the most important factors for precision. By the size of wholemount *Drosophila* brains ( $\sim 500 \times 250 \times 250 \mu\text{m}$ ) we were forced to use an 20x/0.70 PL APO objective. To gather as much data as possible at this low magnification we sampled each confocal slide with 1024x1024 Pixels resulting in an lateral optical resolution of  $0.65 \mu\text{m}$ . The high numerical aperture of the objective allowed to scan with a minimal axial resolution of  $0.8 \mu\text{m}$  resulting in data sets with about 200 slides per brain. Two channels (expression pattern and reference channel) were scanned with a signal intensity sampled at 8-bit. These parameters sum up to a file size of about 400MB each.

Regular 32-bit computers today are not capable of processing the VIB protocol on data sets of this size ( $\geq 512 \times 512$  pixels). Therefore data sets bigger than  $512 \times 512$  pixels had to be resampled. To avoid loss of information during the process of standardization the step of resampling is done after the interactive

processes of segmentation (VIBscissors, VIBlabelWizard). So these can be accomplished at high resolution.

#### **4.1.8 Expert options:**

Checking 'Expert options:' unfolds advanced configurations. These are implemented to allow for high throughput application of the VIB protocol.

#### **4.1.9 Transform by:**

In addition to the default transformation (see 0 on page 15) three other transformations are implemented in the VIB protocol and can be selected via this multi-menu.

##### **4.1.9.1 VIBregistrationTransformation (RT)**

The transformation method VIBregistrationTransformation is a global rigid transformation based on principle component analysis (PCA) of the grey values of the 3D images. Using the Amira module 'Registration' rigid transformation of the file group's data sets onto the Template data set is computed, using an iterative optimization algorithm [90]. This process correlates the grey values of the 3D images allowing isotropic scaling of the Sample. Thereby the scaling is applied after rotation and translation of the Sample. Thus scaling artifacts can be avoided to a large extent. The module of the method is the VIBgreyTransformation (chapter 4.2.2.9 on page 25)

##### **4.1.9.2 VIBlabelSurfaceTransformation (LST)**

The transformation method VIBlabelSurfaceTransformation is a global rigid transformation based on the functionality of the Amira module 'AlignSurfaces' [90]. The LST generates a triangular approximation of the interfaces between the Exterior and the Interior of all the Materials defined in the LabelFields of the Sample and the Template using the Amira module 'SurfaceGen'. Surfaces are aligned in their entirety to each other by iteratively minimizing the root mean square distance between corresponding surfaces [90]. This process is called the iterative closest point algorithm (ICP) [91]. The module of the method is the VIBlabelSurfaceTransformation (chapter 4.2.2.10 on page 26).

##### **4.1.9.3 VIBcenterTransformation (CT)**

The transformation method VIBcenterTransformation computes a global rigid transformation of the Samples on the basis of the centers of gravity of the Materials. These are stored in the corresponding statistics files by the module VIBtissueStatistics. The module creates landmark sets from the coordinates of the neuropils' centers of gravity. Landmark sets represent specific points or markers in 3D space. On the basis of these data sets a rigid transformation is

computed by minimizing the sum of the squared distances between corresponding points. I.e., the module moves the points of the Sample as close as possible onto the points of the Template without changing their relative position to each other. The result is returned as a 4x4 transformation matrix and written to the corresponding statistics file.

The module of the method is the VIBcenterTransformation (chapter 4.2.2.11 on page 26).

#### **4.1.9.4 VIBlabelDiffusion (DT)**

For computing a non-rigid transformation the VIBdiffusionTransformation (DT) is the most costly but most precise transformation in the VIB protocol. It consists of three steps. Beginning with the algorithms of the CT a global rigid transformation of the Sample onto the Template is applied, followed by a local rigid transformation (VIBlabelDiffusionTransformation). In this step for each of the LabelFields the 3D overlap of corresponding Materials is maximized without taking into account the degree of overlap of the other Materials using parts of the functionality of the LST. By this as many contradictory transformations are computed as Materials are defined in the LabelFields. In the last step (VIBdiffusion) the contradictory transformations are applied to their corresponding Materials and non-labeled areas in between are transformed following a modified heat transfer equation [86]. This step results in a VectorField which is directly applied to the 3D images. The non-rigidly transformed 3D image files are saved in the VIB/output/warped folder from where they are recalled by the process of standardization.

The modules of the method are VIBlabelDiffusionTransformation and VIBdiffusion (chapter 4.2.2.12 and chapter 4.2.2.13 on pages 26f).

All four procedures lead to an alignment of the standardized reference channel in combination with the Gal4 expression patterns. Additionally, the transformations based on LabelFields create probability maps of the appearance of the Materials. By these the quality of the transformations can be judged intuitively.

#### **4.1.10 Cluster computing:**

To speed up the work on very large file groups, the files can be processed on several computers running the VIB protocol in parallel. Internal blocking of the current file while it is processed prevents redundant computation in the cluster if 'cluster computing' is enabled. This is accomplished by writing nearly empty text files into the folders of the files which have to be locked. These files have the same name as the corresponding file to be blocked but have a different file

extension. This extension is constructed automatically from the name of the locking process and the suffix 'LCK'. By this approach files can be used in parallel by different processes but not by multiple instances of the same process on different computers. The common pattern "LCK" facilitates the recovery of lost lock-files after a potential system crash.

#### **4.1.11 Batch run all groups:**

The batch run can be extended to all file groups following the selected file group by enabling this option.

#### **4.1.12 Batch run:**

The VIB protocol can be run completely automatically, if all interactive steps (mainly the segmentation) are done beforehand. Batch run can be activated if LabelFields are not needed (Amira's Registration) or as soon as for each image data set a LabelField exists in the folder VIB-root/labels. This can be controlled by hitting the button 'Show group' (see 0 on page 12). Batch running the VIB protocol computes all needed steps automatically according to the settings done in the VIBconfig.hx. In the ground state of the protocol the batch run is confined to the current file group. Batch run is started with this button.

#### **4.1.13 Debug level:**

This is a switch between three levels (0-2) of verbosity of the VIB protocol seen in the Amira console. This output also is appended to the log.txt file needed for debugging. At levels >0, the 'Jump to Script' menu appears which enables direct selection of any module included in the configured procedure.

#### **4.1.14 Navigate:**

In interactive mode the 'Navigate' buttons lead through the process of standardization by loading the appropriate modules and files. The progress of the protocol is displayed by the number of the current module next to the total number of modules needed.

## 4.2 The VIB protocol

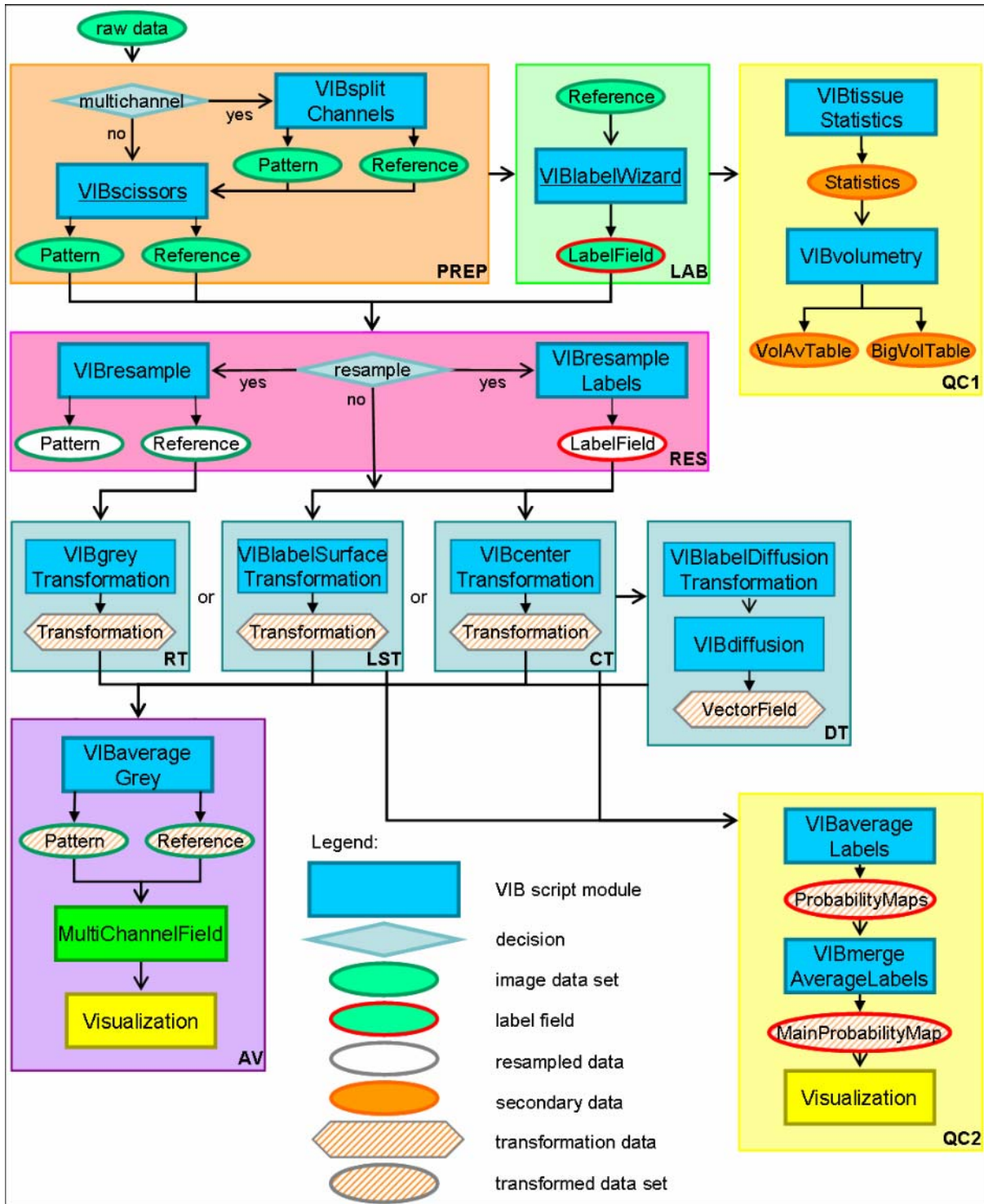


**Figure 4: Flowchart of the VIB protocol.** The process starts with the import of raw data (upper left). Sections: PREP (light brown): In the steps of preprocessing the imported 3D images are prepared for standardization. These steps include optional resampling and electronic removal of unwanted parts of the 3d images. LAB (light green): During the labeling LabelFields are constructed on the basis of the reference channel; QC1 (light yellow): The first quality control evaluates the LabelFields by basic statistical comparisons of the Material's volumes; RT, LST, CT, DT (light blue): The transformation processes align the

**Samples to the Template rigidly (RT, LST, CT) or non-rigidly (DT); QC2 (light yellow):** The second quality control for the evaluation of the alignment creates **MainProbabilityMaps** for each file group. These can be controlled visually and statistically; **AV (purple):** The step of averaging fuses each channel of the 3D images of a file group to an average intensity image.

**Icons:** Ovals: data; squares: processes; diamonds: decisions; hexagon: transformations. **Color code:** green: 3D images; red: LabelFields; blue: processes/scripts; orange: spreadsheets; yellow: visualization; white: resampled data; hatched: transformed data. **Arrows:** open: data input to processes; closed: writing data to files.

#### **4.2.1 Flowchart**

The VIB protocol uses a configurable set of script modules (chapter 1 on page 10) to manage the process of registration and standardization of brain structures and corresponding Gal4 expression patterns. The modular architecture of the protocol facilitates the flexibility and robustness of the process even on instable computer systems, a feature saving lots of time and frustration.

##### **4.2.1.1 Preprocessing (PREP)**

To cope with the large data volume of high resolution files the raw image data have to be preprocessed before being fed into the actual process of alignment and standardization. This preprocessing (Figure 4, light brown box, PREP) starts with the splitting of the data sets if needed (see chapter 4.2.2.2 on page 22). Depending on the registration algorithm to be used unwanted appendages can be removed electronically (see chapter 4.2.2.3 on page 23). For reasons of RAM capacities of today's computers, high resolution data larger than 512x512 pixels in x-/y-dimension have to be resampled before processing (see chapter 4.2.2.5 and chapter 4.2.2.6 on page 24). On more advanced computer systems (64 bits) this step of preprocessing is dispensable and therefore can be switched off in the configurations menu of the VIB protocol.

From the preprocessing there are two ways leading to the standardization. The module **VIBgreyTransformation** (Figure 4, light blue box, see chapter 4.2.2.9 on page 25) is the fastest standardization procedure. However it is the least precise method. Therefore it only can be recommended for a quick screen but not for a thorough analysis of anatomy. More precision can be achieved using label based standardizations like **VIBlabelSurfaceTransformation** (see chapter 4.2.2.10) or **VIBcenterTransformation** (see chapter 4.2.2.11). The best results are obtained with the non-rigid approach of the VIB protocol, the **VIBlabelDiffusionTransformation** (see chapters 4.2.2.11 - 4.2.2.13), which combines the rigid alignment approaches and enhances them by a step of non-

rigid transformation. However, as these alignment methods mainly work on LabelFields, the images data have to be segmented.

#### **4.2.1.2 Labeling (LAB)**

LabelFields (green oval, red rim) are created by segmenting the raw data manually using the module VIBLabelWizard (Figure 4, light green box, see chapter 4.2.2.4 on page 23). Segmentation is manually executed on the basis of the reference channel in original resolution to attain highest accuracy of the LabelFields. If the original x-/y-dimensions of the raw data are bigger than 512x512 pixels the LabelFields are resampled after completion and stored in a new folder to be read back by the following processes (Figure 4, green chessboard, red rim).

#### **4.2.1.3 Quality Control (QC)**

The VIB protocol has two routines of Quality control, one before standardization for the control of the initial data and one after standardization for the evaluation of the results. In the first routine (QC1) the LabelFields are tested for data integrity by statistical measures (Figure 4, light yellow box, see chapter 4.2.2.7 and chapter 4.2.2.8 on page 25).

In the first step the module VIBtissueStatistics creates a statistics file for every LabelField of the selected file group. The statistics files have two layers of data. On the one hand a statistics file consists of a table of the volumes of the LabelFields' Materials. It is created by counting the number of voxels of each Material and multiplying this number with the actual size of a voxel. These data are stored with the coordinates of the Materials centers of gravity. On the other hand a statistics file contains a list of parameters which is used to store the parameters of the rigid transformations performed during the process of standardization (CT, DT see chapter 4.1.9.3 and chapter 4.1.9.4 on pages 15f).

In the second step the module VIBvolumetry provides basic volumetric measurements of the LabelFields. It reads out the statistics files of the selected file group and creates two tables the volumes of the LabelFields' Materials (BigVolTable, VolAvTable, see chapter 4.2.2.8 on page 25). These are exported to "comma separated values" format (csv) and can be loaded into any spreadsheet, compared and used to control the quality of labeling. Inconsistencies in labeling can easily be found and analyzed by exceptionally big or small volumes of the labeled Materials.

The second routine of quality control (QC2) creates a MainProbabilityMap of the LabelFields' Materials (see chapter 4.2.1.3 on page 20f). The MainProbabilityMaps are grey value images coding for the probability to hit a

Material on a certain position. The quality of alignment easily can be evaluated visually and arithmetically. A good measure of alignment quality deduced from the MainProbabilityMaps is the core-to-seam measure (see chapter 5.2.2 on page 32) we developed during the choice of Template (see chapter 0 on page 29)

#### **4.2.1.4 Registrations (RT, LST, CT, LDT)**

Depending on the transformation algorithm chosen during the configuration of the process of standardization (chapter 1 on page 10) the VIB protocol carries out the appropriate steps of alignment (light blue boxes, see chapter 4.2.2.9 - 4.2.2.13). Four different methods of transformation are implemented in the VIB protocol.

VIBgreyTransformation	rigid transformation
VIBlabelSurfaceTransformation	rigid transformation
VIBcenterTransformation	rigid transformation
VIBdiffusionTransformation	non-rigid transformation

All rigid transformations are stored in a combination of 16 parameters in the statistics files (see chapter 4.2.2.7 on page 25). Due to enormous file size of VectorFields in the dimensions of the images the non-rigid transformations are not saved as independent files but applied to the corresponding images directly. The transformed images are saved in the protocol's output folder (VIB-root/output).

#### **4.2.1.5 Averaging (AV)**

The step of averaging combines the transformed image files to average grey value images reflecting the typical morphology of the expression patterns investigated (see chapter 4.2.2.14 on page 27). The corresponding LabelFields are fused to probability maps depicting the distribution of each Material (see chapter 4.2.2.15 on page 28). These are combined to a MainProbabilityMap reflecting the distribution of all Materials (see chapter 4.2.2.16 on page 28).

### **4.2.2 The modules**

The VIB protocol has a modular architecture to achieve maximal flexibility during the process of standardization. By means of the modules the user navigates through the protocol. Therefore, basic elements are repeated from module to module, always serving the same functions:

#### 4.2.2.1 Common elements of the VIB script modules

File group: In this dropdown selector a predefined file group can be selected out of the list of file groups defined in the VIBconfig.hx. Navigating through the modules with the buttons 'next script' or 'previous script' this field will be set automatically to the file group predefined in the VIBconfig.hx.

Action: Hitting the action button runs the module for all files in the current file group. (Running the VIB protocol in batch mode no interaction is possible.)

Navigate: Hitting the buttons of the line 'Navigate' leads to the next, the previous or the configuration module (VIBconfig.hx). By these buttons the user is led through the process of standardization. While changing modules many checks of data integrity are performed in the background.

Jump To: For advanced users the Jump menu provides the possibility to skip obsolete modules and jump to a specific module directly. For example while controlling previously created LabelFields the modules VIBsplitChannels and VIBscissors are not needed and therefore can be skipped. The Jump menu is enabled by setting the 'Debug level' in the 'Expert options' >0.

Template: In the modules which are computing the transformation (light blue boxes, see 0 - 4.2.2.13) and in the configuration module (VIBconfig.hx) the Template can be selected from a list of predefined Templates. This list is edited in the configuration module (QV VIBconfig)

#### 4.2.2.2 VIBsplitChannels.hx

This module is only included in the VIB protocol if the number of channels is set greater than one in the line 'File contains channels:' of the VIBconfig.hx (chapter 1 on page 10).

The module VIBsplitChannels loads the original images from the images source (VIB-root/images) and creates automatically as many data modules as channels are stored in these files. Subsequently it saves each of the data modules (i.e. the different channels of the scan) in numbered folders (VIB-root/images-1, VIB-root/images-2, ...). If these folders do not exist the module creates them automatically. These folders are set as the images source for the further processing. To avoid unnecessary processing the module first screens the images folder and target folders and only runs on files which are not yet split. This is done by controlling if there is no corresponding file in the target folder or if the file in the target folder is older than the original file, which means the original file was changed after the last call of this module.

The original images are not changed by this module and stay in the folder VIB-root/images.

Depending on the size of the file group defined during the configuration of the VIB protocol this process can take rather long. Especially if the original data are not located on the local machine but have to be transferred via a network for loading and saving. The time the module will be finished is approximated every time the process uploads a new original image for splitting and is displayed in Amira's main window and the console.

#### **4.2.2.3 VIBscissors.hx**

The module VIBscissors is one of the highly interactive ones. The module VIBscissors is designed to revise the recorded data sets. Unwanted parts of the data set like trachea or the esophagus can be removed electronically. By this even suboptimal preparations can be used in the VIB protocol. Standardizations based on LabelFields (CT, LST, DT) do not really need this step, because after segmentation additional appendices have no influence on the transformation. Nevertheless the quality of the average brain can be enhanced dramatically by removing unwanted tissues which otherwise would blur the average. Using the alignment method VIBgreyTransformation the module VIBscissors is indispensable because large appendices like the esophagus or the connective to the ventral nerve cord would spoil the standardization completely.

Working on single channel data this process never should be processed on the original raw-data because the files processed by the module VIBscissors are changed permanently. Working on multi-channel data the data are split in their channels by the module VIBsplitChannels beforehand. Therefore the original data are not touched by this module in multi-channel data.

The module VIBscissors consecutively loads all files of the selected file group, connects them to a VolumeEdit module [90] which enables the treatment of the actual data set and saves the revised file before opening the next. By this procedure the protocol ensures that all files of the current file group are attended. For direct access to a certain file two dropdown selectors are implemented in the module VIBscissors by means of which a file and a channel can be selected for editing ("File to edit:", "Channel Number:").

#### **4.2.2.4 VIBlabelWizard**

As the other highly interactive modules the VIBlabelWizard is just called in the interactive mode. In the batch mode for control reasons it is called but interaction is disabled.

The labeling of *Drosophila* brains is performed using the reference channel of the split channels. This is the channel containing the neuropil staining. The neuropil areas of interest have to be labeled in all members of the file group

consistently. Currently this has to be done manually using the SegmentationEditor of Amira. All loading, naming and saving is performed by this module. Thereby it is guaranteed that the naming conventions chosen for the images are followed during the process of labeling.

Hitting the Action button loads the file currently selected in the line 'File to edit', attaches a LabelField to it and opens the SegmentationEditor.

For Segmentation it is recommended to maximize the window of the SegmentationEditor. If the labeling is started 'de novo' the Materials have to be newly created in the list of Materials on the left hand side of the SegmentationEditor. This has to be done with a right mouse click in the white area of the list of Materials. As soon as a data set is completely labeled it may be chosen as Template. The list of Materials In the Template then is transferred to the next LabelFields of this file group. Not all Materials of a transferred list have to be labeled. Materials also can be left empty and are not considered during the standardization procedure.

For the creation of *Drosophila* standard brains it is recommended to use the Templates (male/female) provided by the VIB project (chapter 5.3 on page 35). For explanations on the SegmentationEditor please refer to the Amira help.

#### **4.2.2.5 VIBresample.hx**

This module is just called by the VIB protocol if the Checkbox 'Use resampling' in the 'Expert options' of the Configuration module is checked (chapter 1 on page 10). This is set on by default to avoid memory allocation errors.

The module resamples the 3D images of the selected file group to a size of 512 x 512 voxels in the x and y dimensions. Due to the much lower resolution in z-dimension this is not resampled. The resampled files are saved in the appropriate folders (VIB-root/images-small). If folders do not exist they are created by the module. The raw image data are not altered and stay in the folder VIB-root/images.

Resampling leads to a loss of resolution. But for large file sizes (1024 x 1024 x 200 Voxel ~ 400MB) it is the only way to run the protocol on an average computer. Image data larger than 512 x 512 lead to massive memory fragmentation and therefore memory allocation errors on 32-bit systems. This is true especially on computers running Windows™ as operating system. On 64-bit systems (Onyx2, InfiniteReality) the VIB protocol was tested positively without resampling. The step of resampling therefore seems to be dispensable on 64-bit machines and can be switched off. Further testing is planned.

#### **4.2.2.6 VIBresampleLabels.hx**

This module is just called by the VIB protocol if the Checkbox 'Use resampling' in the 'Expert options' of the Configuration module is checked (chapter 1 on page 10). This module resamples the LabelFields of the selected file group to the size the images were resampled before (default: 512 x 512). The resampled LabelFields are stored in the appropriate folders (VIB-root/labels-small) which are created if not already existing. These folders become the source of LabelFields for the further processing.

The original LabelFields are not altered and stay in the labels folder (VIB-root/labels).

#### **4.2.2.7 VIBtissueStatistics.hx**

This module counts separately for each LabelField of the selected file group the number of voxels of each Material. By multiplying this number with the size of a voxel the actual volume is calculated. These data are stored with the coordinates of the Materials centers of gravity in the statistics files ( VIB-root/statistics ).

By measuring the distribution of labeled voxels for each Material the center of gravity is calculated and saved as a virtual Landmark Set. These Landmarks are used by the alignment method VIBcenterTransformation.

#### **4.2.2.8 VIBvolumetry.hx**

The module VIBvolumetry is part of the quality control implemented in the VIB protocol. Using the statistics files this module performs basic statistics on the volumes of the LabelFields. The results are stored in two spreadsheets

#### **4.2.2.9 VIBgreyTransformation.hx**

The module VIBgreyTransformation aligns the Samples of a file group to the Template according to the distribution of Grey values in the reference channel. A principal component analysis (PCA) is computed on the 3D images of the reference channels and the data volumes are aligned to each other by the first three principal axes. Therefore it is important that the Samples which are processed with this module are very tidy and void of additional tissues like the esophagus or trachea.

Functionality:

- load reference channel of Template
- create module Registration
- subsequently for all Samples:
  - load reference channel
  - align to Template
  - save transformation data in the corresponding statistics files.

#### 4.2.2.10 VIBLabelSurfaceTransformation.hx

The module VIBLabelSurfaceTransformation aligns the Samples of a file group to the selected Template by minimizing the distance between the surfaces of the Materials.

Functionality:

- create module SurfaceGenerator
- create module Resample
- load LabelField of Template
- resample LabelField of Template
- create surface of LabelField of Template
- visualize surface
- visualize LabelField of Template with BoundingBox
- create module AlignSurfaces
- subsequently for all Samples:
  - load LabelField
  - resample LabelField
  - create surface of Labelfield
  - visualize surface
  - visualize with BoundingBox
  - align to Surface of Template
  - save transformation data in the corresponding statistics files.

#### 4.2.2.11 VIBcenterTransformation.hx

The module VIBcenterTransformation aligns the Samples of a file group to the Template by minimizing the distance between corresponding centers of gravity of the Materials. For this computation only the rather small statistics files are needed. Therefore this process is very quick.

Functionality:

- load statistics of Template
- create LabelField (needed for LandmarkSets)
- subsequently for all Samples:
  - load statistics
  - create LandmarkSet with two sets of Landmarks (Template/Sample)
  - align Landmarks
  - save transformation data in the corresponding statistics files.

#### 4.2.2.12 VIBLabelDiffusionTransformation.hx

The module VIBLabelSurfaceTransformation aligns the volumes of the Materials of the Samples to the corresponding volumes of the Template. The three-dimensional overlap of the volumes is maximized for each Material individually without taking the overlap of the other Materials into account. Therefore this module results in as many contradictory transformations as Materials are defined in the LabelFields. These transformations are stored in the Samples' statistics files with the name of the Material and fused by the module VIBdiffusion (see next paragraph).

Functionality:

- load LabelField of Template
- visualize LabelField of Template with BoundingBox
- create module Align
- subsequently for all Samples:
  - load LabelField
  - visualize LabelField with BoundingBox
  - subsequently for all Materials:
    - align Sample Material to corresponding Template Material
    - save transformation data with the name of the current Material in the statistics files of the Sample.

#### **4.2.2.13 VIBdiffusion.hx**

The module VIBdiffusion is the second module in the method VIBdiffusionTransformation. This module merges the local rigid transformations computed by the module VIBLabelDiffusionTransformation (see previous paragraph). The area in between the Materials is transformed following a modified heat diffusion equation iteratively. Thereby the grey values are treated as denoting temperature at two different points in time, and the force to establish the heat flow is minimized. In this manner, it is assured that the neuropile areas are mapped rigidly, thus avoiding distortions which do not make anatomical sense (such as eliminating unstained areas when they are anatomically relevant)

Functionality:

- load LabelField of Template
- create module Diffusion
- subsequently for all Samples:
  - load LabelField
  - subsequently for all channels of the 3D images
    - load statistics file
    - load 3D image
    - initialize transformation
    - compute transformation vector field
    - apply vector field to current 3D image
    - save transformed 3D image

#### **4.2.2.14 VIBaverageGrey.hx**

The module VIBaverageGrey creates average intensity maps on the basis of the 3D images and the Transformations which were computed by the preceding modules. Therefore it has two modes which are selected automatically. Following a global rigid transformation (RT, LST, CT) this module first applies the transformation parameters which are stored in the statistics file of each Sample to the 3D images. Subsequently it averages the grey values of each voxel over the whole file group. Following the non-rigid transformation (DT) this module just averages the transformed 3D images, because all steps of transformations are included in these files. In both modes average intensity maps are separately created for each channel of the 3D images.

#### **4.2.2.15 VIBaverageLabels.hx**

Like the grey values of the 3D images get averaged in the module VIBaverageGrey, the LabelFields get averaged in this module. The LabelFields thereby are taken as binary data of the occurrences of the Materials (inside/outside). Therefore averaging of the volumes of the Materials leads to ProbabilityMaps of the distribution of occurrence of the Materials. For each Material a ProbabilityMap is computed separately and stored in the output folder (VIB-root/output/prob/). This avoids the fusion of closely adjacent Materials. The ProbabilityMaps are coded in percent (i.e. the highest value is normalized to 100).

#### **4.2.2.16 VIBmergeAverageLabels.hx**

The module VIBmergeLabelsAverages merges the ProbabilityMaps which were build by the module VIBaverageLabels before to generate MainProbabilityMaps. The ProbabilityMaps of closely adjacent Materials in some cases overlap. At these positions the weight of the ProbabilityMaps decides which Material wins.

## **5 The choice of templates**

The process of standardization is dependent on a Template representing typical brain morphology. The Template image provides the coordinate system to which all other brains become aligned during the process of standardization. Therefore the selection of the Template images is a critical task during the creation of standardized neuroanatomy.

### **5.1 Iterative approach for Template selection**

Hitherto the problem of Template selection was solved by an iterative approach [4] & [6]. This starts with manually screening all specimens and selecting the one which appears most normal due to the judgment of the trained eye of the selector. This is chosen as the primary Template to be used in a first round for standardization. After the standardization the most normal brain out of the standardized brains is chosen as a template (secondary Template) and the process of standardization is run again. This procedure is repeated until the most normal brain after the standardization is identical to the Template selected.

This approach suffers from three major weaknesses. First the outcome is influenced by the selection of the primary Template, because all consecutive steps are just minor improvements of the primary choice. As a test we deliberately selected a deformed specimen as a primary Template. In some cases this leads to suboptimal results even after several iterations. Therefore the primary selection needs to be done by an experienced neuroanatomist which is a general drawback.

Secondly, even a trained user is not free from bias in the selection of the first Template. Variations in the quality of staining or scanning can deceive the quality of the specimen with regards to its morphological normality.

Third, the iterative approach may run into an endless loop between two or more specimens, if their morphology is very similar. In such cases an incontestable selection is impossible and a Template has to be arbitrarily selected out of the group of competing specimens. Therefore the result of the iterative approach of Template selection has only limited reliability due to the potential bias in the selection of the primary Template.

### **5.2 Bias-free approach**

Here we introduce two absolute measures for the normality of neuroanatomy of the specimens for selection as Templates, the overall mean distance of centers

of gravity (mean-cog-distance, mcd) and the core-to seam ratio (core2seam-ratio, c2s).

### 5.2.1 Overall mean distance of centers of gravity

The overall mean distance of centers of gravity (mean-cog-distance, mcd) describes the (overall) mean distance of all Materials' centers of gravity of the current Template to the corresponding centers of gravity of all Samples. This implies that all Samples in a file group are successively defined as Template to which the other Samples are aligned. Alignment is achieved by bringing the centers of gravity of the Samples as close as possible to the corresponding centers of gravity of the Template. As only rigid transformations are applied to the data sets the mcd selects the most normal Sample as the best Template. This represents the "morphologic median" of a file group. In all aspects of variability (deformation, 3D size) it is the most median Sample.

The mcd was developed as a quick search for the best Template. Therefore it uses rigid transformation (CT, see chapter 4.1.9.3 on page 15). During the process of the CT the transformation parameters needed to map a Sample to the current Template are stored in the statistics file of the Sample with a reference to the Template. For every combination of Template and Sample a CT is calculated and the transformations are stored in the statistics files. This information quickly can be read out together with the Materials' centers of gravity, stored in the same file. From this information the mcd can be derived without loading the comparatively big image files of LabelFields.

Due to the global rigid transformation of the CT, deformations or aberrations from normal/wild-type/typical morphology in the current Template result in a big mcd.

$$\text{mean - cog - distance} = \frac{1}{m} \cdot \sum_{S=1}^m \left( \frac{1}{n} \cdot \sum_{M=1}^n D_M \right)_S$$

**Equation 1: The mean-cog-distance is the mean of the mean distance (D) of the Materials (M) centers of gravity from the corresponding center of gravity of the Template (DM) over all Samples (S) of the file group.**

For our *Drosophila* Templates the mcd was computed on groups of 31 female and 28 male brains (CantonS) using LabelFields with 16 Materials (medulla, lobula, lobula plate, mushroom body, antennal nerve, antennal lobe (all bilaterally), ellipsoid body, fan shaped body, protocerebral bridge).

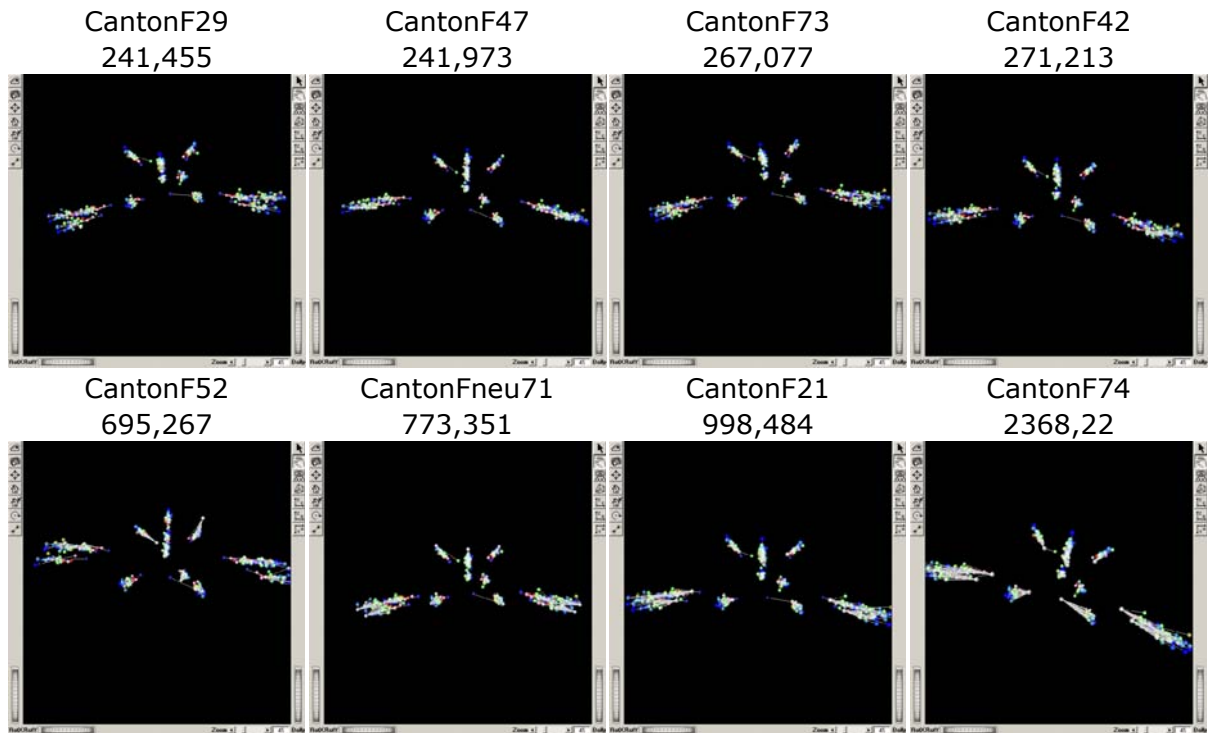


**Figure 5: Exemplary samples of the Mean-cog-distances of 31 female brains (best four vs. worst four). The centers of gravity of the current Template (grey) are connected with a white line to the corresponding centers of gravity of the samples (colored). The smaller the resulting cloud the better the current Template. The size of the cloud is quantified by the mean-cog-distance displayed under the Templates name.**

Using the mcd only the best female Template out of the test populations is CantonF29 and the best male Template is CantonM60. Nevertheless the mcd for CantonF29 (241,455) is notable bigger than that of CantonM60 (163,235). This can be explained by a higher variability in brain volume in the female test population than in the male counterpart (RelDev in Table 4 and

Table 5).

**Table 4: Label based volumetry of the female test population**

Nr	Material	Volume	Deviation	RelDev	StdError	RelStdError	fileCount
0	Exterior	65800300,00	6214550,00	9,44	1116170,00	1,70	31
1	medulla_r	1101040,00	157759,00	14,33	28334,40	2,57	31
2	medulla_l	1093320,00	144072,00	13,18	25876,20	2,37	31
3	lobula_r	368784,00	59400,90	16,11	10668,70	2,89	31
4	lobula_l	370142,00	57125,50	15,43	10260,00	2,77	31
5	lobula_plate_r	197907,00	38631,50	19,52	6938,42	3,51	31
6	lobula_plate_l	199069,00	35617,60	17,89	6397,11	3,21	31
7	mushroom_body_r	158035,00	34473,40	21,81	6191,60	3,92	31
8	mushroom_body_l	160756,00	30712,50	19,11	5516,13	3,43	31
9	ellipsoid_body	36192,90	4758,08	13,15	854,58	2,36	31
10	noduli	10186,00	1719,60	16,88	308,85	3,03	31
11	fan_shaped_body	106997,00	15594,60	14,57	2800,86	2,62	31

Nr	Material	Volume	Deviation	RelDev	StdError	RelStdError	fileCount
12	protocerebral_bridge	20017,00	3054,46	15,26	548,60	2,74	31
13	antennal_nerve_r	14690,00	3800,88	25,87	682,66	4,65	31
14	antennal_nerve_l	14503,00	4504,12	31,06	808,96	5,58	31
15	antennal_lobe_r	192005,00	24505,40	12,76	4401,31	2,29	31
16	antennal_lobe_l	194066,00	25459,60	13,12	4572,67	2,36	31

**Table 5: Label based volumetry of the male test population**

Nr	Material	Volume	Deviation	RelDev	StdError	RelStdError	fileCount
0	Exterior	64739300,00	6714500,00	10,37	1268920,00	1,96	28
1	medulla_r	1042990,00	119043,00	11,41	22497,10	2,16	28
2	medulla_l	1032640,00	112651,00	10,91	21289,00	2,06	28
3	lobula_r	364750,00	43384,10	11,89	8198,83	2,25	28
4	lobula_l	366286,00	42099,20	11,49	7956,00	2,17	28
5	lobula_plate_r	191303,00	24191,20	12,65	4571,71	2,39	28
6	lobula_plate_l	194373,00	23406,30	12,04	4423,38	2,28	28
7	mushroom_body_r	143077,00	19992,70	13,97	3778,26	2,64	28
8	mushroom_body_l	143276,00	20708,20	14,45	3913,48	2,73	28
9	ellipsoid_body	33995,00	3537,50	10,41	668,53	1,97	28
10	noduli	8929,00	1371,38	15,36	259,17	2,90	28
11	fan_shaped_body	95999,30	10218,20	10,64	1931,06	2,01	28
12	protocerebral_bridge	18596,00	3717,25	19,99	715,38	3,85	27
13	antennal_nerve_r	11777,00	4084,49	34,68	771,90	6,55	28
14	antennal_nerve_l	12331,00	2901,11	23,53	548,26	4,45	28
15	antennal_lobe_r	179841,00	24598,90	13,68	4648,75	2,58	28
16	antennal_lobe_l	174276,00	18621,20	10,68	3519,08	2,02	28

For control reasons the same test populations were introduced in two volumetric measures based on rigid and non-rigid transformation.

### 5.2.2 Core-to-seam-ratio

The most obvious advantage of the mcd over the core-to-seam-ratio (c2s) is processing time. The CT is very fast compared to the non-rigid transformation (DT) used in c2s. C2s is a volumetric absolute measure for the normality of a template data set. It describes the ratio between the non overlapping areas (seam) and the overlapping parts (core) of the Materials after transformation.

After rigid or non-rigid transformation the c2s is processed on the basis of the MainProbabilityMap (see chapter 4.2.2.16 on page 28). By separating the areas of low probability (seam;  $10\% < P < 90\%$ ) from those with high probability (core;  $P \geq 90\%$ ) two volumes are generated (). Probabilities of overlap below 10% are excluded from the evaluation, in order to correct for outliers. The ratio of the core volume to the seam volume describes the quality of the alignment and thereby the suitability of the current template.

$$c2s = \frac{V_{core}}{V_{seam}}$$

Equation 2: The core-to-seam ratio is the volume with high probability of overlap ( $V_{core}$ ) divided by the volume of low probability of overlap ( $V_{seam}$ ).

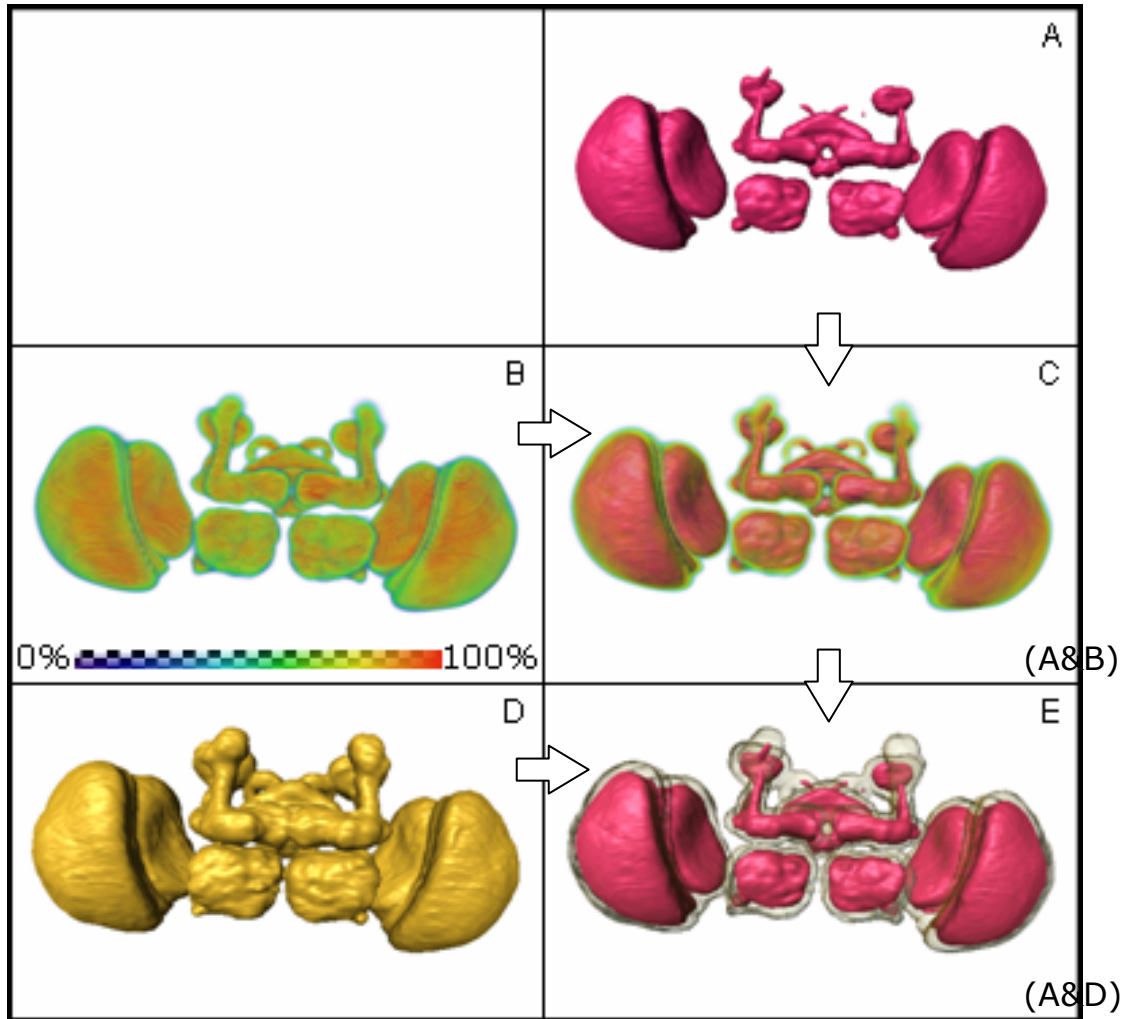


**Figure 6: The principle of the core-to-seam ratio. By thresholding the MainProbMap of a StandardBrains MainPropabilityMap (B, probability of occurrence false color coded) the Materials can be subdivided into the core with a probability of overlap greater or equal to 90% ( $V_{core}$ , A) and the seam with a probability of overlap between 90 and 10% ( $V_{seam}$ , D). C displays the core in proportion to the MainProbabilityMap. E displays the core in proportion to the seam which is rendered transparently.**

### 5.2.3 Core-to-seam ratio after non-rigid transformation (non-rigid c2s)

The non-rigid c2s is the most elaborate measure for the selection of the best Template. It uses the non-rigid alignment of the DT (chapter 4.1.9.4 on page 16) and therefore is very time-consuming. The DT provides the best alignment of the VIB protocol and in general should be used to create standard brains.

Therefore the non-rigid c2s selects the Sample to which the other Samples of the file group can be aligned most precisely using the DT as the best Template.

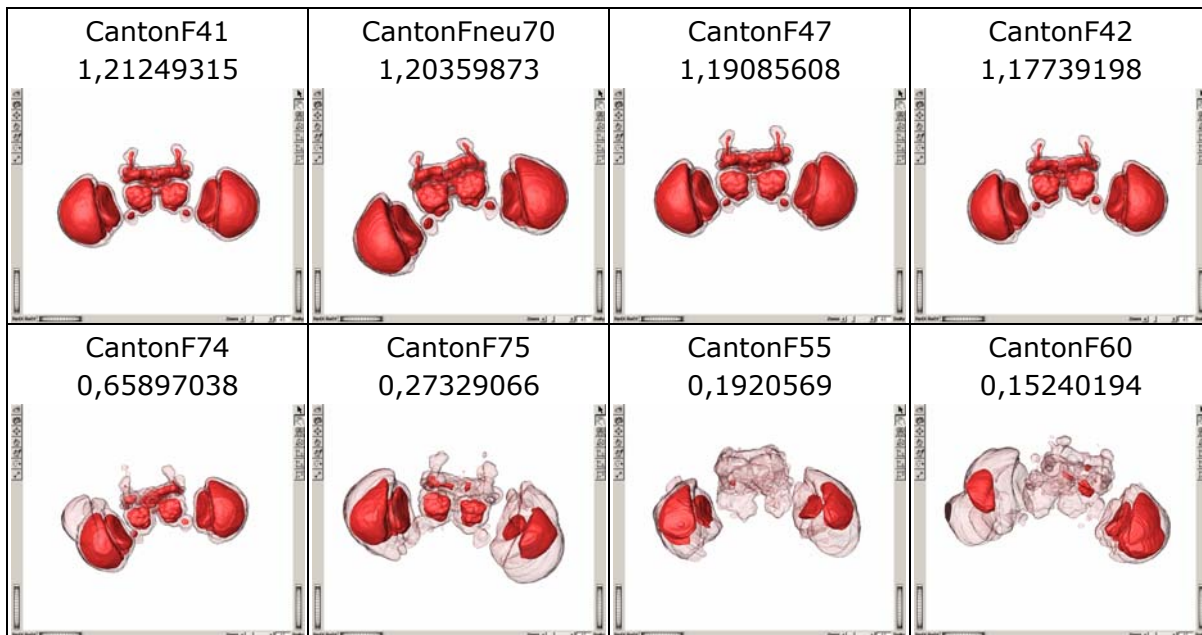


**Figure 7: Exemplary samples of the non-rigid core-to-seam-ratio of 31 female brains (best four vs. worst four). The core volume ( $V_{core}$ ) of the Materials is rendered opaque red. The surrounding seam volume ( $V_{seam}$ ) is rendered transparently.**

Using the non-rigid c2s only for the evaluation of the best Template **CantonF41** is the best female Template and **CantonM60** the best male Template.

#### 5.2.4 Core-to-seam ratio after rigid transformation (rigid c2s)

To confirm the results of the mcd we applied the c2s after rigid transformation using the same algorithms (chapter 4.1.9.3 on page 15). As expected for the CT the alignment of the Samples is much less precise as after non-rigid transformation. This results in rather small core volumes ( $V_{core}$ ) and big seam volumes ( $V_{seam}$ ). This combination gives very small c2s.

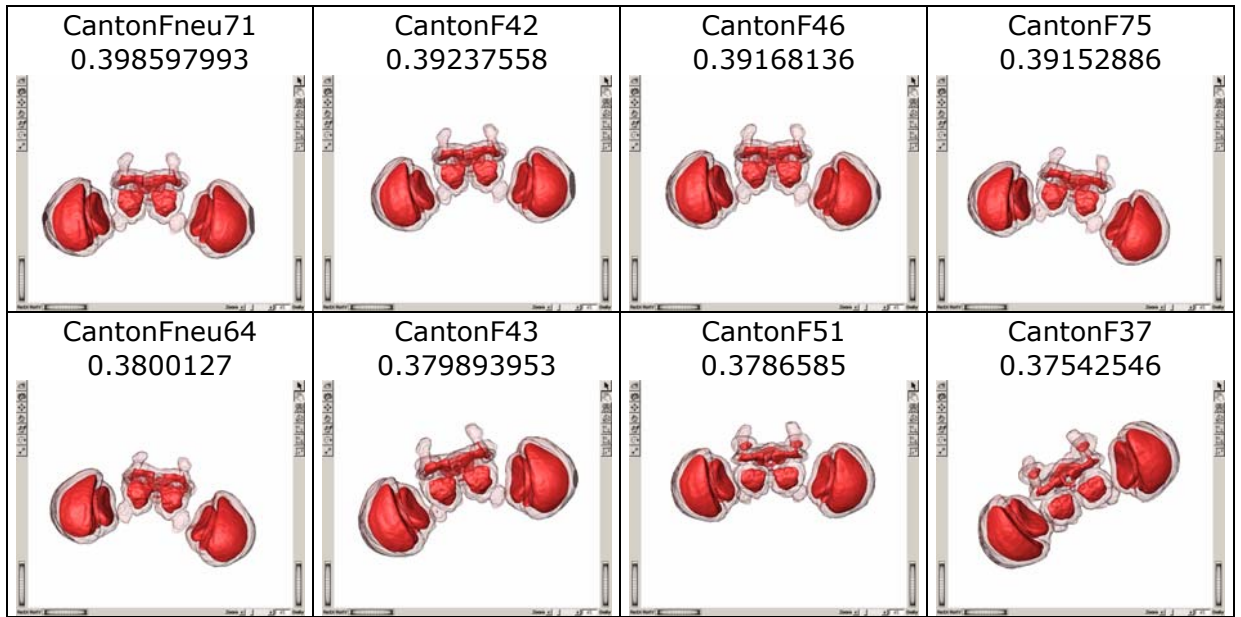


**Figure 8: Exemplary samples of the rigid core-to-seam-ratio of 31 female brains (best eight vs. worst eight). The core volume ( $V_{\text{core}}$ ) of the Materials is rendered opaque red. The surrounding seam volume ( $V_{\text{seam}}$ ) is rendered transparently.**

Due to the invariable low quality of alignment the highest c2s (best Template) differs from the lowest c2s (Template unsuitable) just by the factor 0,9 (female: 0,94; male 0,92). In comparison with the other measures this difference is too small to allow a ranking of 28 respective 31 Samples. Therefore we discarded the rigid c2s from the evaluation of the best Template.

### 5.3 Template data sets for *Drosophila melanogaster*

As expected running the tests for Template selection on the same file groups consisting of 31 female or 28 male wholemount preparations the results are different from each other. While the mcd selects **CantonF29** as the best female Template the non-rigid c2s selects **CantonF41**. Only in the definition of the best male template the measures agree in **CantonM60**. Measuring different parameters with different approaches the probability of perfectly matching results is very low. Nevertheless results of the two meaningful tests (mean-cog-distance, non-rigid c2s) reflect the same tendency by resulting in very similar rankings of the Templates. Therefore these rankings were fused in a meta-ranking for the selection of the best Templates. This was done by adding up the ranking of the mcd and the non-rigid c2s for each Template and sorting the Templates by this sum (see Table 6 and Table 7).

According to the meta-ranking we selected **CantonF47** as the best female Template and **CantonM60** as the best male Template. As the result of the combination of the mcd and the non-rigid c2s they represent the most normal

brains to which the best alignment of the other Samples of the file groups can be achieved.

**Table 6: Meta-ranking of the female Templates. The Meta-ranking is the sum of the mcd and the non-rigid c2s. Due to the very low difference between the best and the worst the ranking of the rigid core-to-seam-ratio is not taken into account.**

CantonF		CantonF47	CantonF29	CantonF42	CantonF41	CantonF70	CantonF67	CantonF73	CantonF28	CantonF43	CantonF30	CantonF46	CantonF26	CantonF22	CantonF58	CantonF60	CantonF71	CantonF75
Mcd	rigid	2	1	4	1 2	1 4	7	3	1 1	1 5	6	1 3	2 2	2 0	5	8	2 9	25
c2s	non-rigid	3	7	4	1	2	1 0	1 7	9	6	1 6	1 3	5	8	2 5	3 1	1 9	29
<b>Meta-ranking</b>		<b>5</b>	<b>8</b>	<b>8</b>	<b>1 3</b>	<b>1 6</b>	<b>1 7</b>	<b>2 0</b>	<b>2 0</b>	<b>2 1</b>	<b>2 2</b>	<b>2 6</b>	<b>2 7</b>	<b>2 8</b>	<b>3 0</b>	<b>3 9</b>	<b>4 8</b>	<b>54</b>
c2s	rigid	5	1 3	2	8	1 3	1 9	1 0	7	2 9	1 4	3	1 1	6	2 0	1 5	1	4

**Table 7: Meta-ranking of the male Templates. The Meta-ranking is the sum of the mcd and the non-rigid c2s. Due to the very low difference between the best and the worst the ranking of the rigid core-to-seam-ratio is not taken into account.**

CantonM		CantonM60	CantonM67	CantonM20	CantonM53	CantonM45	CantonM25	CantonM22	CantonM66	CantonM24	CantonM31	CantonM23	CantonM44	CantonM36	CantonM73	CantonM41	CantonM58	CantonM21	CantonM32
mcd	rigid	1	2	3	5	13	11	8	23	19	4	6	14	7	12	15	25	21	28
c2s	non-rigid	1	3	4	13	5	7	11	2	6	22	21	16	24	19	18	8	15	26
<b>Meta-ranking</b>		<b>2</b>	<b>5</b>	<b>7</b>	<b>18</b>	<b>18</b>	<b>18</b>	<b>19</b>	<b>25</b>	<b>25</b>	<b>26</b>	<b>27</b>	<b>30</b>	<b>31</b>	<b>31</b>	<b>33</b>	<b>33</b>	<b>36</b>	<b>54</b>
c2s	rigid	19	8	9	26	10	27	21	20	26	25	6	4	22	2	3	5	7	1

For test reasons or reimplementations of the template data sets the original images can be requested from VIB@neurofly.de on a DVD.

## 6 Towards a nomenclature for neuropil areas

Intense work has been performed on the analysis of the neuroanatomy of the fly brains in the last decades. A precious base was provided by N. J. Strausfeld in 1976 publishing an illustrated atlas of the brain of the blowfly (*Calliphoridae*) [92]. This still is one of the most important sources for learning insect brain neuroanatomy. In 1994 Kei Ito published a set of annotated serial sections of silver-stained wild-type *Drosophila* adult brains electronically [93]. Armstrong et al. 1995 created an internet based platform for neuroanatomical studies on the fly brain [94]. Many neuropil areas were named in these approaches. However, the named regions were not completely delimited with respect to each other. Therefore, (e.g.) the dimensions of the neuropil areas could not be determined. Moreover, the names in the atlases on *Calliphora* and *Drosophila* did not always conform to each other, leaving open the possibility of species differences. General agreement can only be found on the most prominent neuropil areas, the mushroom bodies, the central complex, the optic lobes and the antennal lobes. Especially in the protocerebrum the nomenclature remained inconsistent. In particular, regions lacking in some regions an obvious border such as the lateral horn, led to diverging nomenclatures.

For a long time large areas of the fly protocerebrum did not have a generally accepted name and remained little investigated. Today, an increasing number of studies are trying to relate structure and function in the fly brain [95]. This makes it necessary to define all neuropil areas and to arrive at a common nomenclature for them. We therefore decided to provide a complete segmentation of the *Drosophila* brain on the basis of the reference staining for the VIB Project (nc82). In immunohistochemical stainings with nc82 neuronal tracts and glial sheaths appear dark because these are areas of low synapse density. These borders we followed to find demarcations of neuropil areas. To test for reliability of the patterns of the neuropil borders and the repeatability of labeling we defined the new neuropil areas in three wild-type Samples (Canton S). After standardization we reassigned the Material names to the corresponding areas in the MainProbabilityMaps. Thereby we included only areas in which all three LabelFields agreed in the occurrence of the same Material (Figure 9).

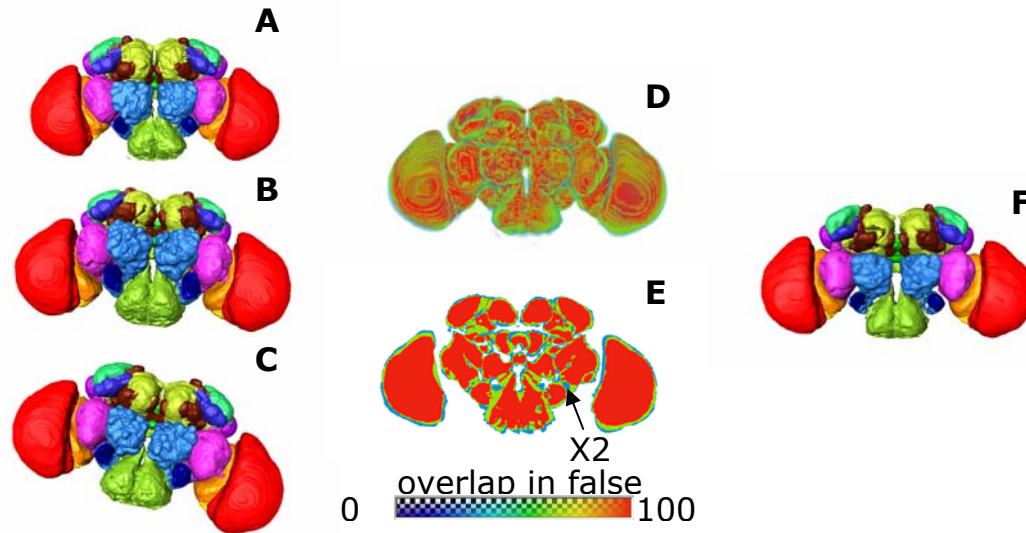


**Figure 9: Standardization of enhanced LabelFields. A, B, C,:** 3D reconstruction of individual LabelFields in original spatial orientation. **D, E:** MainProbabilityMap of standardization of A, B and C. Red codes for overlap of the same Material in all Samples, green codes for Overlap in two Samples and blue codes for areas with only one occurrence of a certain Material. **F:** Standard LabelField. Areas of high accordance (red areas in D and E) were assigned to the corresponding Materials.

The three registered samples showed a high degree of accordance of distribution of the Materials of the LabelFields. Therefore, most of the Materials in the individual LabelFields could also be encountered in the standardized brain. Only two small neuropil areas got lost in the process of standardization. One of them is the very slim Material X1 in Figure 10A. Although other areas of similar size (og, pb, eb) can be found the X1 area breaks into two pieces and is nearly undetectable in the standardized LabelField (Figure 10B).

The other one is a rather large area ventrally to the ventro-lateral protocerebrum (vlp, Figure 9B ). This area (X2 in Figure 9E and Figure 10A) was intentionally not labeled bilaterally in one of the Samples to test the standardization algorithms. The missing Material had no influence on the alignment of the Samples.

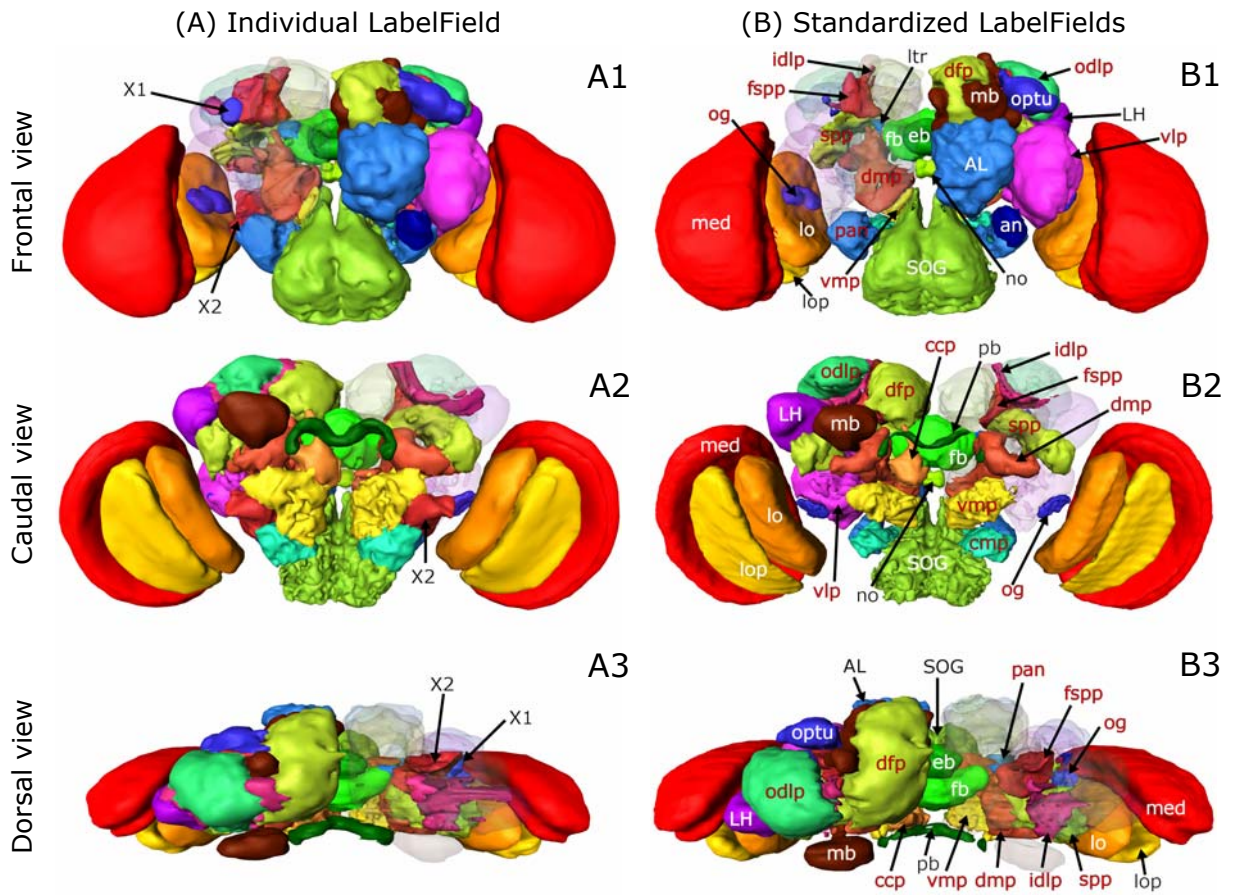


**Figure 10: 3D Reconstruction of the enhanced nomenclature for neuropil regions. In the left hemisphere all neuropil areas are visualized opaque. In the right hemisphere the distal-most neuropils are rendered transparent to uncover the underlying neuropil structures. A: Individual LabelField including all new neuropil structures. B: Standardized LabelFields (N=3).**

**Table 8a: Defined neuropil areas in the enhanced nomenclature. 12 new areas were defined.**

New Material names	
og	Optic glomerulus
fspp	Frontal super-peduncular protocerebrum
spp	Super-peduncular protocerebrum
idlp	Inner dorso-lateral protocerebrum
dlp	Dorso-lateral protocerebrum
dfp	Dorso-frontal protocerebrum
vlp	Ventro-lateral protocerebrum
dmp	Dorso-medial protocerebrum
vmp	Ventro-medial protocerebrum
pan	Proximal antennal nerve
cmp	Caudo-medial protocerebrum
ccp	Caudo-central protocerebrum

**Table 8b: : Defined neuropil areas in the enhanced nomenclature. 13 existing neuropil names and delimitations were adopted.**

Already existing names of neuropil areas	
mb	Mushroom body
fb	Fan shaped body
ltr	Lateral triangle
eb	Ellipsoid body
pb	Protocerebral bridge
no	Noduli
SOG	Sub esophageal ganglion
med	Medulla
lo	Lobula
lop	Lobula plate
AL	Antennal lobe
an	Antennal nerve
LH	Lateral horn
optu	Optical tubercle

Following the given demarcations in nc82 stainings, the whole fly brain can be reliably classified into 25 neuropil areas. The list of 13 neuropil areas with indisputable names was extended by another 12 newly defined areas. The names for the new areas were chosen following the earlier studies by Otsuna, Ito and Strausfeld as far as a significant overlap of the given already named regions and the newly defined areas could be established. Areas which had no name before were newly named according to their location in the brain.

### **Optic glomerulus – og**

The optic glomerulus is one of the most conspicuous new areas defined by nc82 staining. This area is silhouetted against the surrounding ventro-lateral protocerebrum with a very strong fluorescent signal. As nc82 marks presynapses we conclude that the synapse density in this area is remarkably high. The position of this area and unpublished findings in the laboratory of Kei Ito suggest that this area is involved in the processing of visual information.

### **Super-peduncular protocerebrum – spp**

Dorsally adjacent to the peduncle the spp extends from the inner angle between the mushroom body peduncle and the vertical lobe to the frontal margin of the mushroom body calyx. Medially it is delimited by the neuropil of the central complex and laterally it reaches as far as the outer margin of the protocerebrum.

### **Frontal super-peduncular protocerebrum – fspp**

Anterior to the spp and adjacent to the vertical lobe of the mushroom body the tetragonal fspp is located. Whereas the broader base has contact to the spp the

opposite angle is pointing upwards along the vertical lobe and reaches up to the bifurcation of the  $\alpha$ - and  $\alpha'$ -lobe.

### **Dorso-lateral protocerebrum – dlp**

The dlp is the most dorsal neuropil area of the fly brain which builds the uppermost margin in frontal view. It is divided into two parts, the outer dlp (odlp) and the inner dlp (idlp). The idlp is a thin cup shaped layer separating the odlp from the underlying spp. Laterally the odlp reaches down between the lateral horn (LH) and the optical tubercle as far as to the ventro-lateral protocerebrum.

### **Dorso-frontal protocerebrum – dfp**

The dfp is a massive neuropil structure reaching from anterior of the protocerebral bridge frontally surrounding the horizontal lobe of the mushroom body and down to the base of the antennal lobe. This area definitely has to be subdivided into smaller, functional compartments in the future. However, using nc82 staining further reliable delimitations were not discernible in this area.

### **Ventro-lateral protocerebrum – vlp**

The vlp is located directly proximal to the optic lobes. In this area further processing of visual information might take place as reported by Otsuna et al. [95]. Housing the og we expect the vlp to resolve in smaller functional units in the future as well.

### **Dorso-medial protocerebrum – dmp**

Ventrally adjacent to the mushroom body peduncle the dmp reaches from the anterior base of the mushroom body calyces to the ventral part of the posterior margin of the dfp at the level of the antennal lobes. This slim structure builds the dorsal part of the medial protocerebrum, ventrally encasing the central complex.

### **Ventro-medial protocerebrum – vmp**

Anteriorly squeezed between the dmp and the dorsal tip of the SOG (subesophageal ganglion) the vmp reaches through the ventral protocerebrum to its caudal margin. Thereby the posterior end is much wider than the anterior one. Medially it is confined by the oesophagus and laterally it abuts on the vlp.

### **Proximal antennal nerve - pan and caudo-medial protocerebrum - cmp**

The ventral most part of the protocerebrum hosts the mechanosensory region of the antenna and therefore may be a functional unit. However, due to differences in the texture of the nc82 staining we divided this area into two

distinct Materials. Further analysis using Gal4 expression patterns should be performed to verify the structure of these areas.

**Caudo-central protocerebrum – ccp**

Posterior to the fan shaped body and anterior to the protocerebral bridge a small neuropil area is located. Due to its prominent position the borders of this small area are easy to define. The ccp was not described before. Thus we selected this name because of its position in the brain.

## **7 Material and Methods**

### **7.1 Flies**

All flies were raised on corn-meal food [96] in a 14-10 hours light-dark cycle at 25°C and 60% relative humidity.

Females from the homozygous enhancer trap line OK107-GAL4 or 201Y-GAL4 were mated to males homozygous for the UAS-reporter. In most cases this is UAS:mcd8GFP, in all other cases this is mentioned separately

For preparation we used 3-4 days old flies.

**Table 9: List of UAS responders used in the reporter test scans.**

Name	Bloomington Stock Number	ASCI Genotype	Chromosome	Insertion Site	Date	Donor	Citation
P{UAS-mCD8::GFP.L}LL5	5137	y[1] w[*]; P{w[+mC]=UAS-mCD8::GFP.L}LL5	2		03/19/1999	Liqun Luo	[97]
P{UAS-mCD8::GFP.L}LL6	5130	y[1] w[*]; Pin[Yt]/CyO; P{w[+mC]=UAS-mCD8::GFP.L}LL6	3		03/19/1999	Liqun Luo	[97]
P{UAS-lacZ.NZ}20b	3955	w[1118]; P{w[+mC]=UAS-lacZ.NZ}20b	2		08/28/1997	Yash Hiromi	[98]
P{UAS-lacZ.NZ}J312	3956	w[1118]; P{w[+mC]=UAS-lacZ.NZ}J312	3		08/28/1997	Yash Hiromi	[98]
P{UAS-EGFP}8	5428	P{w[+mC]=UAS-EGFP}8, w[1118]	1		10/14/1999	Eric Spana	[99]
P{UAS-EGFP}5a.2	5431	w[1118]; P{w[+mC]=UAS-EGFP}5a.2	2	029C	10/14/1999	Eric Spana	[99]
P{UAS-EGFP}34	5430	w[1118]; P{w[+mC]=UAS-EGFP}34/TM3, Sb[1]	3	086E13-18	10/14/1999	Eric Spana	[99]
P{UAS-lacZ.B}Bg4-1-2	1776	w[1118]; P{w[+mC]=UAS-lacZ.B}Bg4-1-2	2	21-60	07/05/1995	Norbert Perrimon	[100]
P{UAS-tau-lacZ.B}2	5829	y[1] w[*]; P{w[+mC]=UAS-tau-lacZ.B}2	2		06/22/2000	Andrea Brand	[101]
P{UAS-n-syb.eGFP}2	6921	w[*]; P{w[+mC]=UAS-n-syb.eGFP}2	2		04/08/2003	Kendal Broadie	[102]
P{UAS-n-syb.eGFP}3	6922	w[*]; P{w[+mC]=UAS-n-syb.eGFP}3	3		04/08/2003	Kendal Broadie	[102]
UAS:lacZ KI2			2			Eike Kieber	[103]
UAS:lacZ KI3			3			Eike Kieber	[103]

**Next page: Table 10: List of Gal4 lines**

Material and Methods

Name	Bloomington Stock Number	ASCIIGenotype	Chromosome	Breakpoints or Insertion Site	Date	Donor	Citation
201y	4440	w[1118]; P{w[+mW.hs]=GawB}Tab2[201Y]	2	56D	6/22/2000	L. Cherbas	[104]
mb247-36y			2	46C	1996	R. A. Schulz	[105]
ok107	854	w[*]; P{w[+mW.hs]=GawB}OK107	4		7/25/2000	L. Cherbas	[104]
H24						T. Raabe	[106]
59y			1	11E		D. Armstrong	[107]
189y						D. Armstrong	[108]
104y			2	26D		D. Armstrong	[109]
154y			3	61C		D. Armstrong	[110]
210y			3	70B		D. Armstrong	[107]
C271						D. Armstrong	[111]
121y			3	71B		D. Armstrong	[112]
C005						D. Armstrong	[113]
c205						D. Armstrong	[114]
007y			2	25		D. Armstrong	[113]
78y			3	84D		D. Armstrong	[113]
GH146			2	51B-C		G. Heimbeck	[115]
NP225				8E10	28/07/03	GETDB	[116]
1.3TβH						S. Hampel	unpub.
4.6TβH						S. Hampel	unpub.
NP7088				49D6	28/07/03	GETDB	[117]
tdc	9313	w[*]; P{w[+mC]=Tdc2-GAL4.C}2	2		12/07/2005	J. Hirsh	[118]
NP938				7D2	28/07/03	GETDB	[116]
NP208				7D2	28/07/03	GETDB	[116]
THCam							[119]
TH3							[119]

## 7.2 Immunocytochemistry

Flies were raised under standard conditions and killed with ether. Brains were dissected under cooled phosphate buffered saline (PBS) and fixed in precooled 2% paraformaldehyde (PFA) overnight at 4°C. To permeabilize the tissue all washing or incubation was conducted in PAT (PBS plus 1g/100ml bovine albumin (Sigma, A6793), 0,5% Triton X 100(Sigma, X-100). After removal of the PFA (3x20 mins PAT) specimens were blocked with 3% normal goat serum/PAT for 1h at room temperature. Excess blocking solution was removed and specimens were incubated with 1:1000 dilution of highly cross absorbed anti-green fluorescent protein antibody (A-6455, MoBiTec, Goettingen, Germany) in PAT overnight at 4°C. Specimens were thoroughly washed in PAT and then incubated with 1:10 dilution of nc82 [7] monoclonal antibody overnight at 4°C.

Secondary antibodies were goat anti-mouse F(ab')<sub>2</sub> coupled to indocarbocyanine fluorophore Cy3 (Jackson Immuno Research, West Grove, PA) diluted 1:250 and highly cross-adsorbed Alexa Fluor® 488 goat anti-rabbit IgG (H+L) (A-11034, MoBiTec, Goettingen, Germany) diluted 1:100 in PAT. Incubation was overnight at 4°C. To reduce background staining the specimens were washed in PAT for the next three days with gentle agitation at 4°C. The specimens were mounted in Vectashield diluted 3:1 with PBS.

### 7.2.1 nc82/anti-GFP standard double staining protocol

1<sup>st</sup> day:

Dissect in Ringer solution.

Fix in 2% FA overnight at 4°C, use precooled well and FA.

2<sup>nd</sup> day:

Wash in PAT three times 20 mins at room temperature.

Block with 3% NGS in PAT at RT.

Incubate in 1<sup>st</sup> primary antibody: α-GFP (1:1000) in PAT overnight at 4°C.

3<sup>rd</sup> day:

Wash in PAT three times 20 mins at room temperature.

Incubate in 2<sup>nd</sup> primary antibody: nc82 (1:10) in PAT overnight at 4°C.

4<sup>th</sup> day:

Wash in PAT three times 20 mins at room temperature.

Incubate in 1<sup>st</sup> and 2<sup>nd</sup> secondary antibodies: Cy3 (1:250) / Alexa488 (1:100) in PAT

overnight at 4°C.

5<sup>th</sup> to 8<sup>th</sup> day:

Wash in PAT as long as possible ( 2.5 days minimum)

Mount in Ringer diluted Vectashield (1:3)

### **7.2.2 Antibodies:**

- 1<sup>st</sup> primary antibody : Anti-GFP, polyclonal rabbit, Molecular Probes (A-6455)
- 1<sup>st</sup> secondary antibody: Alexa488, goat-anti-rabbit, Molecular Probes (A-11034)
- 2<sup>nd</sup> primary antibody: nc82, mouse, from Dr. Alois Hofbauer
- 2<sup>nd</sup> secondary antibody: Cy3 goat-anti-mouse, JacksonImmunoResearch (115-166-003)
- Normal goat serum (NGS), Sigma (G-9023) or JacksonImmunoResearch (005-000-121)

### **7.2.3 Chemicals:**

Paraform-aldehyde (Sigma, P1213)

Phosphate buffered saline (PBS)

- 130mM NaCl
- 4,7mM KCl
- 0,74mM KH<sub>2</sub>PO<sub>4</sub>
- 0,35mM Na<sub>2</sub>HPO<sub>4</sub>
- 1,8mM MgCl

at pH 7,4

bovine albumin (Sigma, A6793)

Triton X 100(Sigma, X-100)

#### **7.2.3.1 Mounting:**

PBS diluted Vectashield, 1:3

### **7.3 Confocal microscopy**

Whole-mount brains were scanned with a Leica TCS-SP1 confocal microscope, equipped with a Kr/Ar laser and a Leica PI Apo 20X NA 0.7 IMM lens. Frontal series of entire brains were taken each  $\mu\text{m}$  in z-direction with 1024 X 1024 pixel resolution using an average zoom of 0,8 to make the specimen fit to the optic field. The resulting optical resolution is 0,6 X 0,6 X 1  $\mu\text{m}$ .

Excitation and emission filters were adjusted appropriately to the labels of the secondary antibodies and endogenous GFP.

For the excitation of the combined signal of Alexa488 and endogenous GFP a Laser at 488nm was used, recording fluorescence signal in the range from 493 to 559nm. Cy3-based fluorescence was excited with 458nm and detected in the range from 607 to 701 nm.

Three-dimensional reconstruction and standardization was performed with Amira (Indeed/Mercury) using the Virtual Insect Brain protocol ([www.neurofly.de](http://www.neurofly.de)).

## **8 Applications of the VIB protocol**

### **8.1 Reporter-test-scans**

Directed expression of transgenes by the P[Gal4] technique [35] has become a versatile tool in studies on learning and memory as well as neuroanatomy in recent years.

Originally we had planned to standardize different aspects of neuroanatomy in the *Drosophila* brain. Besides the obviously interesting approach of standardizing the neuroanatomy of the whole outline of the Gal4-positive cell population we tried to standardize sub-compartments. This was supposed to lead to a better understanding of the anatomy and wiring of distinct neuron populations on each other. We were looking for reporters with reliable expression of an immunohistochemically detectable marker. Therefore we screened 10 UAS:reporters which divide into three groups.

- -Nuclear markers;
- -markers for synaptic regions (e.g. EGFP tagged Synaptobrevin);
- -markers for the entire cell,(transgenes directed to the cytosol or the membrane).

Controls of the Gal4-lines (without UAS:reporter) and UAS-reporters (without Gal4-driver) were performed on the homozygous (parental) stocks. In some UAS:reporter lines expression of the reporter without a Gal4-driver (leaky expression) could be detected. If the leaky expression was strictly confined to a certain region these lines could be used to provide landmarks in studies which were focused on other regions. However, in most cases the leaky expression showed patterns widely spread over the whole brain spoiling the analysis of Gal4-driven expression. One such UAS:reporter with obviously leaky expression (EGFP3) will later be described in detail.

For the reporter test scans we used three Gal4-lines which were reported to have a Gal4 expression pattern specific for the mushroom bodies. These are the lines Gal4-201y, Gal4-ok107 and Gal4-mb247. Due to the confined expression patterns these Gal4-lines were used in several behavioral experiments for the investigation of the role of the mushroom bodies in learning and memory formation.

#### **8.1.1 Gal4-201y**

The Gal4-line 201y comes from the collection of Kim Kaiser [120], [121]. In the adult brain this line expresses Gal4 in Kenyon cells of the mushroom bodies, in the pars intercerebralis and in the thoracic ganglion. The line exhibits an extensive staining in the  $\gamma$ -lobe, whereas only faint staining is observed in the a

and  $\beta$ -lobes. In the peduncle, most of the staining is restricted to an outer ring ( $\gamma$ -fibers). A small dot in the center may correspond to the immunopositive core fibers of the  $\alpha$ - and  $\beta$ -lobes ( $\alpha/\beta$ -fibers). The following is a short summary of studies using this Gal4 expression pattern.

### **Studies on learning and memory.**

Conolly et al. 1996 [104] was able to disrupt aversive associative olfactory learning by expressing constitutively activated stimulatory heterotrimeric guanosine triphosphate binding protein  $\alpha$  subunit ( $G\alpha_S^*$ ) in the mushroom bodies using Gal4-201y and Gal4-ok107. Although the associative olfactory learning in experimental flies was significantly reduced the effect in Gal4-201y was the weakest under the tested Gal4-lines.

Martin et al. 1998 [122] questioned the influence of the mushroom bodies on locomotor activity driving tetanus toxin light chain (Cnt-E, [123]) with Gal4-201y (and other Gal4-lines). Only P[GAL4]201Y/Cnt-E flies show a significant increase in activity compared to their respective controls. Therefore Martin et al. conclude the mushroom bodies as a center of locomotor inhibition.

Zars et al. 2000 [112], [124] was able to partially rescue the rutabaga memory defect by driving wild-type cDNA in the mushroom bodies using Gal4-201y. In other Gal4-lines with a stronger expression in the  $\alpha$ - and  $\beta$ -lobe they achieved even better results. Therefore the rutabaga memory defect could be located to the mushroom bodies. Mutant rut flies with the GAL4 element mb247 in combination with the P[UASGAL4-rut1] transgene showed memory scores statistically indistinguishable from wild-type flies. Due to the high specificity of the expression pattern to the mushroom bodies in Gal4-mb247 the rutabaga dependent behavioral phenotype localized to the mushroom bodies.

Manoli et al. 2005 [125] investigated the role of the male-specific isoform of the transcription factor fruitless (FruM) on courtship condition. For the analysis of the influence of the mushroom bodies FruM was inhibited by the expression of UAS-fruMIR driven by Gal4-201y and Gal4-ok107. This led to a reduced courtship conditioning to mated females (i.e., males do not learn not to court recently mated females, which display high levels of rejection).

Joiner et al. 2006 [126] investigated the regulation of sleep in *Drosophila*. Driving UAS-PKA under the control of Gal4-201y result in a significantly increase of sleep while waking behavior is not altered.

### **Developmental studies.**

Tettamanti et al. 1997 [111] focused their work on the investigation of the development of the mushroom bodies. Therefore the expression of  $\beta$ -galactosidase or GFP was driven by Gal4-201y (and other Gal4-lines). Expression of the UAS:reporters was found to have an abrupt onset which coincides with the hatching and also can be observed in the adult animal. Anatomical analysis of the expression patterns shows that in the mushroom body four cell body clusters give rise to four distinct fascicles of neurites/axons.

Kurusu et al. 2000 [127] assayed the influence of the genes *eyeless*, *twin of eyeless*, and *dachshund* on the development of the mushroom bodies and used Gal4-201y as a marker for the mushroom bodies. Thereby they found no expression of Gal4-201y-driven expression in newborn Kenyon cells in third instar larvae. Therefore the proliferation of  $\gamma$ -neurons seems to be completed before third instar.

Zhu et al. 2003 [128], 2005 [129] carried out a study on the development of the mushroom bodies using the MARCM technique [130] on the basis of Gal4-201y, Gal4-ok107 and other Gal4 lines. Due to the observations on the Gal4-201y expression pattern which is located predominantly in the  $\gamma$ -lobes they concluded that the Kenyon cell population building up the  $\gamma$ -lobe do not contribute in the formation of the fourfold regions of the calyces described by Tettamanti et al. [111].

Watts et al. 2003 [131] studied the influence of the Ubiquitin-Proteasome System on the proliferation and axon pruning of Kenyon cells by driving the expression of yeast ubiquitin protease (UBP2) in the  $\gamma$ -lobes using Gal4-201y as a driver. Defects in axon pruning were apparent while no effect on cell proliferation was detectable.

Ramaekers et al. 2005 [132] studied the neuroanatomy of the expression pattern in the olfactory pathway of middle to late third instar stage. Therefore this approach was focused on the Gal4 expression in the mushroom body precursor cells. Using the MARCM technique on the basis of Gal4-201y, Gal4-ok107 and Gal4-mb247 the connectivity of the mushroom bodies was dissected. At the chosen developmental stage these are the  $\gamma$ -neurons because the neurons which building up the  $\alpha$ - and  $\beta$ -lobes are born later. This study showed that in contrast to the adult brain there is no converging and diverging connectivity in the larval olfactory pathway.

### **Other studies using 201y as a reference.**

Michel et al. 2004 [133] investigated *Drosophila* Fragile X Mental Retardation1 Mutants using a Gal4-201y UAS-GFP recombinant for the visualization of the mushroom bodies. Thereby they found that  $\beta$ -lobe fibers of *dfmr1* extend across the midline, sometimes sufficient to cause apparent fusion of the right and left  $\beta$ -lobes while  $\gamma$ -lobe fibers do not extend across the brain midline.

Gu et al. 2006 [134] succeeded in obtaining in situ whole-cell recordings from adult Kenyon cells. For visualization of the Kenyon cells GFP expression was driven in the neurons by Gal4 *ok107* or 201y. Comparisons of the signal of labeled (GFP+) and unlabeled (GFP-) cells were enabled by GFP expression driven by Gal4-201y due to its incomplete expression pattern. No significant differences were found between the signal of GFP+ and GFP- Kenyon cells.

#### **8.1.2 Gal4-ok107**

The Gal4 line *ok107* was discovered by a screen of the O’Kane Lab and first mentioned by Conolly et al in 1996 [104]. An ample description of this line according to its insertion locus can be found at Adachi et al [135]:

“A GAL4 enhancer trap, OK107, was initially isolated as an enhancer trap line that shows strong MB expression in the adult brain. Its P-element is inserted on chromosome 4, where *ey* is located. By PCR and sequencing, the exact location of the OK107 insertion was found to be 6.5 kb upstream of the first exon of *ey*. OK107 is confirmed to be expressed in the embryonic MB primordia as well as the larval MBs. Double immunostaining verified colocalization of OK107 expression and *Ey* in the brain, in that all GAL4-expressing neurons in OK107 indeed express *Ey*, although many *Ey*-expressing cells in other regions of the CNS do not express OK107 GAL4. In MBs, OK107 faithfully recapitulates the *Ey* expression throughout brain development. The coexpression of OK107 and *EY* in MBs was further confirmed in a complementary experiment, in which OK107 was used to drive a dominant-negative form of *Ey*. The phenotypes observed in this experiment reproduce the range of MB phenotypes observed in *ey* mutants (Adachi, 2003 and references therein). ”

Due to its expression pattern which is reported to be confined to the mushroom bodies [97] this line was introduced into the many behavioral and morphological experiments dealing with the structure and function of this brain structure.

McGuire et al. 2001 [136] describe that the expression of *shibire* (*shits*) driven by Gal4-ok107 leads to a loss of odor avoidance under restrictive conditions.

Gu et al. 2004 [137] report minimal rescue of the phenotype of a mosaic *ninaD* mutant by the expression of UAS-*ninaD* driven by Gal4-ok107. Due to these results they conclude that *ninaD*, which is postulated to encode the scavenger receptor responsible for  $\beta$ -carotene cellular uptake by Kiefer et al. and therefore is expected to act in the retina only, is active in the mushroom bodies as well.

Agrawal et al. 2005 [138] describe the loss of the  $\alpha'$  and  $\beta'$  lobes and a strong reduction of the number of fibers in the  $\gamma$  lobes due to the expression of UAS-Httex1p Q93 (polyglutamine (polyQ) responsible for the neurodegenerative effects of Huntington's disease) under the control of Gal4-ok107. They also describe a reduction of the number of cells in the median bundle from  $\sim 20$  to  $\sim 8$ , which is the first mention that Gal4-ok107 expresses in this cell population as well. Further on they mention changes in the number and morphology of neurons in the ventral ganglia.

Sakai et al. 2006 [139] compared the influence of the central complex and the mushroom bodies on courtship behavior by driving the expression of UAS-*shi*<sup>ts1</sup> with ok107 (and other Gal4-lines). Due to significantly lengthened initiation phase and reduced courtship activity at high temperature in these animals as well as in other Gal4-lines expressing UAS-*shi*<sup>ts1</sup> in the mushroom bodies (30y, c772) they concluded that this neuropil structure is responsible for courtship initiation and maintenance.

Li et al. 2004 [140] studied the dynamics of the Alzheimer's disease using *Drosophila* as a model organism. Therefore expression of *Drosophila* amyloid precursor-like proteins (APPL) was driven together with EGFP in the mushroom bodies using Gal4-ok107 or Gal4-mb247 as drivers. An influence of APPL on the gross organization of the mushroom bodies could not be found by over-expression of two APPL-variants.

### **8.1.3 Gal4-mb247**

The expression pattern of Gal4-mb247 is highly specific for the Kenjon cells. Cell counts revealed about 700 Gal4-positives cells in this line [141]. This is about 28% of the Kenjon cell population equally distributed in all lobes of the mushroom bodies. In spite the relatively small number of cells changes in the behavior and the ability to learn certain tasks could be elicited by expression of transgenes in these cells. Thanks to the specificity of this Gal4-line to the mushroom bodies these results can be put down this neuropil structure:

Isabel et al. 2004 [142] investigated formation of the different memory phases in the mushroom bodies driving UAS-shi<sup>ts</sup> by Gal4-mb247 and other Gal4-lines. Using the ala-mutant which is lacking the vertical lobes they were able to pin down the formation of ARM and LTM to these structures. In contrast to earlier work they found ARM and LTM to be mutually exclusive. Therefore they conclude that ARM and LTM may involve the same group of neurons.

Baier et al. 2002 [143] used the line Gal4-mb247 for the regulation of synaptic output of the mushroom bodies while investigating aggressive behavior. Inhibiting synaptic output by the expression of the catalytic subunit of bacterial tetanus toxin (UAS-Cnt-E) led to a strongly reduced aggression.

Schwärzel et al 2002 [103] used Gal4-mb247 to block Mushroom body output during olfactory learning and/or memory retrieval. Thereby they were able to show, that the olfactory memory can be formed and stored for up to 3 hr in this subset of Kenyon cells. This memory can be acquired in the absence of Kenyon cell synaptic output and can still be abolished by blocking the Kenyon cell output 3 hr later. This implies that the molecular mechanisms underlying 3 hr olfactory memory are located within Kenyon cells.

#### **8.1.4 The UAS-reporters**

Besides UAS:reporters which are expressing fluorescent markers like green fluorescent protein we used some UAS:reporters expressing  $\beta$ -galactosidase. Even though both transgenes were used as epitope for immunohistochemical staining we finally refrained from the  $\beta$ -galactosidase expressing reporters. The signals of reporters expressing fluorescent markers generally were superior to the signals basing on the expression of  $\beta$ -galactosidase. Especially in fine the arborizations of dendrites the strength of the signal is crucial. Expressing a green fluorescent protein as an epitope for the immunohistochemical staining bears the advantage of significant signal enhancement by endogenous fluorescence.

All approaches we carried out with multiple closely related UAS:reporter lines and lines visualizing the same aspect of the Gal4-positive cells.

##### **8.1.4.1 Nuclear marker expression for the standardization of cell body position**

For the standardization of cell body positions we crossed the test Gal4-lines (Gal4-201y, Gal4-ok107, Gal4-mb247) to two UAS:reporter lines expressing nuclear  $\beta$ -galactosidase (see Table 11: UAS:reporter for the visualization of

nuclei.). These lines are closely related to each other due to the insertion of the same genetic construct in two different locations of the genome.

**Table 11: UAS:reporter for the visualization of nuclei.**

Name	Comment (flybase.org)
P{UAS-lacZ.NZ}20b	Y. Hiromi and S. West, insertion second chromosome SV40 T NLS-lacZ fusion in pUAST, expresses nuclear $\beta$ -galactosidase, Y.H.
P{UAS-lacZ.NZ}J312	Y. Hiromi and S. West, insertion on third chromosome SV40 T NLS-lacZ fusion in pUAST, expresses nuclear $\beta$ -galactosidase, Y.H.

The P-elements (pUAST) contain the lacZ gene fused with the nuclear localization signal (nls) derived from the SV40 large T gene and an intron and poly(A) signal derived from SV40. [<http://www.blackwell-synergy.com/toc/dgd/36/5>]Therefore the expression of  $\beta$ -galactosidase is localized to the nucleus.

The result of the standardization of cell body position was disappointing. The nuclear localization sequence appears not to be able to force all fluorescing molecules to the nucleus but also areas which are void of nuclei like the lobes of the mushroom bodies were stained immunohistochemically.

Although the staining was not as specific to the nuclei as expected big cell clusters like the Kenyon cells can be standardized by the VIB protocol (Figure 11). These areas could be transformed like any other structure in the specimen. In some (rare) cases we observed shearing artifacts between the labeled volumes (e.g. mushroom body calyx) and the directly adjacent areas (e.g. Kenyon cell cluster) (see discussion). That means the areas of special interest should be transformed uniformly, either rigidly or non-rigidly. Because the Kenyon cell cluster closely surrounds the mushroom body calyx we waived the labeling of the mushroom bodies to avoid potential transformation artifacts between the calyces and the Kenyon cells. The transformation without the mushroom bodies as Landmark neuropil is satisfactory.

In a mayor computer system failure all data of these experiments were lost. Therefore the results of this study are represented by two other crosses (Gal4-201y x UAS:lcaZ.B, Gal4-201y x UAS:EGFP3).

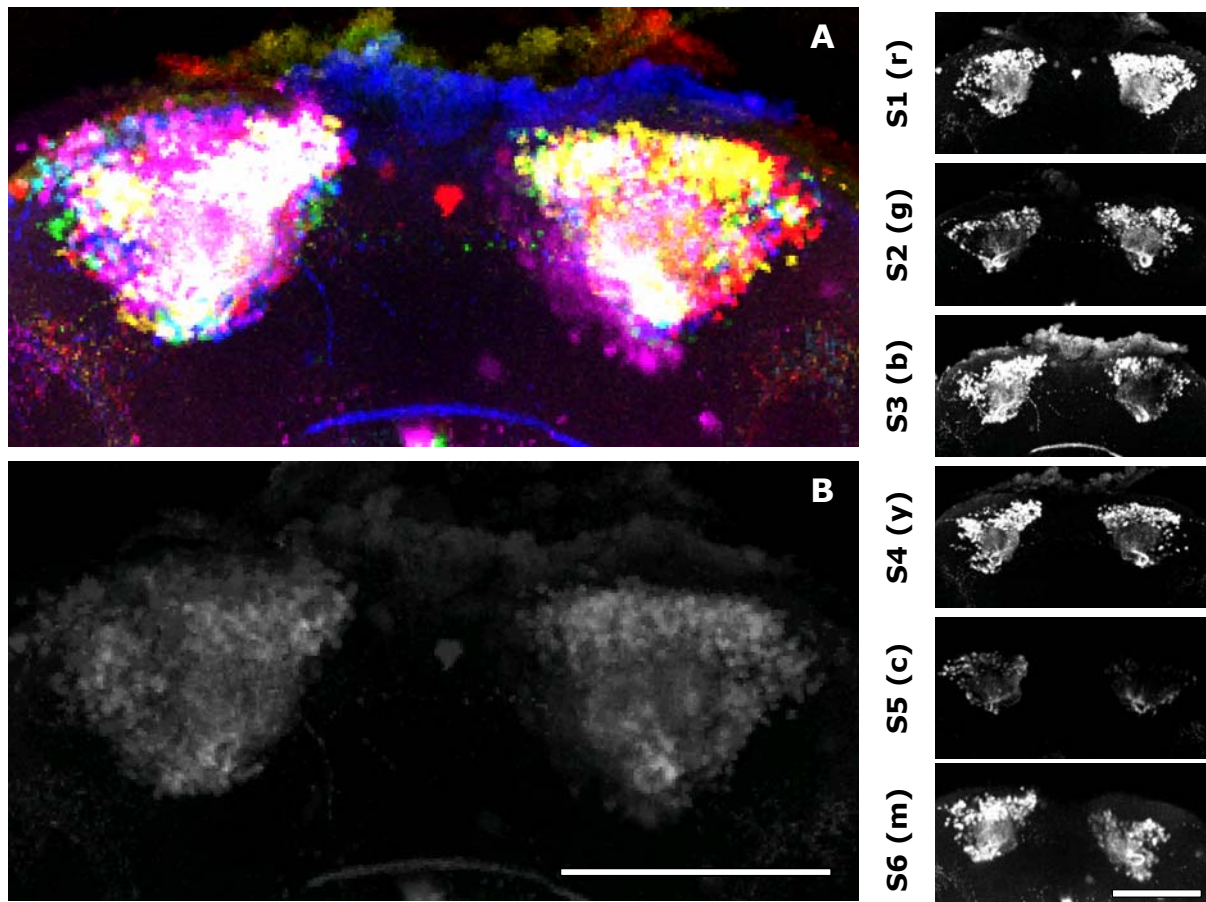


**Figure 11: Standardized Kenjon cell clusters of six animals (Gal4-201y x P{UAS-lacZ.B}Bg4-1-2). In the upper image (A) the individual clusters (right column) are false colored and superimposed. In areas of overlap the colors merge additively to white. The lower image (B) shows the average of the upper image. Individual signals which are caused by interindividual variability are suppressed while common structures are pronounced. S1-S6: Sample1 -Sample6, r: red; g: green, b:blue, y:yellow, c:cyan, m: magenta, scalebar: 100 $\mu$ m**

Due to the high variability of the position of individual cell bodies the standardization of single cell bodies can only lead to a crude area of high probability to encounter a specific cell body. A precise transformation of the same cell body in two or more specimens can not be achieved, because in the specimens specific cell bodies rarely are located at the very same position (Figure 12).

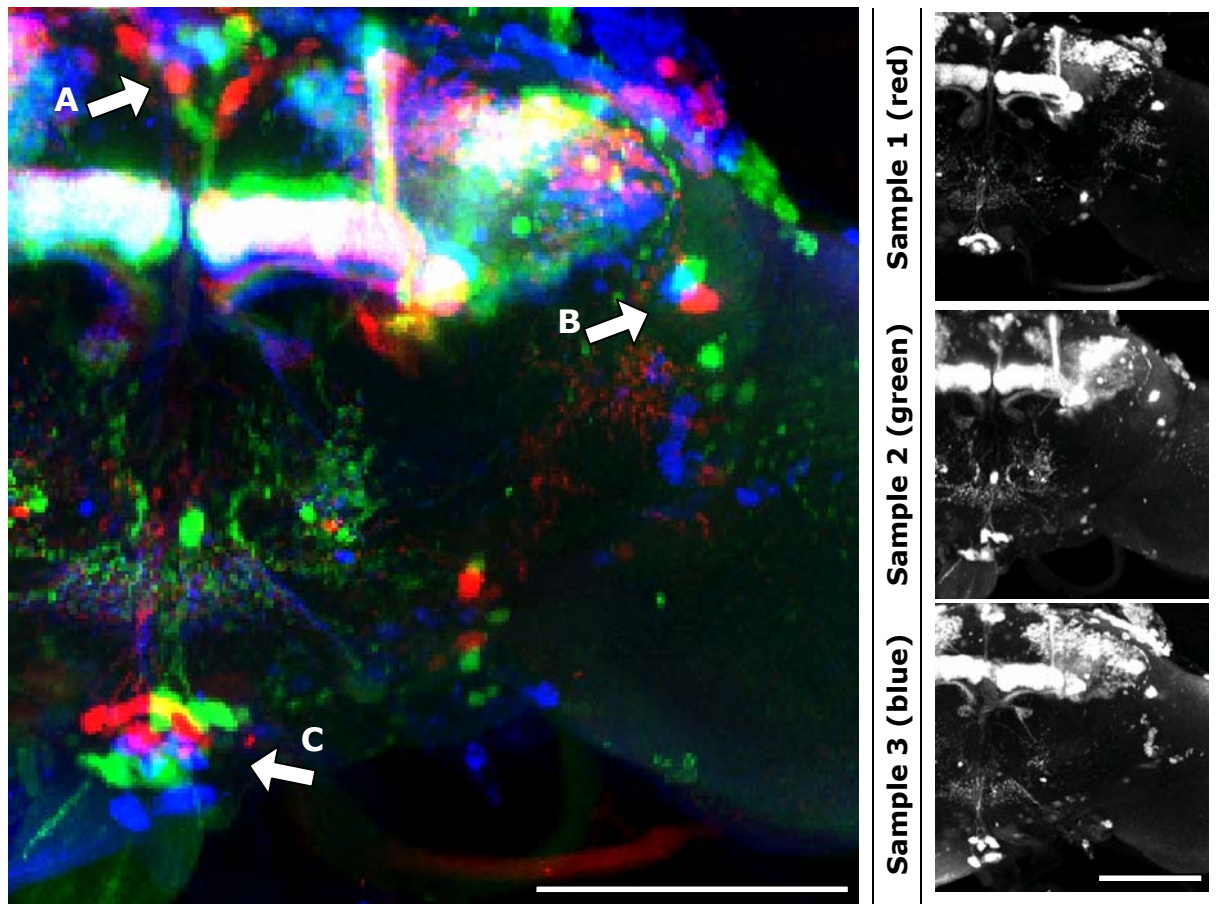


**Figure 12: Comparison of standardized cell body positions in three animals (Gal4-201y x EGFP3). Arrows are pointing to cell clusters with well defined positions. In no case alignment of the cell bodies is achieved due to high interindividual variability of call body position. A: Pars intercerebralis, B: prominent single cell latero-frontal of the lateral horn, C: Cell cluster of the ventral unpaired midline neurons (VUM). Scalebar: 100 $\mu$ m.**

Forcing the VIB protocol to transform the cell bodies on each other leads to strong distortions in the surrounding areas. Therefore we refrained from further standardization of cell body positions.

#### **8.1.4.2 Presynaptic marker expression for the standardization of synapses**

Besides the structure of the Gal4-positive cells (which is investigated further down) the connectivity and direction of signal transduction was a matter of interest during the development of the VIB protocol. Information about the input- and output-regions of the studied Gal4-positive cells could provide new insights into the wiring and function of the *Drosophila* brain.

A first approach was carried out on the presynaptic endings of the Gal4-positive cells by expressing GFP-tagged synaptobrevins. Synaptobrevins are small

integral membrane proteins of secretory vesicles with molecular weight of 18 kilo Dalton (kDa) that are part of the vesicle associated membrane protein (VAMP) family. Synaptobrevin is one of the SNARE proteins (**S**oluble **N**SF<sub>(N-ethylmaleimide sensitive factor)</sub> **A**ttachment **R**eceptor) involved in formation of the SNARE complexes. Out of four  $\alpha$ -helices of the core SNARE complex one is contributed by synaptobrevin, one by syntaxin, and two by SNAP-25. SNARE proteins are the key components of the molecular machinery that drives fusion of membranes in exocytose. Therefore the GFP-tagged version of synaptobrevin stains the output region of the Gal4-positive cells by staining presynaptic vesicles.

For the standardization of the output regions of the Gal4-positive cells we crossed the test Gal4-lines with two closely related UAS:n-syb-EGFP lines (see Table 12)

**Table 12: UAS:reporters for the visualization of presynapses.**

Name	Comment (flybase.org)
P{UAS-n-syb.eGFP}2	May be used to label synaptic vesicles, K.B., homozygous
P{UAS-n-syb.eGFP}3/TM3	May be used to label synaptic vesicles, K.B., balanced over TM3

EGFP is a green fluorescent with enhanced light emission due to two mutations which affect the folding of the molecule. The construct coding for the EGFP-tagged synaptobrevin was inserted into the second (P{UAS-n-syb.eGFP}2) and third chromosome (P{UAS-n-syb.eGFP}3). The insertion on the third chromosome is balanced over TM3. As the heterozygous progeny which is not carrying the balancer but the reporter construct was used both crossings were comparable in respect of the numbers of copies of the construct. Therefore this study describes the effect of the insertion site of the construct on the expression pattern.

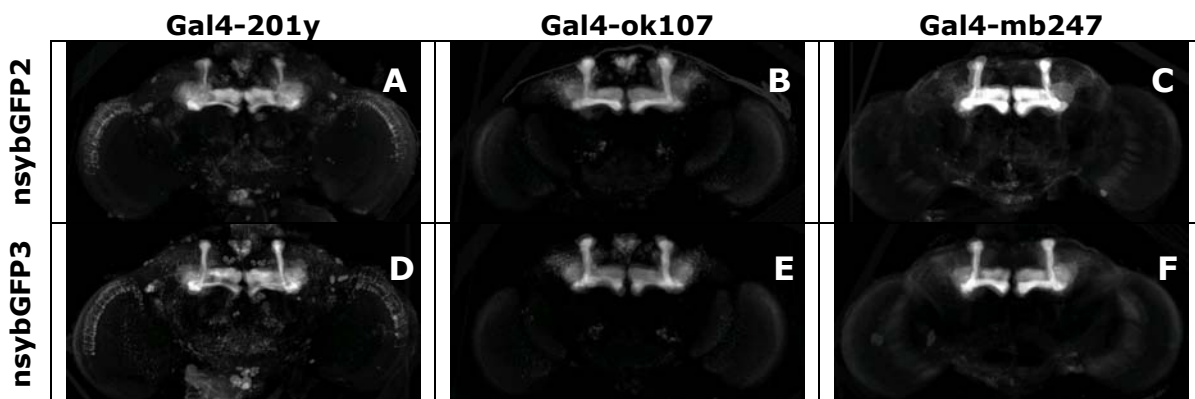


**Figure 13: Standardized expression patterns of the test Gal4-lines crossed to P{UAS-n-syb.eGFP}2 or P{UAS-n-syb.eGFP}3/TM3. N<sub>A</sub>:6, N<sub>B</sub>:7, N<sub>C</sub>:6, N<sub>D</sub>:6, N<sub>E</sub>:7, N<sub>F</sub>:9**

Similar to the nucleus specific reporters the reporters we used in this study were less specific than expected. Besides the presynaptic areas which were intensively stained, fluorescent signal was found all over the cell. This may be due to the synthesis of the fluorescent protein at the cell body and its transport to the presynapses. Thereby the whole volume of the cell gets stained. In the crosses with the test Gal4-lines which have strong Gal4-expression in the Kenyon cells we found strong EGFP expression in the whole mushroom body. Even in the calyces where no presynaptic terminals have ever been reported in Kenyon cells, intense staining is found. Therefore, this approach did not prove very useful for the specific staining of presynaptic areas.

The influence of the insertion site of the construct on the expression pattern was rather weak. The expression of the UAS:reporter with the insertion on the second chromosome was slightly stronger than the expression of the insertion on the third chromosome. Especially driving the reporters with Gal4-ok107 or Gal4-mb247 revealed these quantitative differences (Figure 13 B/E and C/F). Qualitative differences in the expression patterns were not detectable.

**8.1.4.3 Cytoplasmatic and membrane bound marker expression for the standardization of arborization patterns**

The overall morphology of the investigated cell populations is the basis of the creation of an atlas of standardized brain anatomy. Therefore we first focused on the search for a strong and reliable UAS:reporter expressing ubiquitously in the cytoplasm or in the membrane of the driving cells. These expression characteristics lead to a labeling of the complete cell. Thereby the reporters with cytoplasmatic expression are expected to label predominantly big volumes like somata or big axons because in these lots of fluorescent molecules can accumulate and generate a strong signal. In the fine arborizations of the dendrites the cytoplasmatic reporters are assumed to give rather weak signals due to the small volumes. In contrast, the reporters with membrane bound expression are thought to label the areas of fine arborizations much stronger due to the high proportion of membranes in these areas. Big volumes may be labeled weakly, due to the relatively small surface – in comparison to the volume. Therefore cytoplasmatic and membrane bound markers should complement each other perfectly.

**Table 13: UAS:reporters for the visualization of entire cells.**

Name	Comment (flybase.org)
P{UAS-mCD8::GFP.L}LL5	MARCM set, GFP labels the cell surface (mouse CD8 is a transmembrane protein), highly concentrated in neuronal processes, L.L. Viable P insertion, but stock is segregating CyO, K.C. 1/00
P{UAS-mCD8::GFP.L}LL6	MARCM set, GFP labels the cell surface (mouse CD8 is a transmembrane protein), highly concentrated in neuronal processes, L.L.
P{UAS-EGFP}8	cytoplasmatic expression of enhanced green fluorescent protein
P{UAS-EGFP}5a.2	cytoplasmatic expression of enhanced green fluorescent protein
P{UAS-EGFP}34	cytoplasmatic expression of enhanced green fluorescent protein
P{UAS-tau-lacZ.B}2	microtubule-bound bet-galactosidase
P{UAS-lacZ.B}Bg4-1-2	cytoplasmatic $\beta$ -galactosidase, N.P.
P{UAS:lacZ}KI2	cytoplasmatic expression of $\beta$ -galactosidase
P{UAS:lacZ}KI3	cytoplasmatic expression of $\beta$ -galactosidase

mCD8-GFP is a protein fusion between the murine lymphocyte receptor CD8 and EGFP. It accumulates at the plasma membrane of most cells. Expressing mcd8GFP in neurons results in the visualization of the whole cell.

The construct EGFP is a version of GFP from Clontech that has two brightness/folding enhancing mutations and has been optimized for human codon usage. [99] The construct was inserted into the first, second or third chromosome (EGFP1, EGFP2, EGFP3).

Three variations of cytoplasmatic expression of  $\beta$ -galactosidase were included in this approach. All of them carry the gene for  $\beta$ -galactosidase of *E. coli* abbreviated as *Ecol/lacZ*. P{UAS-lacZ.B}Bg4-1-2 was constructed by Norbert Perrimon and carries the Insertion of the P-element on the second chromosome. The other two were constructed in our lab by Eike Kibler and carry insertions of the *Ecol/lacZ* on the second or third chromosome (KI2, KI3).

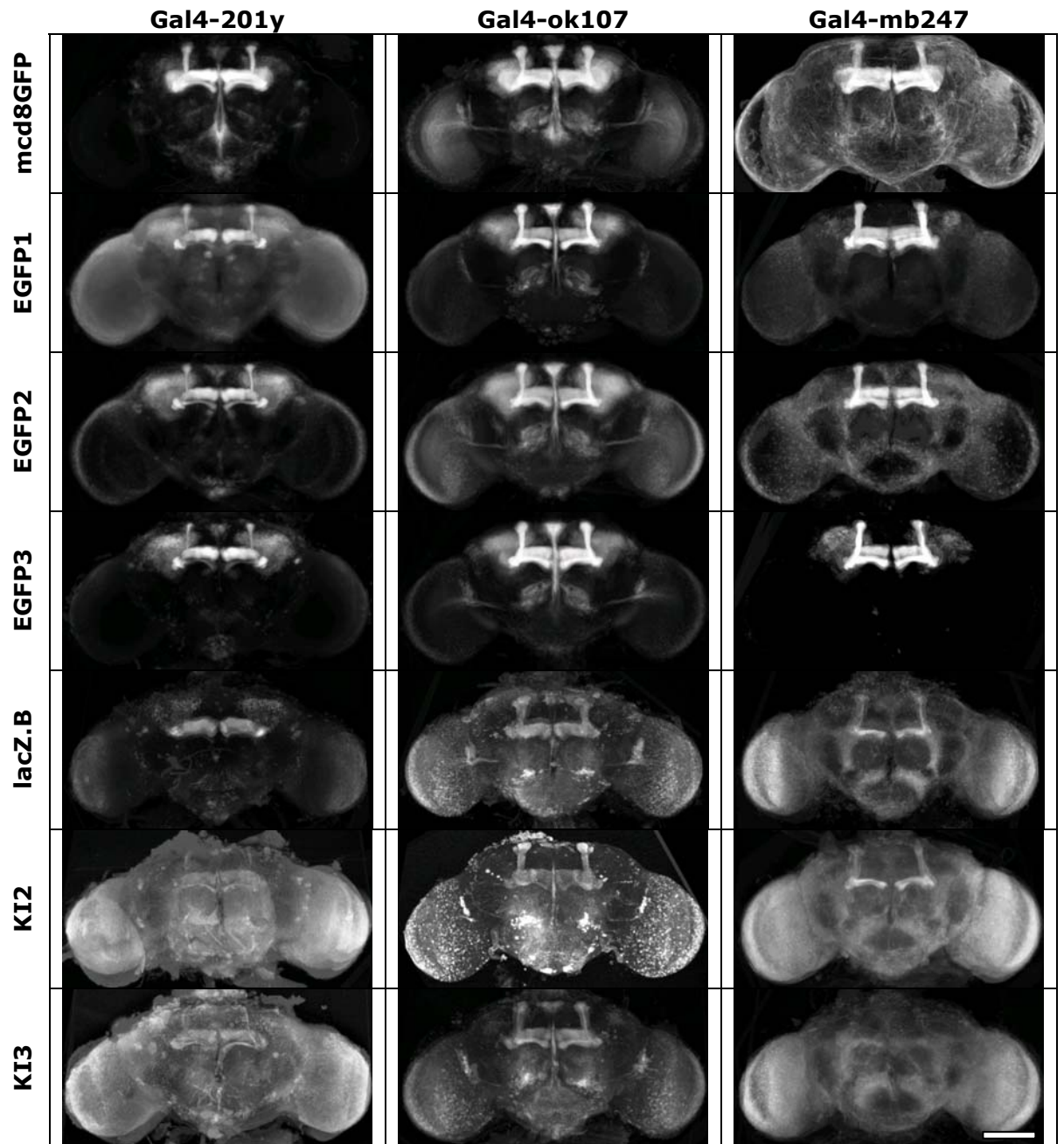


**Figure 14:** Visualizaion of the expression pattern of Gal4-201y, Gal4\_ok107 and Gal4-mb247 by cytoplomatic UAS:reporters. Numbers of standardized specimens are listed in Table 14. Scalebar: 100µm.

**Table 14:** Numbers of standardized brains in Figure 14.

N	Gal4-201y	Gal4-ok107	Gal4-mb247
mcd8GFP	16	17	15
EGFP1	12	14	8
EGFP2	18	16	8
EGFP3	11	10	5
lacZ.B	8	6	8
KI2	4	4	7
KI3	4	6	9

### **Membrane bound expression of fluorochrome (mcd8GFP)**

As expected was the visualization of the Gal4-expression pattern most precise and most detailed in crosses with UAS:mcd8GFP. Due to the strong aggregation of labeled membranes in the neuropil these structures are intensively stained. The combination of endogenous and immunohistochemical fluorochrome makes an eminently strong signal. Even the very small cell bodies of the Kenjon cells are only stained weakly (Figure 16A).

### **Cytoplasmatic expression of fluorochrome (EGFP)**

Cytoplasmatic expression of enhanced green fluorescent protein (EGFP) leads to a weak but evenly distributed signal. Even immunohistochemical counter staining does not enhance the signal to strength of mcd8GFP (Figure 16B). This may be due to a loss of EGFP -molecules during the immunohistochemical procedure. The immunohistochemical protocol involves many indispensable steps of washing and permeabilization of the tissue. Floating in the cytoplasm without stable connection to any cell components EGFP may get washed out of the specimen during the immunohistochemical protocol. Therefore its own fluorescence is weakened and the number of epitopes for the immunohistochemical protocol is diminished. Without immunohistochemical counter staining of the EGFP this tends to bleach quickly under the confocal microscope during scanning.

UAS:EGFP1 and UAS:EGFP2 showed considerable expression without Gal4-driver (leaky expression). UAS:EGFP1 shows a faint but repeatable signal in the mushroom bodies, the ellipsoid body and - even weaker - in the fan shaped body. Due to strong signal amplification during data acquisition at the confocal microscope in expression patterns of Gal4-lines with low expression levels these signals may become apparent. Therefore in contrast to the crosses with UAS:EGFP2 and UAS:EGFP3 the expression pattern of Gal4-201y appears to include the ellipsoid body if crossed to UAS:EGFP1 (Figure 14). Analyzing the control data (homozygous UAS:reporters without Gal4-driver) shows that in the reporter line UAS:EGFP1 the expression of EGFP in the ellipsoid body is autonomous and not dependent on a Gal4-driver (Figure 15).

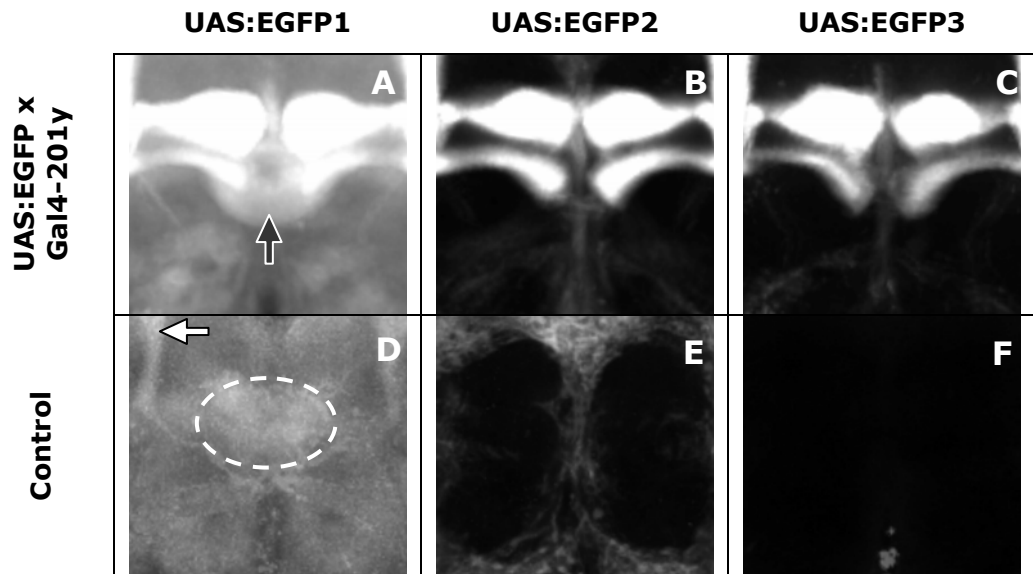


**Figure 15: EGFP expression in the central complex. All images strongly over amplified. Upper row: Gal4 expression pattern of Gal4-201y visualized by UAS:EGFP1 (A), UAS:EGFP2 (B) or UAS:EGFP3 (C). Lower row: Autonomous expression of EGFP. The expression of EGFP in the ellipsoid body in A can be found as well without Gal4-driver (dashed circle in B). UAS:EGFP2 (E) shows weak autonomous expression of EGFP in the cell body layer. Due to the reticular structure of this pattern this could be glial cells.**

In Gal4-lines with stronger expression patterns like Gal4-ok107 and Gal4-mb247 the fluorescence in the ellipsoid body is not visible due to the much lower amplification at which these specimens are scanned under the confocal microscope. This effect is called the 'full-moon-effect' and will be discussed later.

### **Cytoplasmatic expression of $\beta$ -galactosidase (lacZ)**

The effect of bleaching the epitope also applies to the cytoplasmatic expression of  $\beta$ -galactosidase. In the latter case this effect may be even more dramatic because the molecule of  $\beta$ -galactosidase is much smaller than the molecule of EGFP. Therefore it can be washed out of the tissue much more easily. Another disadvantage of the expression of  $\beta$ -galactosidase for the usage as an immunohistochemical epitope is the fact that  $\beta$ -galactosidase has no fluorescence itself. The fluorescent signal is based only on the fluorochrome of the immunohistochemical staining (Figure 16C). Therefore the expression of cytoplasmatic  $\beta$ -galactosidase ends up in a vicious cycle: the immunohistochemical protocol is absolutely indispensable for the visualization of the expression pattern but its washing steps is removing the cytoplasmatic epitope before it can be detected.

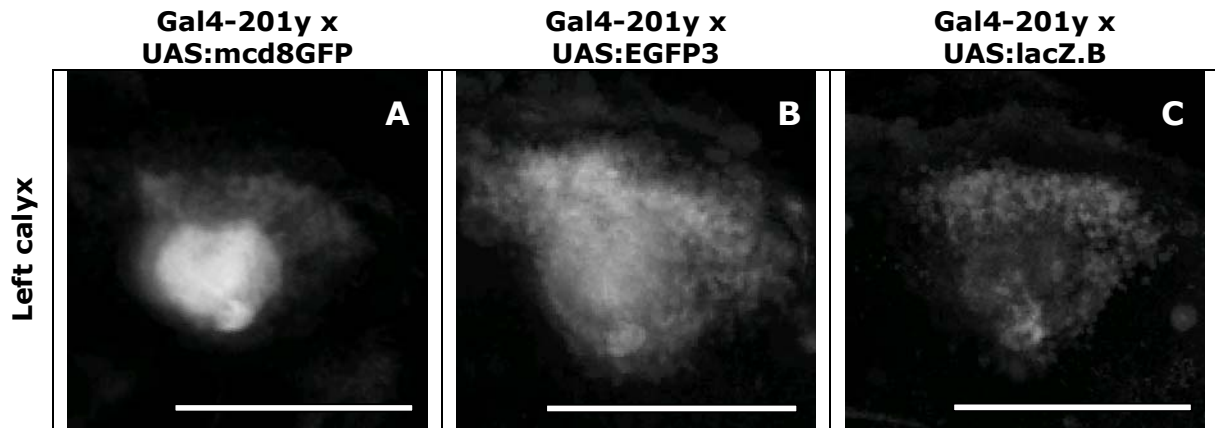


**Figure 16: Comparison of staining intensity of standardized calyces. Projections of the same standard volume reveal the staining characteristics of the different reporter types. While UAS:mcd8GFP intensively stains the Gal4-positive neuropil, lacking the somata, UAS:EGFP3 evenly stains both structures. UAS.lacZ.B produces the weakest signal in the Gal4-positive cells.  $N_A:16$ ,  $N_B:11$ ,  $N_C:8$ ; scalebar 100  $\mu\text{m}$**

### 8.1.5 Conclusion

Comparing the fluorescent signals in the progeny of crosses between the test Gal4-lines and eleven different UAS:reporters lead to a clear result. The UAS:reporter mcd8GFP is the most appropriate one for the creation of an atlas of standardized neuroanatomy. Primarily aiming for the standardization of the arborization pattern of Gal4-positive cell populations a strong and reliable fluorescent signal in all parts of the cell is needed. Representing the areas of synaptic transmission and processing of neuronal signals the fine dendritic ramifications need to be most intensely stained. These requirements were only met by UAS:mcd8GFP. The other tested lines were either insufficient in strength of fluorescent signal or not as specific as expected. Therefore we decided to build up the standard atlas on the expression of mcd8GFP. Standardized expression pattern of other markers e.g. pre- and postsynaptic areas can be added to the atlas as soon as suitable UAS:reporters are found.

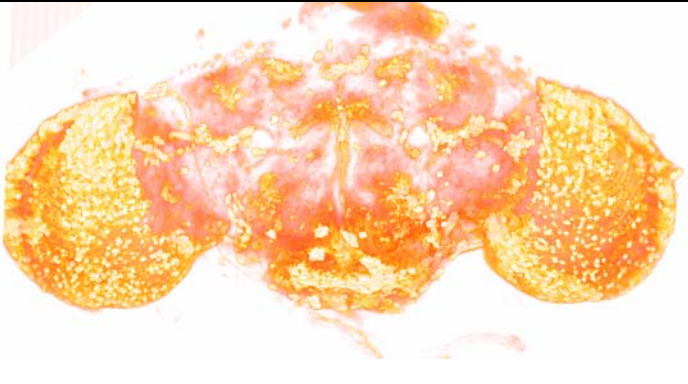
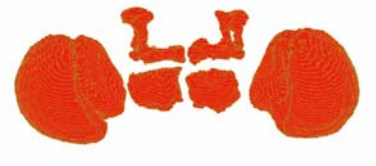
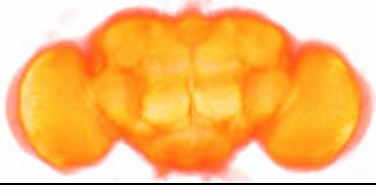
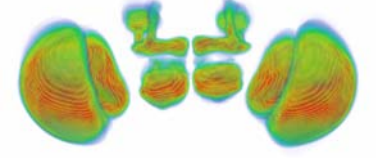
## 8.2 Comparison of Gal4 expression patterns in the central complex

Liu et al. [110] localized the memory traces for the 'elevation' of a pattern in the flight simulator in neurons of the fifth layer of the fan shaped body (F5-neurons). They could show that driving the expression of the wild-type *rut* gene in a *rut* mutant background by several Gal4-lines (*rut2080/Y;UAS-rut+/+;Gal4-driver/+*) the memory for 'elevation' could be restored. Therefore some cells in the investigated expression patterns are sufficient to rescue the *rut* memory defect. By driving the expression of a constitutively active form of

the Gas protein subunit (Gas\*) [104] using two of these Gal4-lines a full suppression of the memory of 'elevation' in the test animals could be shown. This led to the conclusion that the Gal4-positive cells are necessary and sufficient for the rut dependent memory formation for 'elevation'. The following Gal4-lines were used for the rescue experiment: 104y, 121y, 154y, 210y, C005, C205 and C271.

Standardizing the expression patterns of five of these lines (104y, 121y, 154y, 210y, C005) we found the overlap of the expression patterns less precise and less restricted than described in Liu et al..

Visualizing the standardized expression patterns for reasons of quality control of the alignment the wide distribution of the Gal4 expression pattern becomes obvious (Figure 17). The question which arose during examination of the expression patterns was, whether the F5 layer in the fan shaped body is the only common area in all of the Gal4 expression patterns as reported by Liu et al.. This question can be addressed on the basis of standardized expression patterns by arithmetic processing of corresponding voxels.

	Gal4 epression pattern		Reference
104y		nc82	
		MainProb	
121y		nc82	
		MainProb	

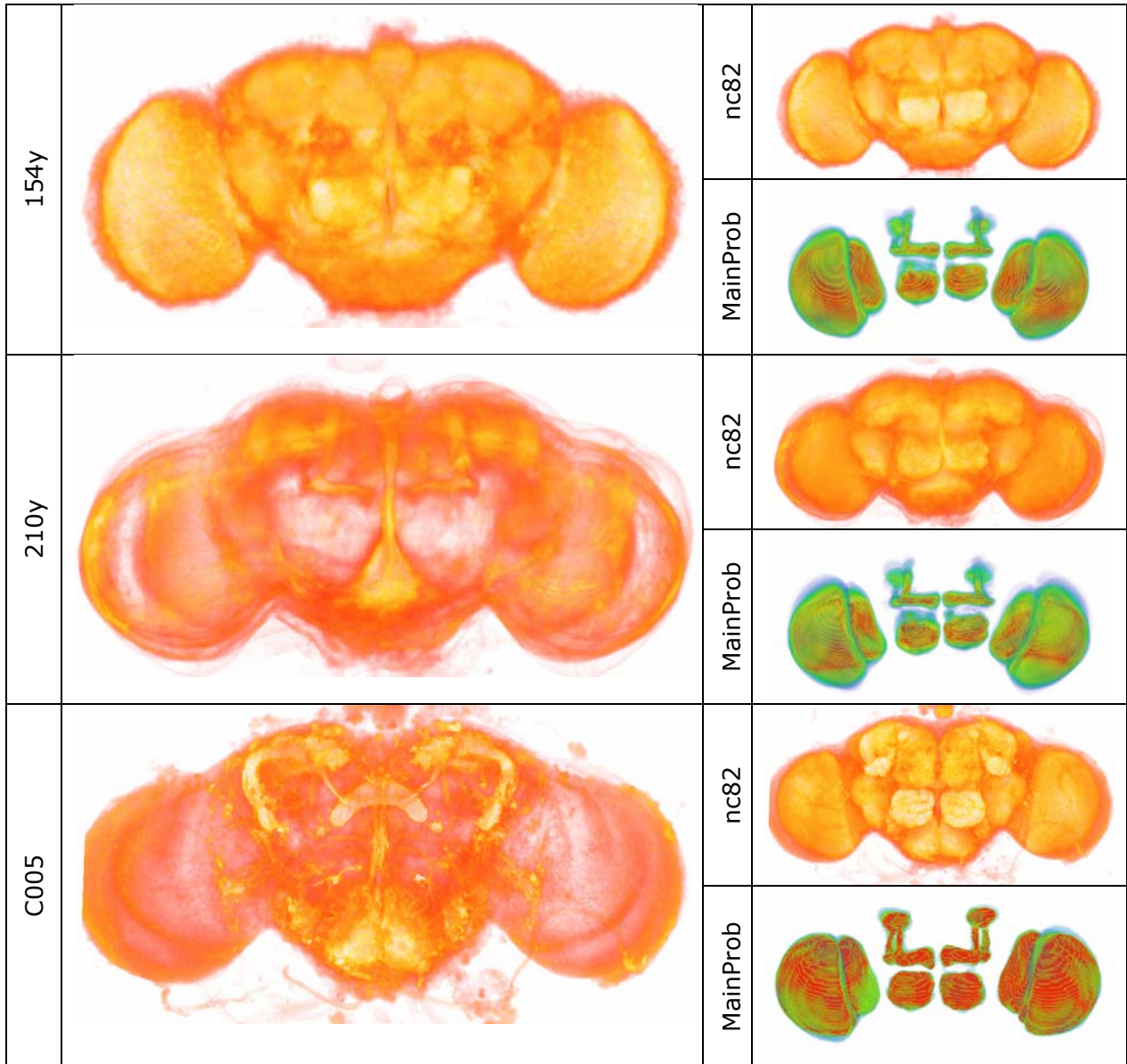


**Figure 17: Quality of standardization.** In direct volume rendering the standardized Gal4 expression patterns, and in the Reference channel neuropil structures are clearly recognizable. The high amount of red in the MainProbabilityMaps (MainProb) indicates the high degree of the alignment quality. In 104y only one Sample was aligned to the Standard. Therefore the pattern is more crisp but at the same time less representative. The MainProb of 104y is all red because there is no deviation in a file group with just one sample.

False color code for fluorescence signals:

(dark)  (bright);

False color code for MainProb: (low)  (high)

### 8.2.1 Image processing for the comparison of expression patterns

The process of standardization transfers the anatomy of the Samples to the same coordinate system. In this way the corresponding areas in the all standardized Samples are positioned at the same coordinates in the standard coordinate system. Therefore it is possible to apply voxel-wise arithmetic measures on the standardized expression patterns. Normalized pointwise multiplication of two standardized Gal4 expression patterns highlight the areas of high fluorescence signal intensity (bright) in both Samples whereas areas of low fluorescence signal intensity remain dark. At the same time areas which are of high intensity only in one of the multipliers are darkened by the low values of the other multiplier.

$$Q(x, y, z) = \frac{S_1(x, y, z) \times S_2(x, y, z)}{256}$$

**Equation 3: Normalized pointwise multiplication of two 3D 8bit-images. Each voxel of the first Sample ( $S_1(x,y,z)$ ) is multiplied with the corresponding voxel of the second Sample ( $S_2(x,y,z)$ ). The result is divided by 256 to normalize the values to 8-bit.**

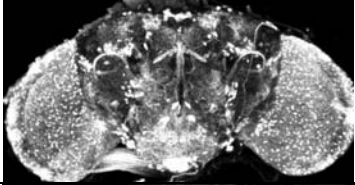
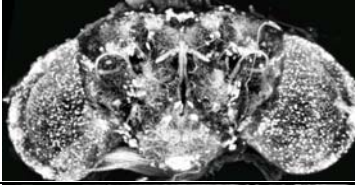
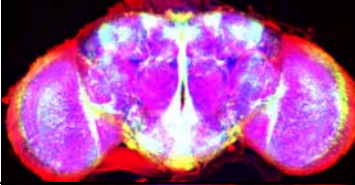
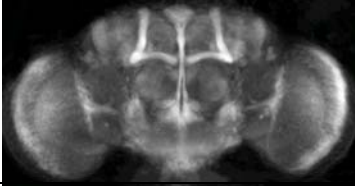
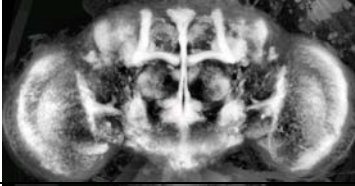
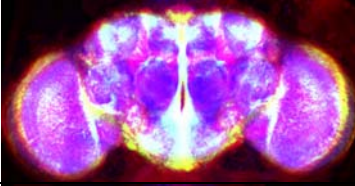
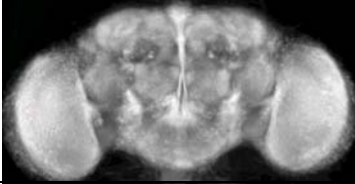
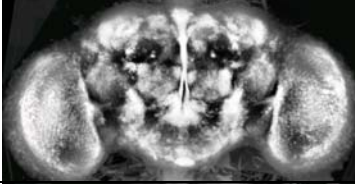
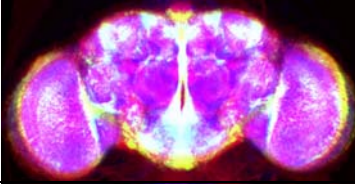
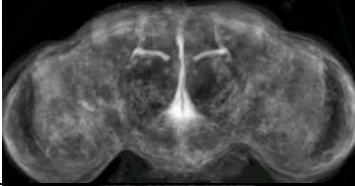
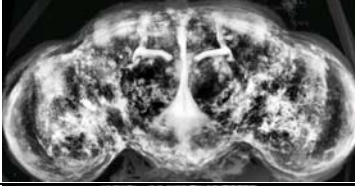
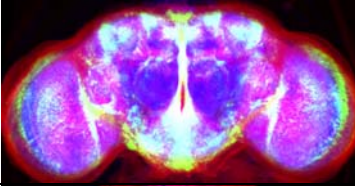
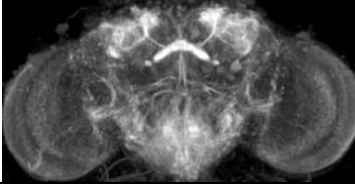
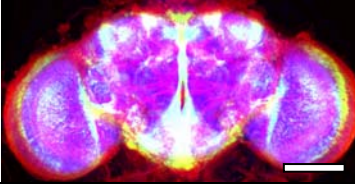
Due to the restrictions of Amira for the processing of multiple 3D images the values of fluorescence intensity are transferred from unsigned integers (0-255) to floating-point numbers before multiplication to avoid data register overflow. The interim result subsequently is multiplied by 256. Thereby it is normalized to 8 bit and comparable with the original data.

$$Q_n(x, y, z) = \left( \frac{S_1(x, y, z)}{256} \times \frac{S_2(x, y, z)}{256} \times \dots \times \frac{S_n(x, y, z)}{256} \right) \times 256$$

**Equation 4: Normalized pointwise multiplication of multiple 3D images. To avoid overflow of the data register the individual intensity values are normalize to 1 before multiplication.**

For the arithmetic analysis of expression patterns we decided for a multiplication over the mean of the intensity values. Thereby high intensity values are more amplified than low intensity values and the visual analysis of common structures of the standardized Gal4 expression patterns is facilitated. Nevertheless, the results are of low contrast if the arithmetic analysis is applied on the original distribution of grey values in the standardized expression patterns. Therefore a contrast limited adaptive histogram equalization (CLAHE) on the standardized expression pattern was applied. CLAHE was originally developed for medical imaging and has proven usefull to enhance low-contrast

images such as X-ray films. The CLAHE algorithm partitions the images into contextual regions and applies the histogram equalization to each one. This evens out the distribution of used grey values and thus makes hidden features of the image more visible. The full grey spectrum is used to express the image. Using CLAHE for contrast enhancement the information about global differences in fluorescence intensity between the standardized expression patterns gets lost because distribution of grey values is reorganized. An overall weak signal after CLAHE is not distinguishable from a strong one (Figure 18). Because in this study we were not comparing signal intensities but looking for overlap of expression patterns, this can be accepted. Therefore signal enhancement using CLAHE was the most favorable.

	Standardized expression pattern	Standardized expression pattern after CLAHE	Overlay of standardized Gal4 expression pattern (red); common Gal4 expression pattern (green) and reference staining (blue)
104y			
121y			
154y			
210y			
C005			

**Figure 18: Comparison of the intensity of standardized expression patterns with their common aspects. The left column displays the standardized expression patterns without normalization of fluorescent signal intensity (CLAHE) in grey values. The middle column shows the same data after contrast enhancement using CLAHE. The right column shows the same data as in the middle column (red) superimposed with the common aspects of all patterns listed (green) and a standardized reference neuropil staining (reference, nc82) (blue). Scalebar: 100µm**

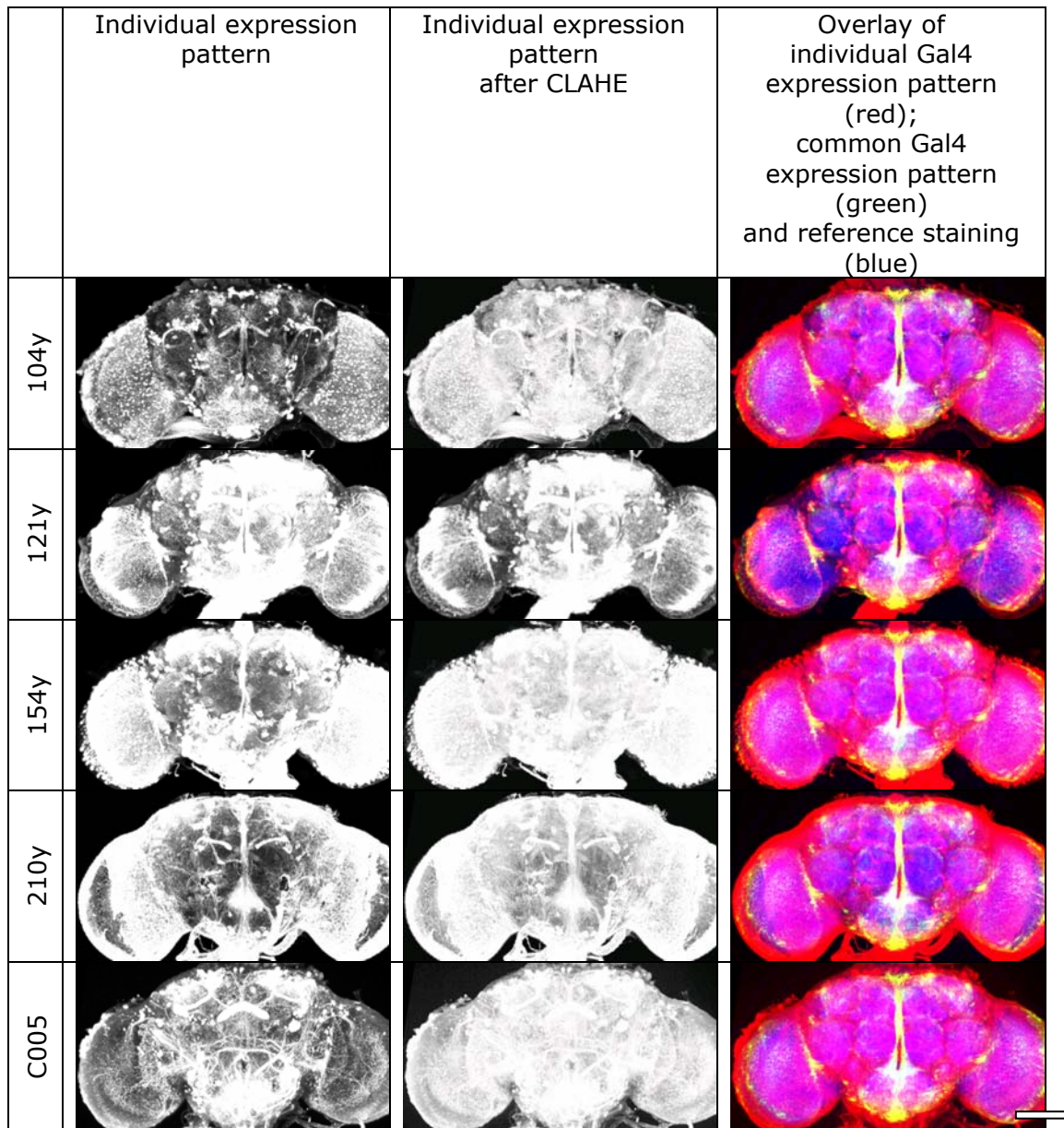


**Figure 19: Comparison of the intensity of individual expression patterns with their common aspects. The left column displays the original expression patterns without normalization of fluorescent signal intensity (CLAHE) in grey values. The middle column shows the same data after contrast enhancement using CLAHE. The right column shows the same data as in the middle column (red) superimposed with the common aspects of all patterns listed (green) and a standardized reference neuropil staining (reference, nc82) (blue). Scalebar: 100 $\mu$ m Due to the high contrast in individual Samples the application of CLAHE does not make sense for visualization. However, for the computation of common aspects of the expression patterns it is indispensable, because it normalizes signal intensity from one Sample to the other.**

This color scheme applies for all following colored figures of this chapter: In areas in which the Gal4 expression pattern (red), the common aspects of the expression pattern (green) and the reference (blue) overlap the colors add up to white. Parts of common Gal4-expression outside the neuropil (tracts, somata) are yellow and individual Gal4 expression pattern in the neuropil is magenta.

### **8.2.2 Analysis of standardized Gal4 expression patterns interfering with the memory for 'elevation'**

Pairwise arithmetic analysis provides insight into the common aspects of the Gal4 expression patterns (Figure 20). As expected the more patterns are included into the analysis (grey fields in Figure 20) the smaller the common areas become. Including all five expression patterns in the analysis results to very few common areas compared to the widespread shape of the individual patterns (Figure 21). Nevertheless the common pattern is much more widespread than expected.

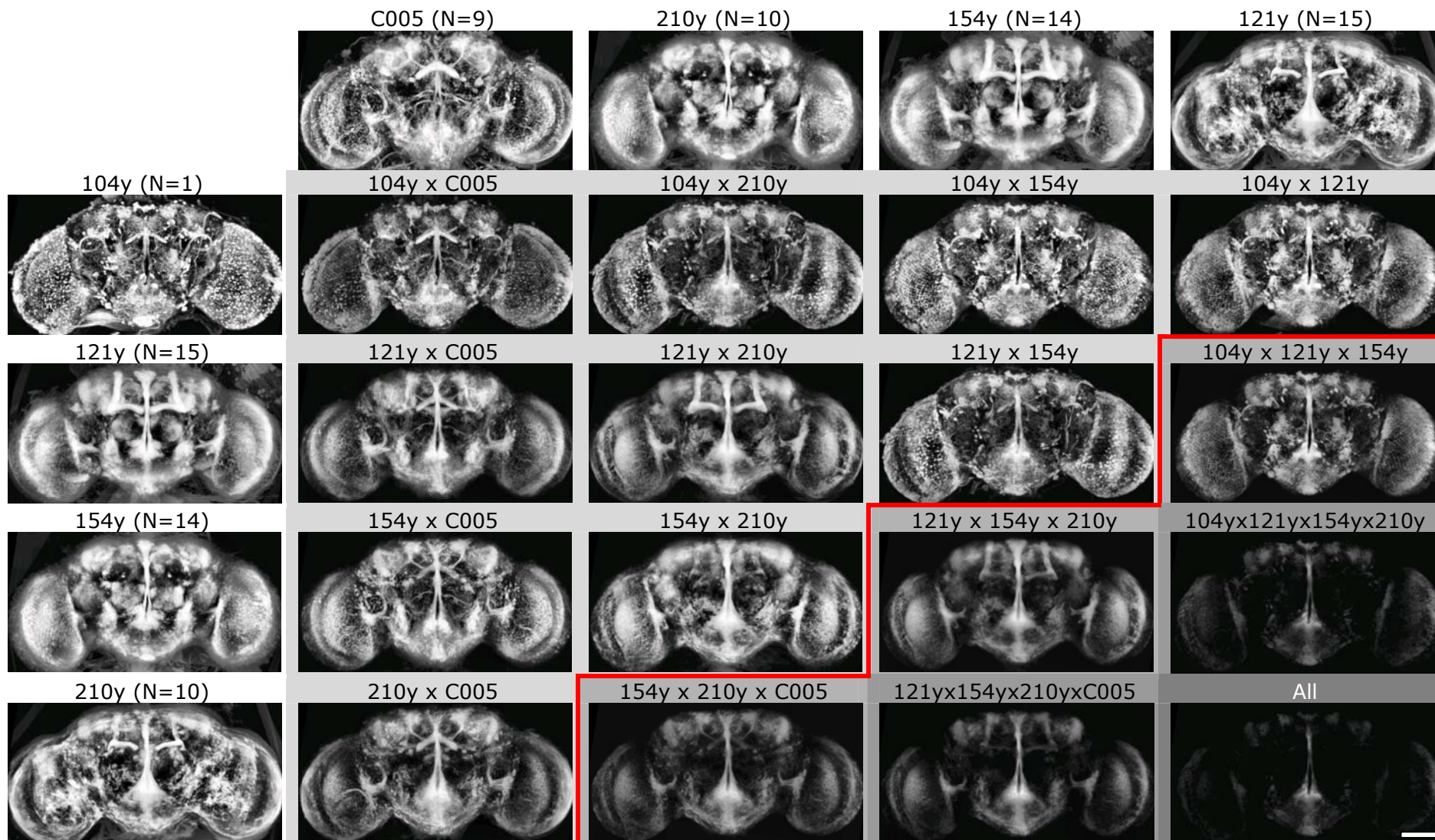
Nevertheless the common pattern is much more widespread than expected.

These areas can be subdivided in

- the ventral brain with subesophageal ganglion (SOG) and antennal nerves (AN) (see chapter 8.2.2 on page 71),
- the pars intercerebralis (PI) together with the median bundle and the tritocerebrum(see chapter 8.2.3 on page 74),
- the optic lobes (OL) (see chapter 8.2.4 on page 74),
- the dorsal brain region with the lateral horn (LH) (see chapter 8.2.5 on page 75),
- and the fan shaped body (FB) (see chapter 8.2.6 on page 76).

**Figure 20: Next page. Common aspects of five standardize Gal4 expression patterns. Patterns on pale grey background left and above the red line are normalized pair wise multiplications of the corresponding standardized expression patterns on white background (C005, 210y, 154y, 121y, 104y). Below and right of the red line are displayed the common aspects of the expression patterns of three (light grey background), four (grey background) and all expression patterns (dark grey background). For reasons of comparability the signal amplification is normalized by CLAHE. Scalebar 100µm**

Applications of the VIB protocol



The result of the arithmetic analysis consists of the structures which are of high fluorescence signal intensity in all included patterns. One has to keep in mind that any bright signal in the standardized expression patterns contributes to the common pattern. Therefore the bright structures in the common pattern can only give a hint of the areas of interest for detailed analysis whereas obviously dark areas can be excluded from further analysis. For example the antennal lobes of the investigated Gal4 expression patterns show no common ground at all and therefore are completely void of signal in the depiction of the common pattern (Figure 21).

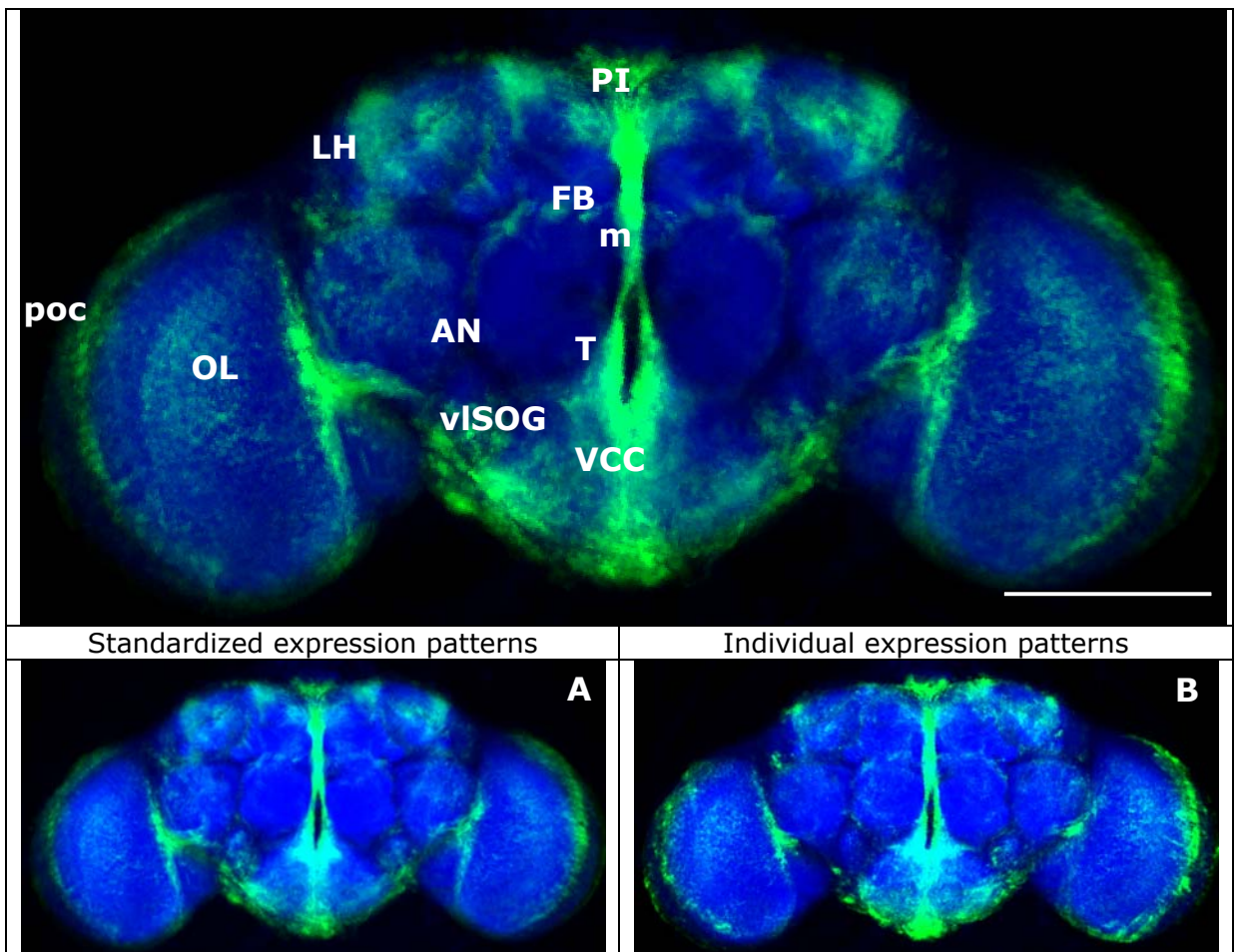


**Figure 21: Common aspects of the expression patterns of C005, 104y, 121y, 210y and 154y (Figure 20 lower right corner) in green. A standardized reference expression pattern (nc82) is superimposed in blue. In addition to CLAHE strong signal amplification is applied to the common expression patterns. A: The common pattern is processed on the basis of the standardized expression patterns displayed in Figure 20, i.e. the common pattern of 49 specimens of different Gal4-drivers. B: Common pattern of five arbitrarily selected Samples, one of each Gal4-driver line. In some areas the common pattern intensity diverges from the standardized pattern but all common aspects of A are apparent in B and vice versa.**

**PI: pars intercerebralis, LH: lateral horn, FB: fan shaped body, m: medial bundle, poc: primary optic chiasm, AN: antennal nerve, T: tritocerebrum, OL: optic lobes, vISOG: ventro-lateral part of the**

**subesophageal ganglion (SOG), VCC: ventral cell body cluster. Scalebar 100µm**

The common pattern in the primary optic chiasm (poc) distal of the medullae is due to a preparation artifact. Many specimens show strong immunohistochemical staining at this position as well as on the whole surface of the specimen. This effect may be explained by unspecific cross reactions of the antibodies to structures of disrupted cells as without any immunohistochemical staining these fluorescent signals are much less prominent.

**8.2.3 Expression in the pars intercerebralis (PI) and the ventral brain with subesophageal ganglion (SOG) and antennal nerves (AN)**

Most prominent in the common fluorescence signal is the median bundle (m) including dorsally the pars intercerebralis (PI) and ventrally the dorsal part of the subesophageal ganglion (SOG) which is the tritocerebrum (T).

Besides the tritocerebrum two additional areas in the SOG are part of the common expression pattern of all investigated Gal4-lines: The lateral parts of the ventro-lateral SOG (vISOG) and the ventral cell body cluster (VCC) (Figure 22).

In the area of the VCC the ventral unpaired midline neurons (VUM) are located, neurons that are reported to be octopaminergic and play a key role in appetitive associative learning [144]. Therefore this cell body cluster is of special interest in many behavioral experiments. However, as mentioned before the position of cell bodies is highly variable and therefore standardization of single cell body positions is not possible. Thus we just can state that there are Gal4-positive cells in the VCC in all of the standardized Gal4 expression patterns. However, no statement can be made about the identity of the Gal4 positive cells. Therefore more detailed investigations with higher spatial resolution should be applied in the future.

In the vISOG sparse arborizations overlap in all investigated Gal4 expression patterns. These are mainly concentrated in the posterior part of the vISOG but a common morphology of the expression patterns as observable in the fan shaped body was not found. Rather the expression patterns of the investigated Gal4 lines seem to overlap coincidentally. Nevertheless it is conspicuous that all the investigated Gal4 lines have expression in this area.

Laterally of the SOG common expression can be found in the antennal nerves (AN). Although this signal is spoiled by a staining artifact of the surfaces of the Gal4-210y-specimens in the approach using standardized expression patterns

(Figure 22) it can be confirmed on the basis of individual expression patterns (Figure 23).

#### **8.2.4 Expression in the optic lobes (OL),**

In all investigated Gal4-lines proximal to the optic lobes a large cell population projecting towards the central brain, seems to be Gal4- positive. Unfortunately many cell clusters are located at this position. Again, due to the high variability in cell body position, this approach is not suited to prove the identity of cell bodies in different Gal4 lines. However, even if we can not define exactly the common cell population nor tell its cell number we can state that in all of the investigated Gal4-lines Gal4 positive cells are located proximally to the lobula. Therefore we expect Gal4-expression in the proximal neuropils of the optic lobes (lobula, lobula plate) in all Samples. Actually, expression in the lobula can be found in all investigated expression patterns. However, the distribution of the pattern diverges strongly between the different Gal4 driver lines. The overlap is confined to the most proximal margin of the lobula (Figure 24). In the individual approach this common pattern does not show up (Figure 25). Therefore we assume the common cell body cluster proximal of the lobula contains different cell populations in the different Gal4-lines. Nevertheless, the close proximity of the arborization patterns in the lobula may suggest interactions between these cells.

The same is true for a small area in the medulla, where the expression patterns of all investigated Gal4-lines seem to overlap in one layer. However, the layers in the medulla are very thin and due to the interindividual variability the fluorescence signal of the Gal4 expression patterns becomes blurred during standardization (Figure 24). Therefore expression in neighboring layers may fuse and appear to be located in the same layer. However, in comparisons of transformed individual Samples the Gal4-positive layers were observed to be very close to each other (Figure 25). Due to the different arborization pattern in the medulla it is very improbable that the patterns are caused by the same cell population.

#### **8.2.5 Expression in the dorsal brain region**

In Figure 26 the common aspects of the Gal4 expression pattern in the dorsal brain seem to consist of three distinct parts in each hemisphere. However, one of these structures is based on the same cell population with a rather complex arborization pattern described as F5 neurons by Liu et al.. The other part of the pattern is a bow of about 15µm diameter in the dorso-lateral protocerebrum that runs antero-laterally from the mushroom body calyces directly under the

surface of the dorso-lateral protocerebrum circumventing the lateral horn in maximal distance. It ends anterior the lateral horn, laterally of the heel of the mushroom bodies (Figure 26, black arrow). This pattern looks like a tract connecting caudal and frontal areas of the dorso-lateral protocerebrum. This tract was not described before. The region of the dorso-lateral protocerebrum is not well investigated. Therefore the potential function of this structure is completely unknown.

The cell bodies of the F5 cells are located laterally to the mushroom body calyces. From there the cells project towards the medial side of the tip of the a-lobes where they build a small tufted arborization. This is the medial part of the common aspects in the dorsal brain (Figure 26, white arrow). Further, they project anterior to the fan shaped bodies, where they form a layer of arborizations (white open arrows). Analyzing standardized expression patterns this pattern is clearly visible in only two of the investigated Gal4-lines (Gal4-C005, Gal4-104y). Using individual expression patterns and CLAHE in the other standardized expression patterns at the described positions weak fluorescence can be observed. This is due to the small number of F5 neurons which are Gal4-positive in these lines.

### **8.2.6 Expression in the fan shaped body (FB)**

In the fan shaped body we found the most striking result of this study. The Gal4 expression patterns in the fan shaped body are less specific for single layers as expected. All investigated Gal4 expression pattern show fluorescent signal in at least two layers of the fan shaped body. Following the tentative classification of Liu et al. in Gal4-104y we found fluorescence signal in layer F5 and in a layer near the ventral margin of the fan shaped body that we tentatively defined as F2. This is due to the expression pattern of Gal4-C005, which is very broad in the fan shaped body and extends more ventrally than the ventral band of Gal4-104y. Therefore the area with the most ventral expression in Gal4-C005 was defined as layer F1. Besides this there is strong Gal4 expression in all layers except layer F4 in Gal4-C005. Gal4-121y expresses in F3, F4 and F5, Gal4-210y in F6, F5, F3 and F2 and in Gal4-154 very weak expression can be found in the layers F5 and F3. Because of variability of the sparse F5 arborization pattern in Gal4-154y in the standardized expression patterns this weak signal vanishes (Figure 28). However, in individual analysis this aspect of the expression pattern also in Gal4-154y becomes obvious (Figure 29)

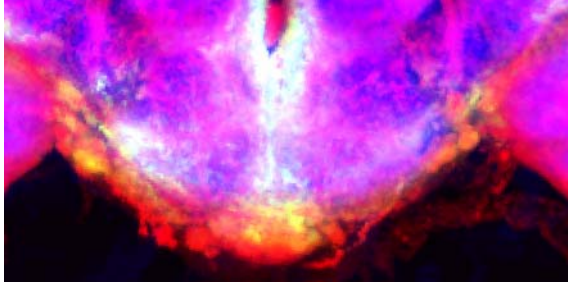
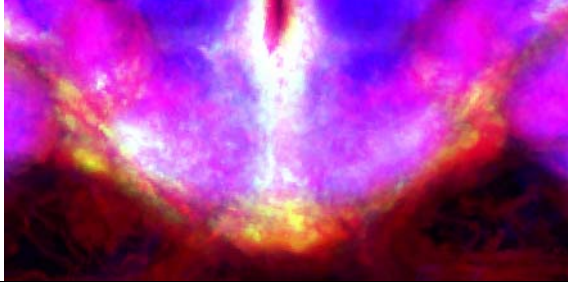
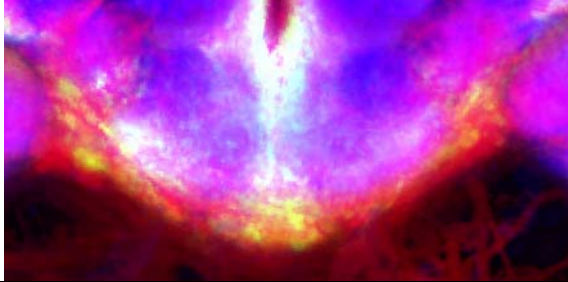
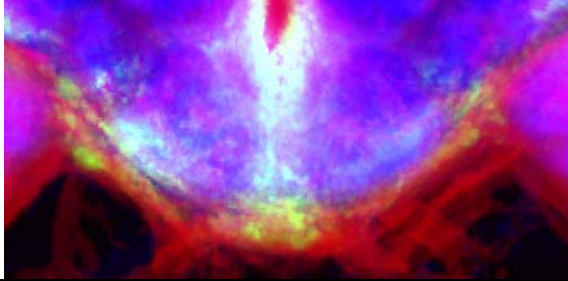
Therefore we can confirm the data of Liu et al. that in the investigated Gal4 expression patterns F5 neurons are included. Table 15 lists the distribution of the expression patterns in the fan shaped body.

However, just a minute overlap of all expression patterns could be found in the most lateral parts what is due to the weak expression in Gal4-154y in the F5 layer.

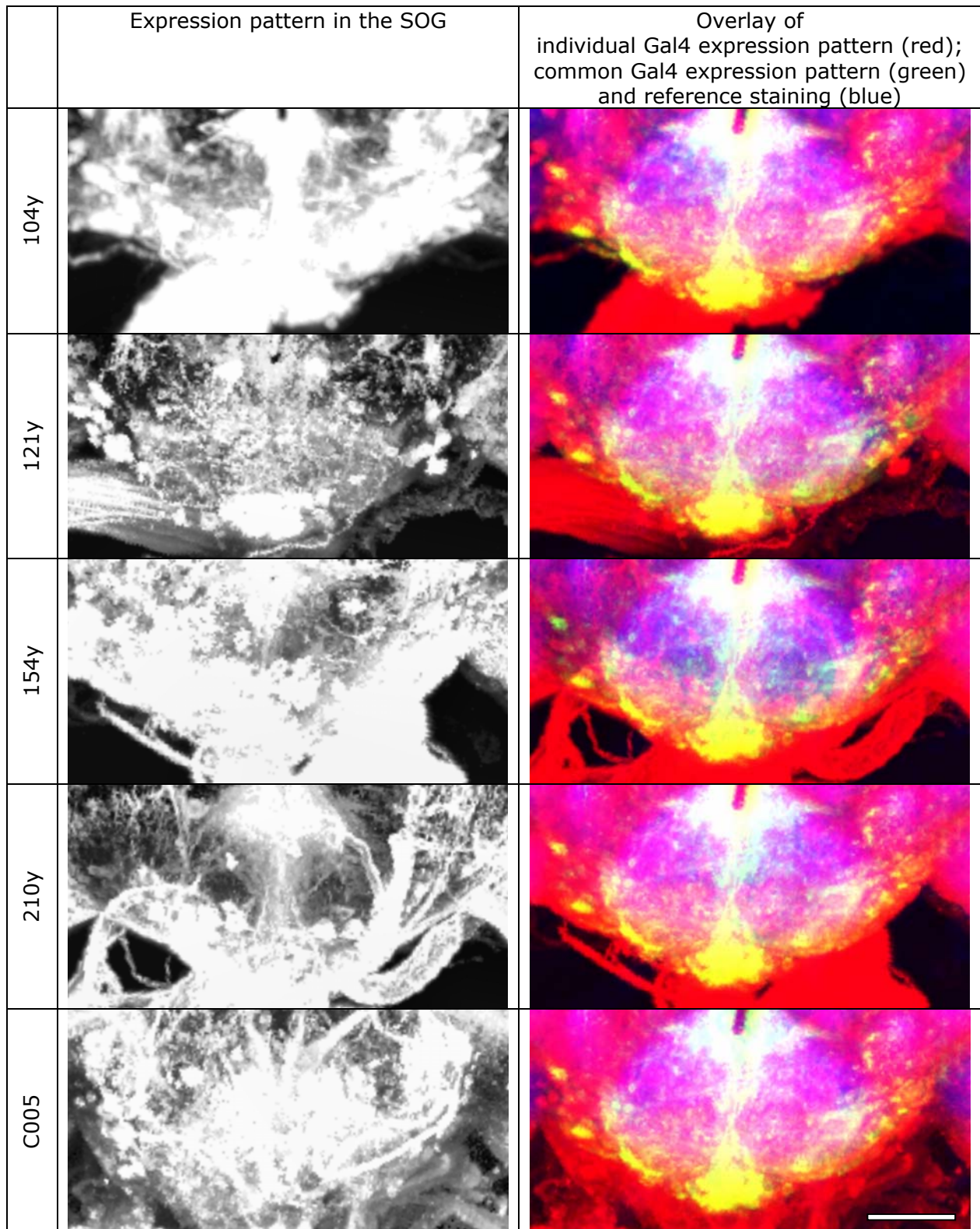
In the F5 layer we also found fluorescence signal in Gal4-lines which were included in the study of Liu et al. and found not to interfere with the memory of 'elevation' (78y, 007y) (Table 15). However, because we can not find fluorescence in the typical tufted arborization in the dorsal brain nor the cell bodies of the F5 neurons we assume these arborizations not to be F5 neurons.

**Table 15: Fluorescence intensity in the layers of the fan shaped body. Scaling from 1 (very weak) to 5 (very strong).**

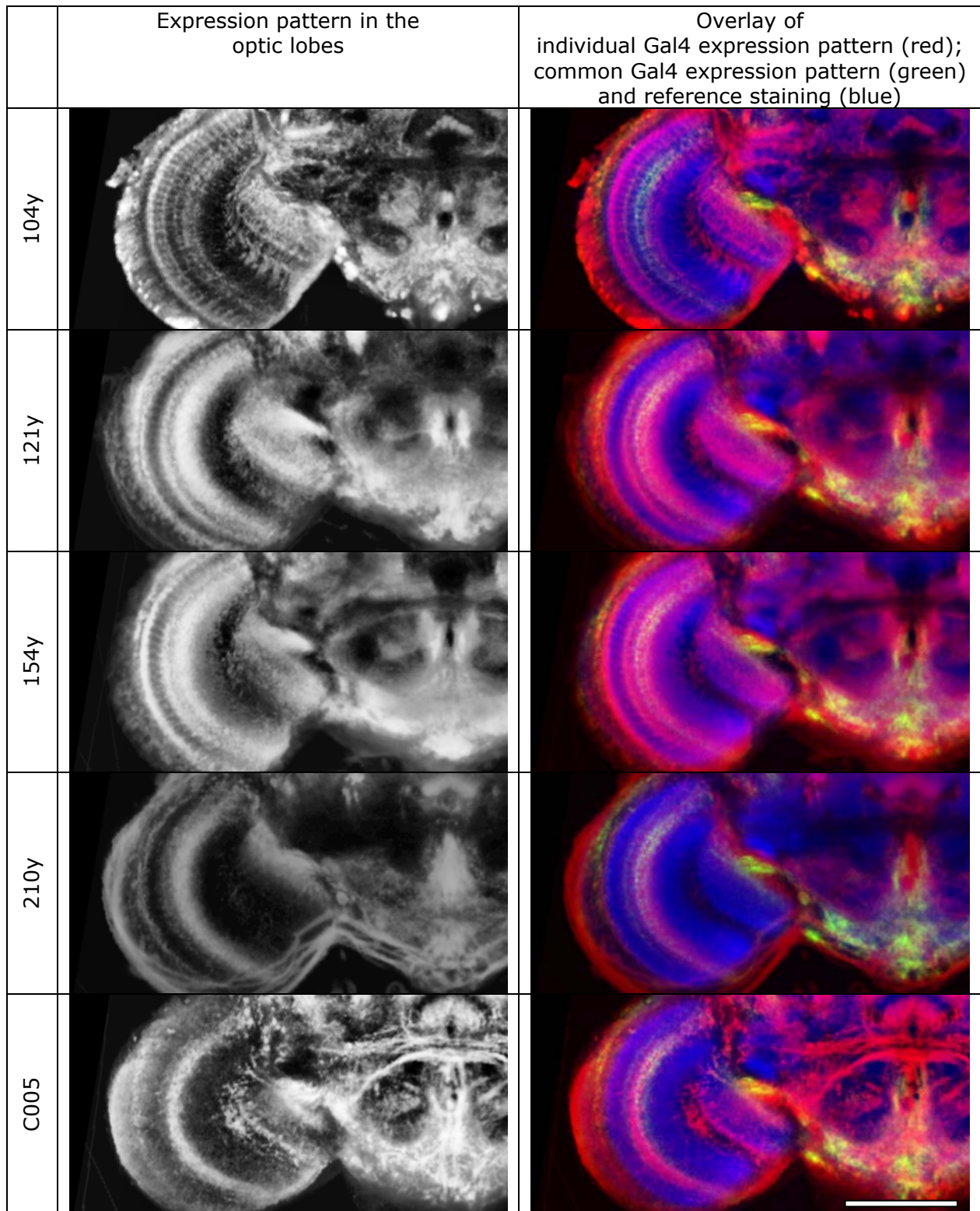
Layer	104y	121y	154y	210y	C005		78y	007y
F6				3	5			
F5	4	3	1	3	4		1	1
F4		1					4	4
F3		2	1	2	3		4	4
F2				2	3			
F1	2				3			

	Expression pattern in the SOG	Overlay of individual Gal4 expression pattern (red); common Gal4 expression pattern (green) and reference staining (blue)
104y		
121y		
154y		
210y		
C005		

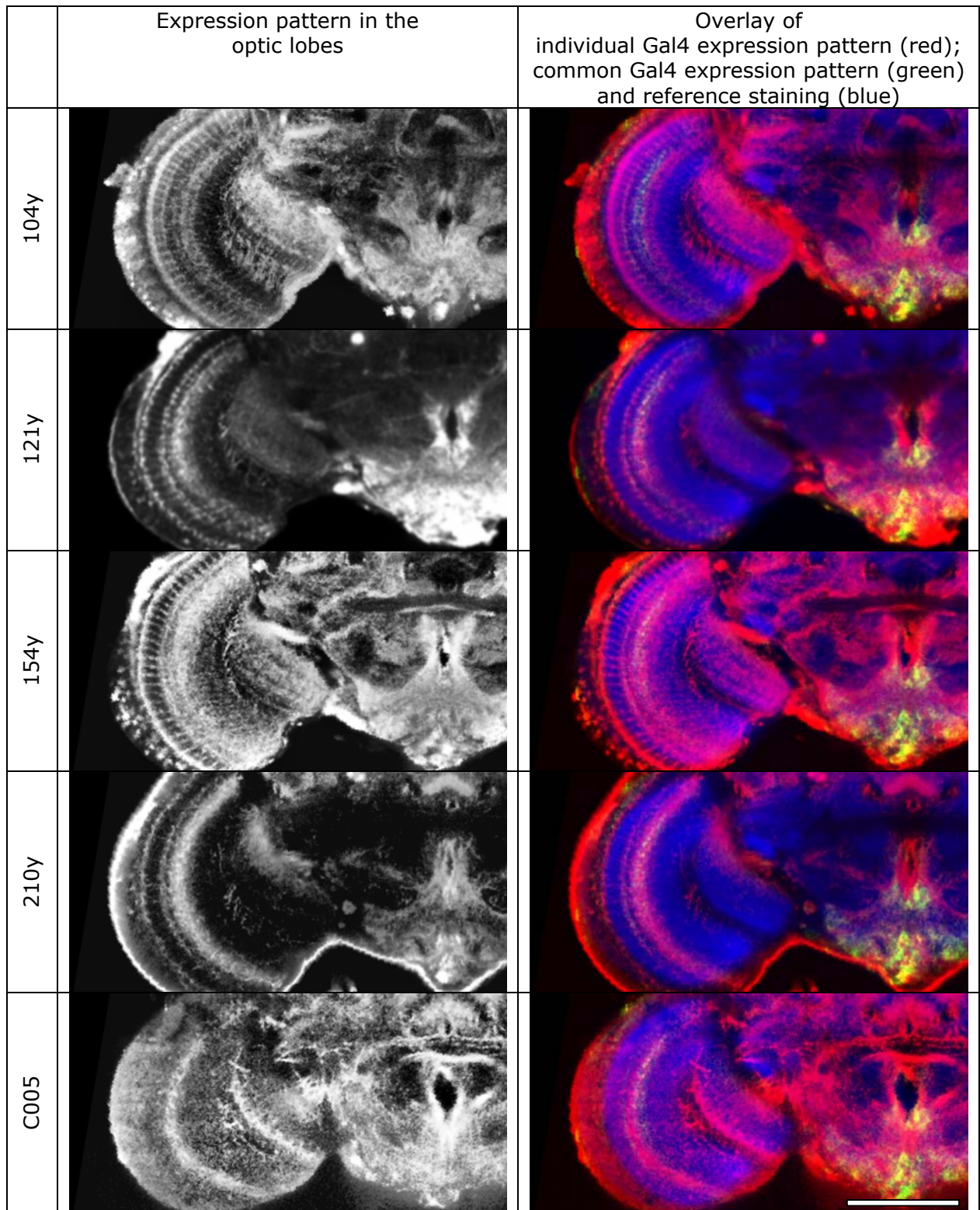
**Figure 22: Comparison of the standardized expression patterns in the subesophageal ganglion (SOG).**



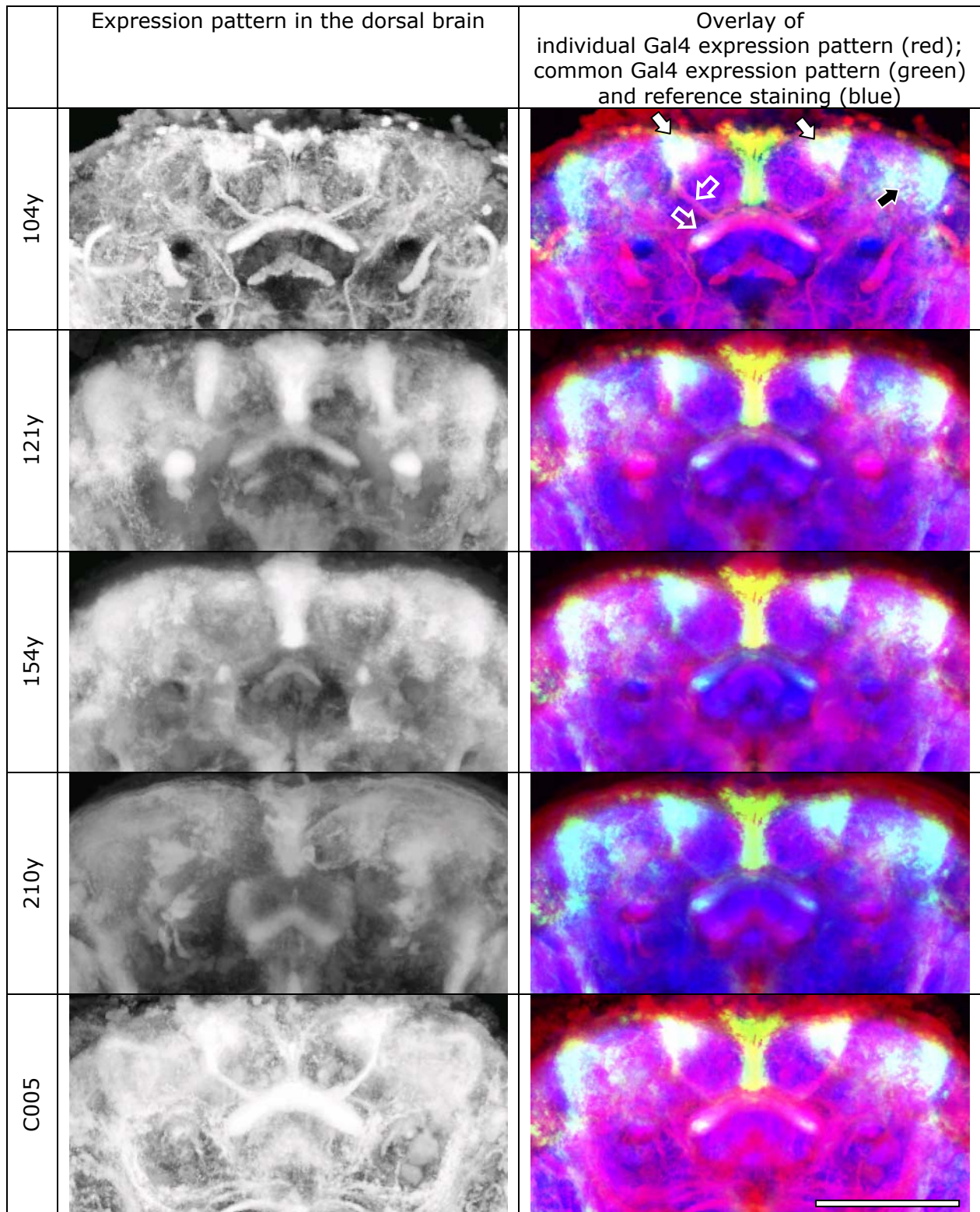
**Figure 23: Comparison of the individual expression patterns in the subesophageal ganglion (SOG).**



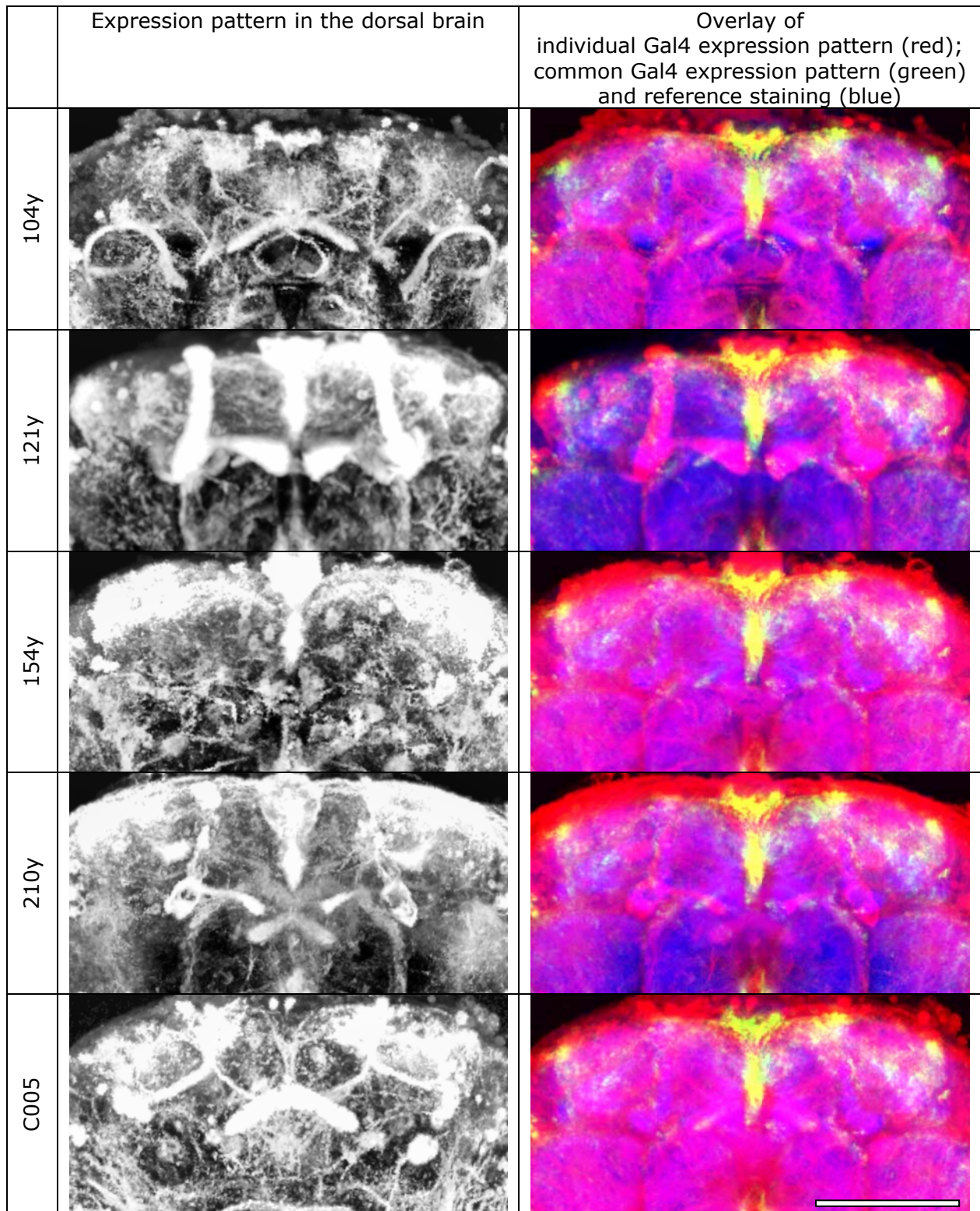
**Figure 24: Comparison of the standardized expression patterns in the optic lobes.**



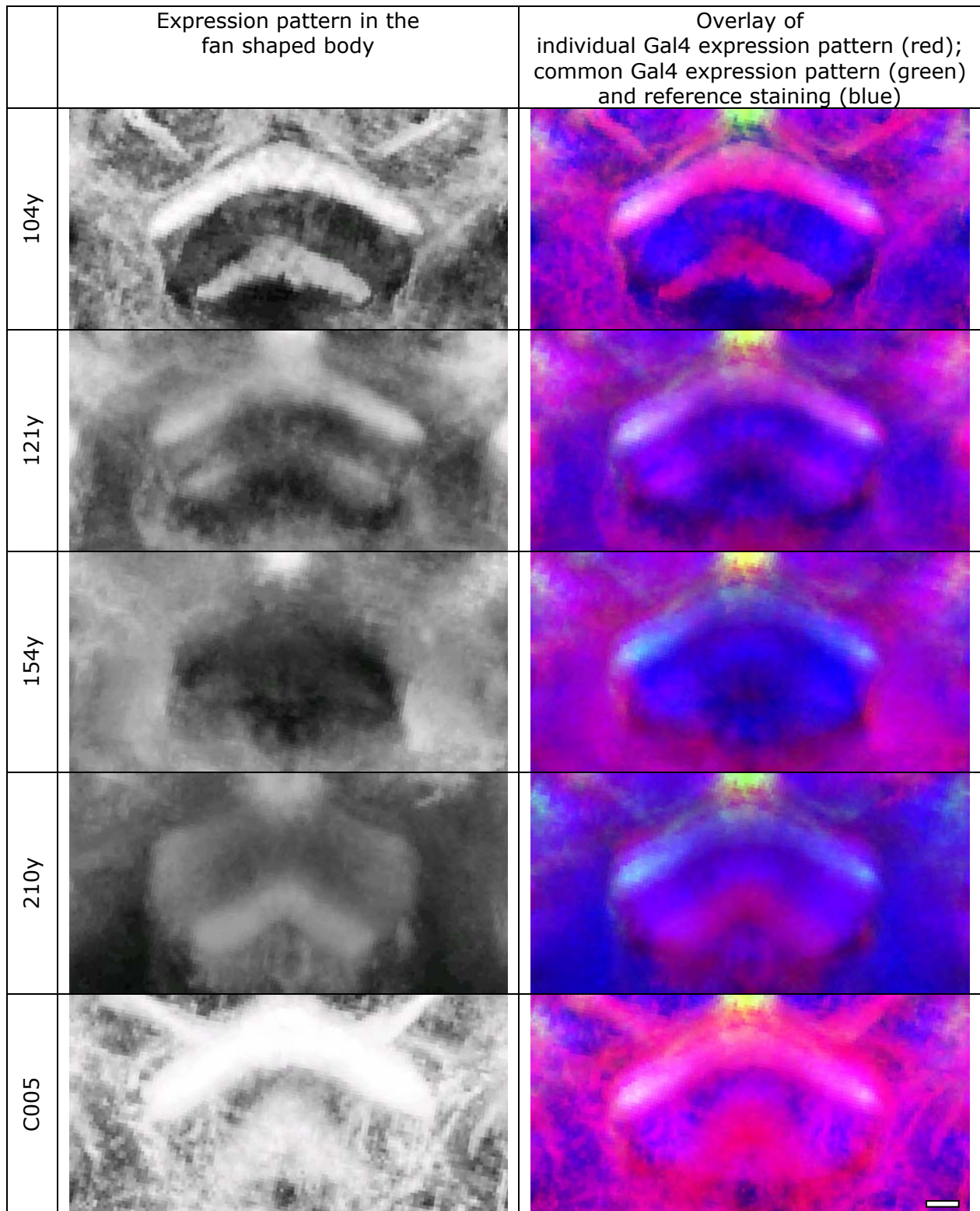
**Figure 25: Comparison of the individual expression patterns in the optic lobes.**



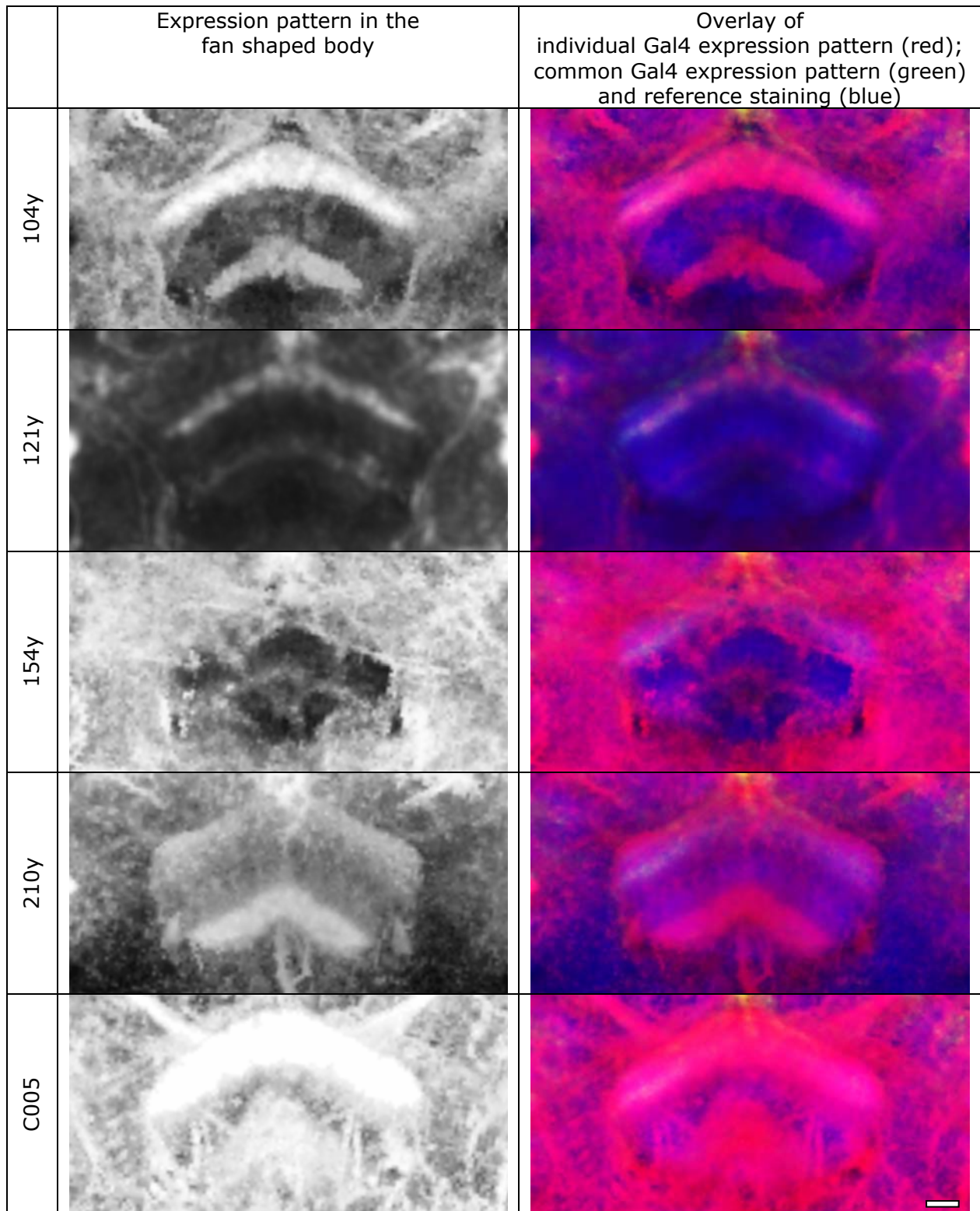
**Figure 26: Comparison of the standardized expression patterns in the dorsal brain.**



**Figure 27: Comparison of the individual expression patterns in the dorsal brain.**



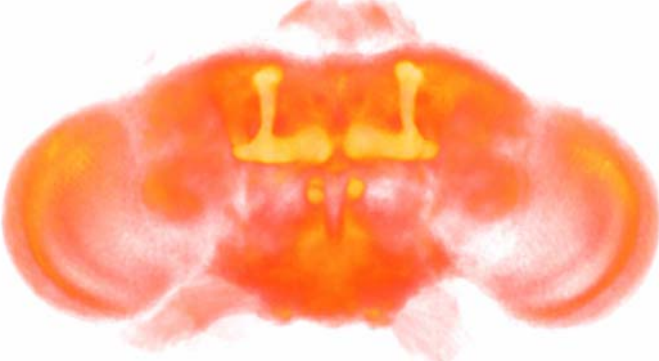
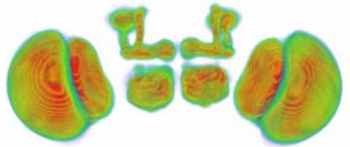
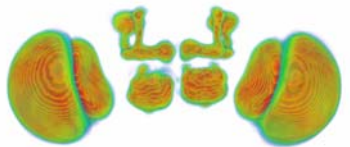
**Figure 28: Comparison of the standardized expression patterns in the fan shaped body.**



**Figure 29: Comparison of the individual expression patterns in the fan shaped body.**

### 8.2.7 Analysis of standardized Gal4 expression patterns which do not interfere with the memory for 'elevation'.

In addition to the expression patterns which were described to have an effect on the memory for 'elevation' as a control we standardized the expression patterns of two Gal4-lines which were reported to have no effect on the memory for 'elevation' and show expression in the central complex. In the ellipsoid body and the protocerebral bridge intense Gal4-expression was observed (data not shown) and in the fan shaped body a strong band in the F3 and F4 layer could be detected (Figure 31). Besides these strong patterns in the central complex a weak fluorescent signal was found in the F5 layer in both Gal4-lines. Due to the fact that no fluorescence was found in the typical tufted arborizations in the dorsal brain or at the position of the F5 neurons' cell bodies we assume, that the observed signal in the F5 layer is based on other cells than F5 neurons.

	Gal4 expression pattern		Reference
007y		nc82	
		MainProb	
78y		nc82	
		MainProb	

**Figure 30: Quality of standardization. In direct volume rendering of the standardized Gal4 expression patterns and the reference channel neuropil structures are clearly recognizable. The high amount of red in the MainProbabilityMaps (MainProb) indicates the high degree of the alignment quality.**

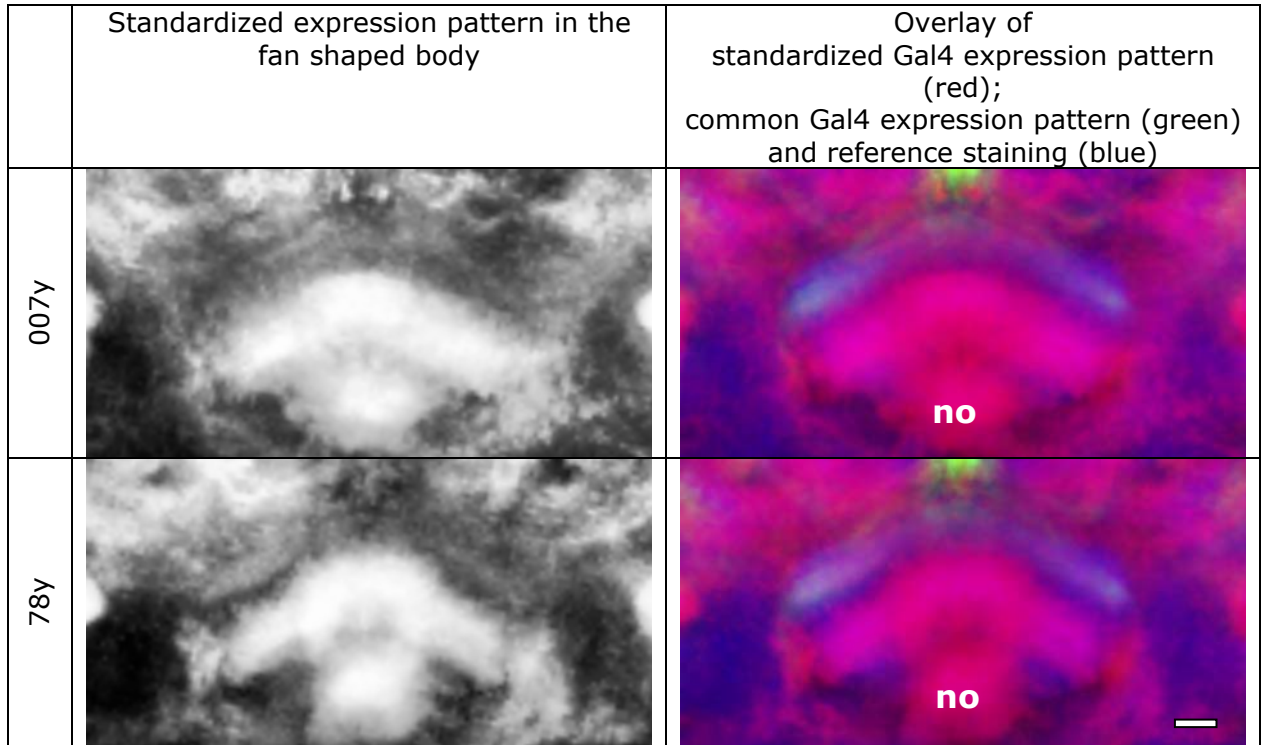


**Figure 31: Expression patterns in the fan shaped body in the non-rescuing lines 78y and 007y. Besides expression in layers F3 and F4 (magenta) weak expression can be found in layer F5. However, this pattern can not be put down to expression in F5 neurons, because neither the tufted arborization in the dorsal brain nor the cell bodies of the F5 neurons show distinct fluorescent signal. Additionally to the expression in the fan shaped body strong expression in the noduli can be observed (no). Scalebar:10**

### 8.2.8 Conclusion

Comparing the expression patterns of five of the seven Gal4 lines used in the study of Liu et al. we were able to confirm some of their findings. Importantly, all Gal4-lines which interfere with the memory for 'elevation', have common expression in the F5 neurons.

Apart from this we found seven areas with a pronounced overlap of the expression patterns. Whether the two lines not investigated here also have expression in these regions remains to be investigated. The overlaps in the VCC and proximal the lobulae were mainly confined to cell bodies. But due to the variability in cell body position and high density of cell bodies at these positions we can not state, that the overlapping fluorescence signal derives from the same cell populations. Furthermore the diverging expression patterns in the lobula neuropil argue against cell identity. Therefore, it is unlikely that these common patterns have an influence on the investigated behavior.

In the medulla common Gal4 expression was found in one layer. Again the common aspects in this layer derive obviously from different cell populations. Nevertheless, due to the precise organization of the medullae direct interaction

of the Gal4 positive cells in the different Gal4-lines can not be excluded. Further investigations focusing on this neuropil could reveal potential interactions of these populations.

In addition to these uncertain areas of common expression we found strong and reproducible common ground in the pars intercerebralis, including the median bundle and the tritocerebrum in all Gal4-lines. If present in the other two lines as well these would be candidates for interfering with the memory for 'elevation'. As described by Zars et al. [112] these brain areas might be involved in spatial learning. In Gal4-78y and Gal4-007y the median bundle is Gal4-positive as well, even though the responsible cells seem to be located slightly more anteriorly.

Another common site of Gal4 expression in all five lines is a bow-shaped area in the dorso-lateral protocerebrum. The function of this area is completely unknown. In the expression patterns of the investigated Gal4 lines the common pattern is always hidden in rather complex surrounding patterns. If it would also be stained in the other two driver lines it would be a further candidate structure for the location of the memory trace for 'elevation'.

On the basis of the five lines studied here, we can not confirm the exclusive overlap of the investigated Gal4-lines in the F5 layer of the fan shaped body but find at least three neuropil areas in which these patterns overlap. In order to question the statement of Liu et al. that the only possible localization of the memory for 'elevation' can be found in the F5 layer of the fan shaped body, we would need to investigate the other two lines.

Nevertheless, in this approach the Virtual Insect Brain protocol has proven useful for the comparison of expression patterns. The retrospect analysis of expression patterns led to the confirmation of described findings. Additionally, it led to the exposure of new details in the common aspects of the investigated expression patterns. Therefore a catalog of standardized expression patterns as used in this study could facilitate the selection of Gal4-lines for experiments. Giving the scientist the possibility to scrutinize the common aspects of the expression patterns to be tested helps to design behavioral experiments and widens the perspective on the collected data.

### **8.3 Standardization of expression patterns specific for olfactory projection neurons**

The olfactory system of the fly is a well organized but complex system. Olfactory information in the fly brain is processed at multiple levels. The first level is constructed by about 1300 receptor cells [145]. Each olfactory receptor

cell hosts only one specific (and at least one unspecific) receptor. This distribution generates odor specific receptor cell types which have special response properties to odors. All receptor cells of the same type project into one or few of 40-50 glomeruli, small subcompartments of the antennal lobes. In the glomeruli the receptor neurons interconnect to local interneurons and projection neurons. In the antennal lobes further processing of the olfactory signal takes place. The next level of olfactory processing lies in the estimated 150 olfactory projection neurons, which are connecting the antennal lobes with the mushroom body calyces and the lateral horn [146], [147]. In the calyces the olfactory projection neurons build large synaptic boutons which are surrounded by large postsynaptic regions of Kenyon cells [148]. The organization and functional role of the lateral horn so far is largely unknown. Therefore we expect there will be more studies coming up in the coming years deciphering the function of the projection neurons and the lateral horn.

To provide a common ground for the comparison of results, for the selection of appropriate Gal4 enhancer trap lines and for the design of new experiments we standardized the expression patterns of two lines specific for olfactory projection neurons (Gal4-GH146, Gal4-NP225). The line GH146 was used frequently in earlier studies for targeting olfactory projection neurons. The following is a short summary of these studies.

### **8.3.1 Gal4-GH146**

Gal4-GH146 stems from the collection of Reinhard F. Stocker in Fribourg and was first described by Stocker et al. in 1997 [115]. Its expression is described as highly selective for olfactory projection neurons during development, continuously from the second larval stage until adulthood.

Ye et al. 2004 [149] performed a study on dopamine dependent attention-like behavior during flight. They found behavioral defects only in animals chronically depleted of dopamine during development. Down-regulation of J-domain protein - a potential co-chaperone in synaptic vesicle release - in the neurons included in Gal4-GH146 showed no effect on attention-like behavior during flight.

Wong et al. 2002 [147] and Jefferis et al. [146] investigated the development of the olfactory pathway for the period from embryo to late pupa using Gal4-GH146 to track down the olfactory projection neurons. In the adult animal both groups estimated about 60% (83 [147], 90 [150]) of the olfactory projection neurons to be included in Gal4-GH146. These neurons have their cell bodies in three anatomically discrete clusters around the antennal lobe neuropil.

Marin et al 2005 [151] used Gal4-GH146 to analyze the remodeling during metamorphosis of persistent olfactory projection neurons (PPNs) that are born in the embryo. They found the PPNs functional in the larva, completely pruned in the first 12 h after pupa formation (APF) and re-extended already after 18h APF. Due to their early birth the PPNs synapse with the Kenyon cells of the  $\gamma$ -lobes.

Ramaekers et al. 2005 [132] studied the development of the olfactory pathway in the third instar larva including Gal4-GH146 as a major population of olfactory input neurons to the mushroom bodies. Thereby they detected an additional glomerulus in the antennal lobes enlarging the number of larval antennal lobe glomeruli to 28. In contrast to the situation in adult animals there is no cellular redundancy in the olfactory pathway of third instar larvae.

Masuda et al. 2005 [152] generated a map of calyx glomeruli, using both anatomical criteria and the pattern of innervation by subsets of the olfactory projection neurons (PNs) (Gal4-GH146 and NP225). Thereby they found the PNs innervating the calyx glomeruli stereotypically while the connections of the Kenyon cells appear to be non-stereotypic. Each calyx glomerulus is innervated by a single PN only but often PNs innervate multiple but few glomeruli. The innervation pattern of the Kenyon cells is much broader. Many calyx glomeruli are innervated by the same Kenyon cell. Converging signals of multiple PNs on downstream Kenyon cells therefore can code for specific olfactory information and allow precise odor discrimination.

Berdnik et al. 2006 [153] investigated the plasticity of the neurons of the olfactory pathway after lesion. They ablated groups of olfactory receptor neurons (ORNs) or olfactory projection neurons (PNs) by conditional expression of toxins. They found that PN dendrites are stable in the absence of their natural presynaptic partners, and inversely that PN dendrites are not essential for maintaining normal axon projections of their partners, the ORNs.

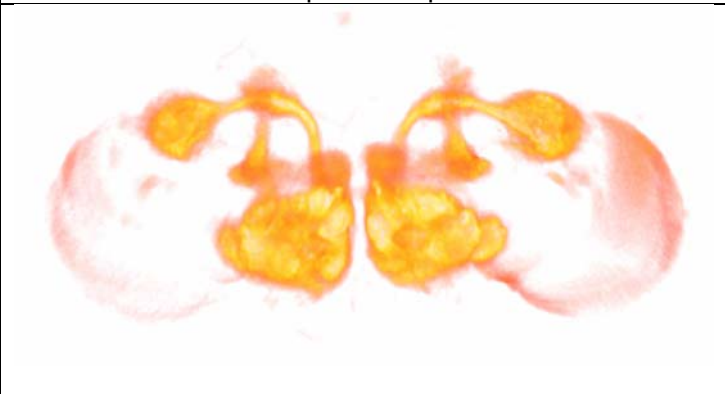
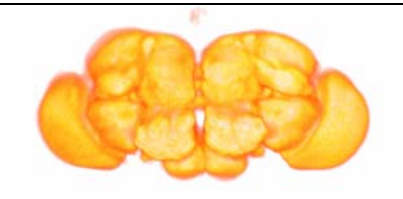
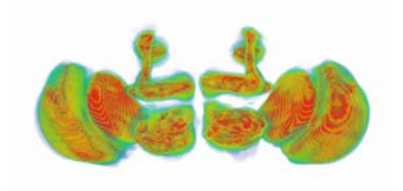
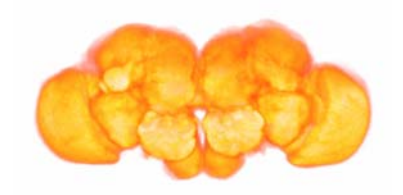
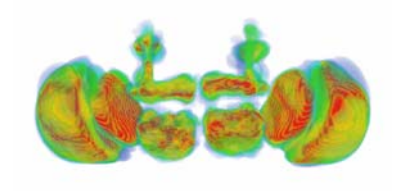
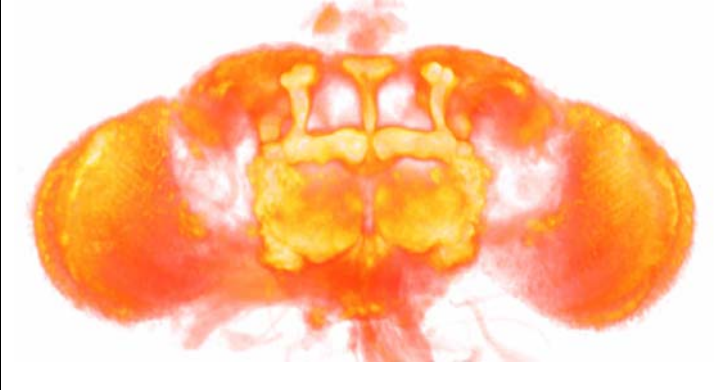
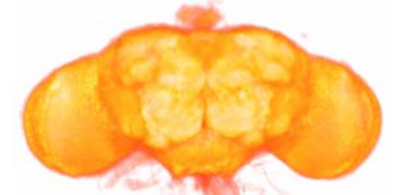
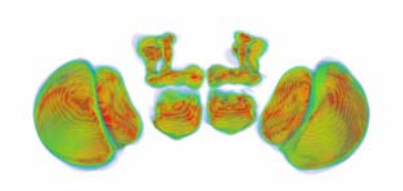
### **8.3.2 Gal4-NP225**

Gal4-NP225 comes from the collection of the NP consortium, Japan. First it was described by Tanaka et al. in 2004 [154] to express in ~70 olfactory projection neurons, which connect to?? 35 out of the total of 43 antennal lobe glomeruli. Using Gal4-NP225 the role of the mushroom body calyx and the lateral horn in processing olfactory signals was investigated. From the structural organization of interconnections between the PNs and the downstream neurons in the calyces and the lateral horn they concluded that the mushroom body is capable

of integrating a wide range of odorant information whereas relatively little integration is assumed to occur in the lateral horn.

Wilson et al 2006 [155] analyzed the influence of the mutation Polyhomeotic (Ph) on the morphogenesis of the brain during metamorphosis. Using the MARCM technique [130] on the basis of Gal4-NP225 (and others) they could demonstrate that due to the loss of Ph the path finding of the neurons is disturbed and the whole brain becomes completely disorganized.

### 8.3.3 Results

	Gal4 expression pattern		Reference
GH146		nc82	
		MainProb	
NP225		nc82	
		MainProb	
59Y		nc82	
		MainProb	

**Figure 32: Alignment quality of expression patterns in olfactory projection neurons (PN). Direct volume rendering of the standardized expression patterns show the typical structures of the expression patterns (left column). The standardized reference channels (nc82) display details of the neuropil surface and the MainProbabilityMaps (MainProb) show a high amount of red labeled overlap of all included LabelField Materials. Therefore the Alignment quality can be assumed as very good .**

False color code for fluorescence signals:

(dark)  (bright);

False color code for MainProb:

(low)  (high)

Comparing the standardized expression patterns of Gal4-GH146 and NP225 we found both less restricted than described. Besides the described expression in the PNs we found a weak expression in all lobes of the mushroom bodies (white arrows in A and B of Figure 33). Additional cell bodies which could be the source of this expression were not detectable in the Gal4-lines. Further investigation in higher resolution should be performed in the future.

Superimposing the standardized Gal4 expression patterns of Gal4-GH146 and Gal4-NP225 with other standardized expression patterns revealed expression in the olfactory projection neurons in another Gal4-line as well. In Gal4-59y which was reported previously to express in the mushroom bodies [141] and the antennal lobes ([www.fly-trap.org](http://www.fly-trap.org)) we found expression in the PNs as well (black arrow in B of Figure 33). In the collection of 22 standardized expression patterns 59y is the only one showing expression in the PNs.

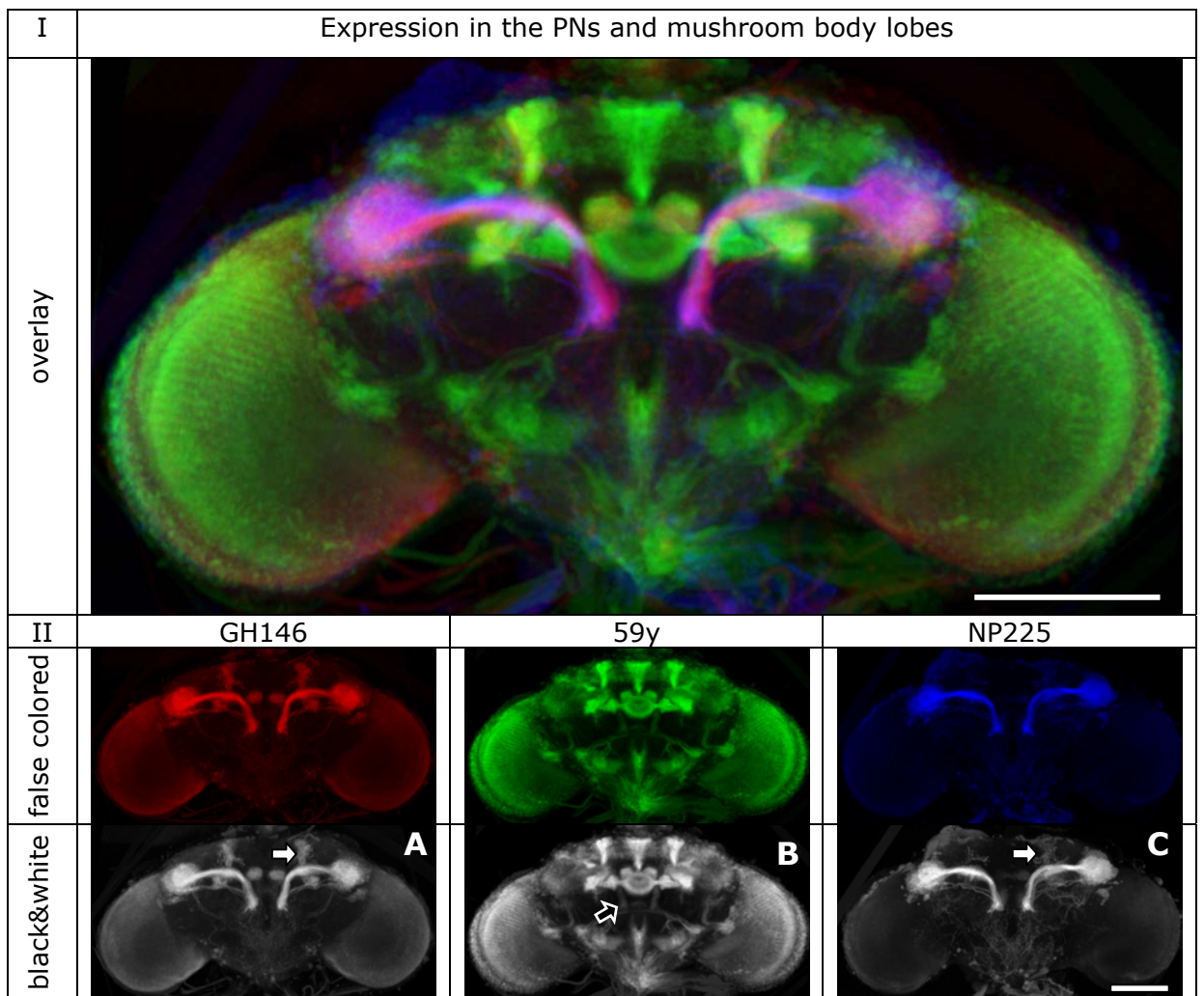


**Figure 33: Restricted projection of Gal4 expression patterns in the olfactory projection neurons (PN). Only the frontal sections including the area of interest are projected to visualize the frontal part of the inner antenno-cerebral tract (iACT) which otherwise is covered by the**

**antennal lobe.**

**I: Overlay of standardized expression patterns in false colors as displayed in II (GH146 red, 59y green, NP225 blue).**

**II: Standardized expression patterns of GH146, NP225 and 59y in false colors (upper row) and grey values (lower row).**

**In A and C additionally to the PN expression can be found in the Mushroom bodies (white arrows).**

**B shows expression in the iACT in the expression pattern of 59y.**

**N<sub>A</sub>:7, N<sub>B</sub>:9, N<sub>C</sub>:6; scalebar 100µm.**

### **8.3.4 Conclusion**

The anatomy of expression patterns in the brain of *Drosophila melanogaster* can be superimposed reliably after standardization. Even small details like neuronal tracts can be retrieved in expression patterns if somehow accentuated in another. Thereby the accentuation can be achieved in diverse ways. A strong fluorescent signal is the easiest marker but an exceptionally weak signal in a fluorescent surrounding could be used as marker as well. Even immunohistochemical stainings using different antibody combinations can be used to narrow down the area of interest for screening. The only precondition which has to be met is the standardization of the marker. Therefore any known aspect in the expression pattern of a given Gal4-line can be used to screen other standardized expression patterns for expression at precisely the same given position. Building up libraries of standardized Gal4-expression patterns and searching for Gal4-lines expressing in a certain region of interest can be facilitated.

### **8.4 Alignment of individual neurons**

In insects, the first levels of processing of visual information are located in the optic lobes. In *Drosophila* the optic lobes consist of the retina and four distinct neuropil areas, lamina, medulla, lobula and lobula plate, the latter two collectively known as lobula complex [156]. Most distal lies the lamina which is directly connected to the photoreceptors of the retina. Proximally and parallel to the lamina lies the medulla which is connected to the lamina via the outer optic chiasm. Proximal of the medulla the lobula and the lobula plate are located. Via the inner optic chiasm these neuropil areas are connected to the medulla and to each other. In all neuropil areas mentioned a multi-layered structure facilitates retinotopic processing (i.e. the neighbourhood relations of the visual input in the retina is retained during the processing of the information in the optic lobes).

Whereas the morphology and wiring of the neuropil areas [156-160] and development of the optic lobes [161-164] is well understood and the knowledge about their function is significantly proceeding [165-168], little is known about

the connections between the optic lobes and the central brain. Recently, Otsuna et al [95] performed a study on visual projection neurons (vpn) connecting the lobula with the ventro-lateral protocerebrum. In ongoing studies K. Shinomiya visualized individual cells of the population of vpns using the flip-out technique [169](unpublished).

#### 8.4.1 3D reconstruction and alignment of individual visual projection neurons.

One of the goals of the StandardBrain is an atlas of the *Drosophila* brain at the single-neuron level. The work of Shinomyia provides the opportunity to extend the VIB protocol to the alignment of these single cell stainings to address the question how these cells do interconnect in the ventro-lateral protocerebrum. Because the existing confocal scans contain the visualized neurons and their direct vicinity only (Figure 34) a new set of Materials had to be established on the basis of the autofluorescence of the tissues recorded as reference channel. The only neuropil areas which were reliably recognizable in all Samples were the lobula, the peduncle of the mushroom body and the projection area of the vpns, which is wrapped by a glial sheath and therefore stands out from the surrounding neuropil (transparent bodies in Figure 35B).

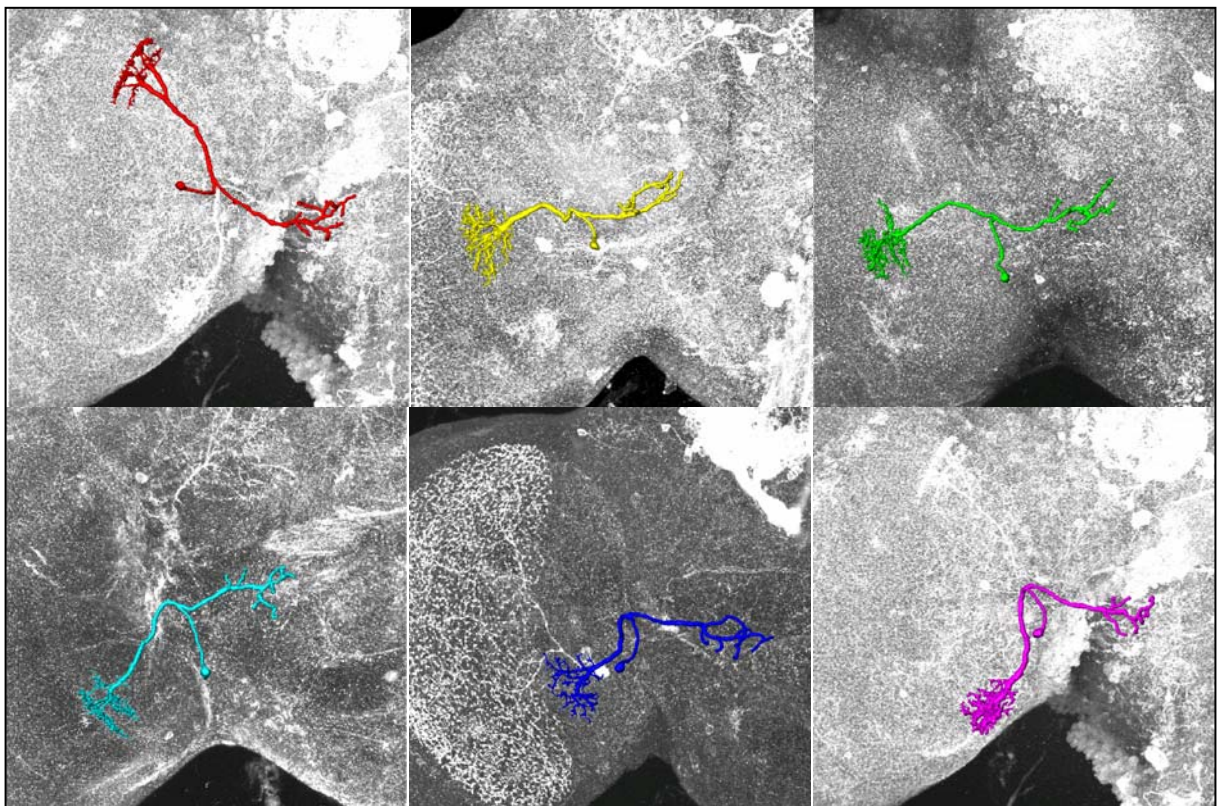


**Figure 34: 3D reconstructions of individual visual projection neurons. The reconstructions are superimposed to a 2D projection of their confocal data set in gray values. Colors like in Figure 35.**

The reconstruction of the three dimensional shape of the visualizes neurons was achieved by the skeletonizer tool of Amira [170, 171]. To test for alignment artifacts the reconstruction was done before (pre) and after alignment (post). Comparisons of the 'post'-surface with the aligned 'pre'-surface showed no significant differences in the structure of the reconstructed neuron.

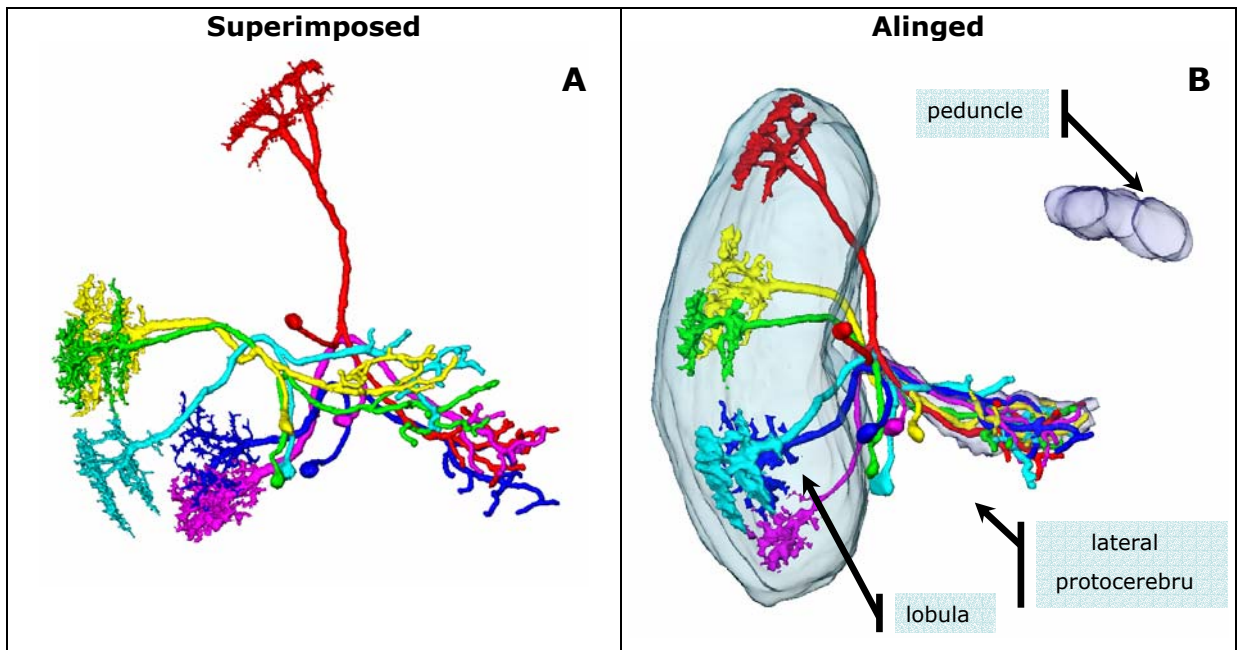


**Figure 35: A: Superimposition of the 3D reconstruction of Figure 34. Before alignment the organization of the cells terminals in the lateral protocerebru are not comprehensible due to the differences in data acquisition.**

**B: Overlay of 3D reconstruction after alignment with the VIB protocol. Alignment was accomplished using three Landmark neuropil areas. These are lobula, peduncle of the mushroom body and projection area of the fibers of interest (transparent bodies). After alignment the input regions in the lobula are assigned to their correct relative position to each other. The organization and potential interactions of the terminals in the lateral protocerebru become obvious.**

#### 8.4.2 Conclusion

Contrary to our expectations the VIB protocol is well suited to support the alignment of single cells. Working on high resolution details of the specimens one has to individually select the Materials that are underlying the transformation. Thus the Samples are aligned to their own common standard coordinate system. The transfer of standardized details to the wholemout standard so far did not succeed. However, adding the Materials used during the alignment of the detailed data to the Template of the wholemout standard may succeed in the future. Approaches like this could eventually help to reach the single-neuron resolution of the StandardBrain atlas.

## **9 Discussion and outlook**

For the integration of anatomical data of different sources and modalities we developed the Virtual Insect Brain protocol for the standardization of insect neuroanatomy. This software is based on a prototype developed 1998 in the Lab of Martin Heisenberg by Karheinz Rein and Malte Westerhoff (aka Zöckler) [85]. A first approach of standardized neuroanatomy using this prototype was published in 2002 presenting the Standard brain of *Drosophila melanogaster* [86].

Comparative work for the honey bee was presented in 2005 by Brandt et al. [87] using another computational approach developed and published by the Zuse Institute Berlin [89].

However, currently the VIB protocol is the only approach available providing a self-contained program structure facilitating the work of untrained users.

### **9.1 The VIB protocol**

The VIB protocol is a combination of versatile functionality and easy usability, to the degree that it can support even unexperienced users. To our knowledge, it currently is superior to all other approaches to the standardization of insect neuroanatomy. Nevertheless, the work on the protocol is by no means finished.

The principle weakness of the VIB protocol is its dependency on Amira. The functionality of this software is outstanding and much help was provided by Konrad Zuse Institute, Berlin (M. Westerhoff-Zoeckler) during the starting phase of the protocol [86]. However, due to its commercial nature (closed source) Amira proved not to be the best platform for the development of custom applications. Also restrictions in functionality and compatibility to common operating systems (namely Macintosh) are mayor drawbacks working with the VIB protocol. Therefore an independent version of the VIB protocol should be developed as soon as possible. The first promising steps in this direction have been taken by J.E. Schindelin and B. Schmid (unpublished).

Outside the VIB protocol, major challenges exist as well. A general shortcoming of the approach of label-based standardization of neuroanatomy is the intense interference of the experimenter with the data. The technique of data acquisition at the confocal microscope has to be standardized. This not only would reduce misinterpretations, it would guarantee comparable data between laboratories, and would even save a considerable amount of time.

Most importantly, manual segmentation has to become automatic. It is time consuming and prone to subjective interpretations. Although some solutions for

the automatic segmentation of human brains exist [172, 173], the implementation of an automatic segmentation of insect brains so far did not succeed. The difficulty in automatic segmentation of the insect brain is mainly due to the high demand on the precision the segmentation has to meet. The low contrast of confocal images and inevitable changes of signal amplification by the operator during data acquisition additionally complicates this approach. A promising mathematical approach was introduced 2005 by J.E. Schindelin [174]. Its implementation presumably will be included in one of the coming, non-commercial versions of the VIB protocol.

## 9.2 The standard brain atlas

During the development and in the start-up phase of the VIB protocol we created a collection of 25 standardized expression patterns. These can be subdivided into two general groups. Of these, 16 were selected due to their reported or observed specificity for a certain neuropil area. Following the focus of our laboratory we concentrated in this study on the mushroom bodies (201y, mb247, ok107, H24, 59y, 189y), on the central complex (104y, 121y, 154y, 210y, C205, C005, 78y, 007y) and on olfactory projection neurons (GH146, NP225). Nine other expression patterns studied were reported to reflect the expression of biogenic amines in the brain. They highlighted serotonergic (NP209), octopaminergic (NP938, tdc, 1.3T $\beta$ H, 4.6T $\beta$ H) and dopaminergic (TH3) neurons. Due to their integration into the StandardBrain atlas they now can be superimposed and analysed in reference to any other standardized expression pattern.

The StandardBrain atlas for *Drosophila melanogaster* finally is working and has already proven useful for investigating the existing 25 standardized expression patterns. Finding Gal4-positive olfactory projection neurons in the Gal4-line 59y (see chapter 8.3) and defining additional common areas in the expression patterns of fan-shaped body Gal4 lines, we demonstrated beyond doubt the functionality of the VIB protocol. The more expression patterns will be added to the atlas, the more powerful this tool will become.

## REFERENCES

1. J Pevsner: **Leonardo da Vinci's contributions to neuroscience.** *Trends Neurosci* 2002, **25**:217-20.
2. J Talairach, P Tournoux: **Co-planar stereotactic atlas of the human brain:** Thieme, New York; 1988.
3. ER Kandell, T Abrams, L Bernier, TJ Carew, RD Hawkins, JH Schwartz: **Classical conditioning and sensitization share aspects of the same molecular cascade in Aplysia.** *Cold Spring Harb Symp Quant Biol* 1983, **48 Pt 2**:821-30.
4. M Ashburner: **Drosophila: A Laboratory Handbook:** Cold Spring Harbor Laboratory Press, New York; 1989.
5. WG Quinn, WA Harris, S Benzer: **Conditioned behavior in Drosophila melanogaster.** *Proc Natl Acad Sci U S A* 1974, **71**:708-12.
6. T Tully, WG Quinn: **Classical conditioning and retention in normal and mutant Drosophila melanogaster.** *J Comp Physiol [A]* 1985, **157**:263-77.
7. JF Hall: **The conditional emotional response as a model of Pavlovian conditioning.** *Pavlov J Biol Sci* 1986, **21**:1-11.
8. Y Dudai: **Neurogenetic dissection of learning and short-term memory in Drosophila.** *Annu Rev Neurosci* 1988, **11**:537-63.
9. G Corfas, Y Dudai: **Habituation and dishabituation of a cleaning reflex in normal and mutant Drosophila.** *J Neurosci* 1989, **9**:56-62.
10. L Liu, R Wolf, R Ernst, M Heisenberg: **Context generalization in Drosophila visual learning requires the mushroom bodies.** *Nature* 1999, **400**:753-6.
11. J Dubnau, T Tully: **Gene discovery in Drosophila: new insights for learning and memory.** *Annu Rev Neurosci* 1998, **21**:407-44.
12. S Waddell, WG Quinn: **What can we teach Drosophila? What can they teach us?** *Trends Genet* 2001, **17**:719-26.
13. M Heisenberg: **Mushroom body memoir: from maps to models.** *Nat Rev Neurosci* 2003, **4**:266-75.
14. RL Davis: **Olfactory memory formation in Drosophila: from molecular to systems neuroscience.** *Annu Rev Neurosci* 2005, **28**:275-302.
15. S Pick, R Strauss: **Goal-driven behavioral adaptations in gap-climbing Drosophila.** *Curr Biol* 2005, **15**:1473-8.
16. R Strauss, M Heisenberg: **A higher control center of locomotor behavior in the Drosophila brain.** *J Neurosci* 1993, **13**:1852-61.
17. R Wolf, M Heisenberg: **Visual space from visual motion: turn integration in tethered flying Drosophila.** *Learn Mem* 1997, **4**:318-27.
18. M Heisenberg, R Wolf, B Brembs: **Flexibility in a single behavioral variable of Drosophila.** *Learn Mem* 2001, **8**:1-10.
19. R Wolf, M Heisenberg: **Basic organization of operant behavior as revealed in Drosophila flight orientation.** *J Comp Physiol [A]* 1991, **169**:699-705.
20. R Wolf, M Heisenberg: **Visual control of straight flight in Drosophila melanogaster.** *J Comp Physiol [A]* 1990, **167**:269-83.
21. A Thum: **Sugar reward learning in Drosophila : neuronal circuits in Drosophila associative olfactory learning.** Würzburg: Universität Würzburg,; 2006.
22. RL Davis: **Olfactory learning.** *Neuron* 2004, **44**:31-48.
23. SE McGuire, M Deshazer, RL Davis: **Thirty years of olfactory learning and memory research in Drosophila melanogaster.** *Prog Neurobiol* 2005, **76**:328-47.

## REFERENCES

24. MD Adams, SE Celniker, RA Holt, CA Evans, JD Gocayne, PG Amanatides, SE Scherer, PW Li, RA Hoskins, RF Galle, et al: **The genome sequence of *Drosophila melanogaster***. *Science* 2000, **287**:2185-95.
25. J Hirsch, JC Boudreau: **Studies in experimental behavior genetics. I. The heritability of phototaxis in a population of *Drosophila melanogaster***. *J Comp Physiol Psychol* 1958, **51**:647-51.
26. J Hirsch: **Studies in experimental behavior genetics. II. Individual differences in geotaxis as a function of chromosome variations in synthesized *Drosophila* populations**. *J Comp Physiol Psychol* 1959, **52**:304-8.
27. J Hirsch, L Erlenmeyer-Kimling: **Studies in experimental behavior genetics: IV. Chromosome analyses for geotaxis**. *J Comp Physiol Psychol* 1962, **55**:732-9.
28. J Hirsch, G Ksander: **Studies in experimental behavior genetics. V. Negative geotaxis and further chromosome analyses in *Drosophila melanogaster***. *J Comp Physiol Psychol* 1969, **67**:118-22.
29. WR Lee, GA Sega, JB Bishop: **Chemically induced mutations observed as mosaics in *Drosophila melanogaster***. *Mutat Res* 1970, **9**:323-36.
30. JB Bishop, WR Lee: **Chromosome breakage in *Drosophila melanogaster* induced by a monofunctional alkylating agent (EMS)**. *Mutat Res* 1973, **21**:327-33.
31. O Ohnishi: **Spontaneous and ethyl methanesulfonate-induced mutations controlling viability in *Drosophila melanogaster*. I. Recessive lethal mutations**. *Genetics* 1977, **87**:519-27.
32. O Ohnishi: **Spontaneous and ethyl methanesulfonate-induced mutations controlling viability in *Drosophila melanogaster*. II. Homozygous effect of polygenic mutations**. *Genetics* 1977, **87**:529-45.
33. O Ohnishi: **Spontaneous and ethyl methanesulfonate-induced mutations controlling viability in *Drosophila melanogaster*. III. Heterozygous effect of polygenic mutations**. *Genetics* 1977, **87**:547-56.
34. CJ O'Kane, WJ Gehring: **Detection in situ of genomic regulatory elements in *Drosophila***. *Proc Natl Acad Sci U S A* 1987, **84**:9123-7.
35. AH Brand, N Perrimon: **Targeted gene expression as a means of altering cell fates and generating dominant phenotypes**. *Development* 1993, **118**:401-15.
36. A Laughon, R Driscoll, N Wills, RF Gesteland: **Identification of two proteins encoded by the *Saccharomyces cerevisiae* GAL4 gene**. *Mol Cell Biol* 1984, **4**:268-75.
37. A Laughon, RF Gesteland: **Primary structure of the *Saccharomyces cerevisiae* GAL4 gene**. *Mol Cell Biol* 1984, **4**:260-7.
38. J Ashburner, KJ Friston: **Nonlinear spatial normalization using basis functions**. *Hum Brain Mapp* 1999, **7**:254-66.
39. J Ashburner, JL Andersson, KJ Friston: **High-dimensional image registration using symmetric priors**. *Neuroimage* 1999, **9**:619-28.
40. J Ashburner, KJ Friston: **Voxel-based morphometry--the methods**. *Neuroimage* 2000, **11**:805-21.
41. KJ Friston, W Penny, C Phillips, S Kiebel, G Hinton, J Ashburner: **Classical and Bayesian inference in neuroimaging: theory**. *Neuroimage* 2002, **16**:465-83.
42. CD Good, RI Scahill, NC Fox, J Ashburner, KJ Friston, D Chan, WR Crum, MN Rossor, RS Frackowiak: **Automatic differentiation of anatomical patterns in the human brain: validation with studies of degenerative dementias**. *Neuroimage* 2002, **17**:29-46.

## REFERENCES

43. J Ashburner, KJ Friston: **Unified segmentation**. *Neuroimage* 2005, **26**:839-51.
44. CH Salmond, J Ashburner, F Vargha-Khadem, A Connelly, DG Gadian, KJ Friston: **Distributional assumptions in voxel-based morphometry**. *Neuroimage* 2002, **17**:1027-30.
45. J Ashburner, KJ Friston: **Why voxel-based morphometry should be used**. *Neuroimage* 2001, **14**:1238-43.
46. J Ashburner, P Neelin, DL Collins, A Evans, K Friston: **Incorporating prior knowledge into image registration**. *Neuroimage* 1997, **6**:344-52.
47. J Ashburner, K Friston: **Multimodal image coregistration and partitioning--a unified framework**. *Neuroimage* 1997, **6**:209-17.
48. JC Mazziotta, D Valentino, S Grafton, F Bookstein, C Pelizzari, G Chen, AW Toga: **Relating structure to function in vivo with tomographic imaging**. *Ciba Found Symp* 1991, **163**:93-101; discussion 101-12.
49. AW Toga, BA Payne: **Animating the 3D structure and function of brain**. *Comput Med Imaging Graph* 1991, **15**:285-91.
50. AW Toga: **A digital three-dimensional atlas of structure/function relationships**. *J Chem Neuroanat* 1991, **4**:313-8.
51. KL Black, JC Mazziotta, AW Toga: **Imaging and functional localization for brain tumors**. *Clin Neurosurg* 1992, **39**:475-81.
52. S Narayan, D Sensharma, EM Santori, AA Lee, A Sabherwal, AW Toga: **Animated visualization of a high resolution color three dimensional digital computer model of the whole human head**. *Int J Biomed Comput* 1993, **32**:7-17.
53. EM Santori, AW Toga: **Superpositioning of 3-dimensional neuroanatomic data sets**. *J Neurosci Methods* 1993, **50**:187-96.
54. AW Toga, KL Ambach, S Schluender: **High-resolution anatomy from in situ human brain**. *Neuroimage* 1994, **1**:334-44.
55. JC Mazziotta, AW Toga, AC Evans, PT Fox, JL Lancaster: **Digital brain atlases**. *Trends Neurosci* 1995, **18**:210-1.
56. JC Mazziotta, AW Toga, A Evans, P Fox, J Lancaster: **A probabilistic atlas of the human brain: theory and rationale for its development. The International Consortium for Brain Mapping (ICBM)**. *Neuroimage* 1995, **2**:89-101.
57. AW Toga, PM Thompson, CJ Holmes, BA Payne: **Informatics and computational neuroanatomy**. *Proc AMIA Annu Fall Symp* 1996:299-303.
58. RC Herndon, JL Lancaster, AW Toga, PT Fox: **Quantification of white matter and gray matter volumes from T1 parametric images using fuzzy classifiers**. *J Magn Reson Imaging* 1996, **6**:425-35.
59. CJ Holmes, R Hoge, L Collins, R Woods, AW Toga, AC Evans: **Enhancement of MR images using registration for signal averaging**. *J Comput Assist Tomogr* 1998, **22**:324-33.
60. PM Thompson, AW Toga: **Detection, visualization and animation of abnormal anatomic structure with a deformable probabilistic brain atlas based on random vector field transformations**. *Med Image Anal* 1997, **1**:271-94.
61. JD Schmahmann, J Doyon, D McDonald, C Holmes, K Lavoie, AS Hurwitz, N Kabani, A Toga, A Evans, M Petrides: **Three-dimensional MRI atlas of the human cerebellum in proportional stereotaxic space**. *Neuroimage* 1999, **10**:233-60.
62. PM Thompson, RP Woods, MS Mega, AW Toga: **Mathematical/computational challenges in creating deformable and probabilistic atlases of the human brain**. *Hum Brain Mapp* 2000, **9**:81-92.

## REFERENCES

63. SM Haney, PM Thompson, TF Cloughesy, JR Alger, AW Toga: **Tracking tumor growth rates in patients with malignant gliomas: a test of two algorithms.** *AJNR Am J Neuroradiol* 2001, **22**:73-82.
64. ER Sowell, PM Thompson, SN Mattson, KD Tessner, TL Jernigan, EP Riley, AW Toga: **Voxel-based morphometric analyses of the brain in children and adolescents prenatally exposed to alcohol.** *Neuroreport* 2001, **12**:515-23.
65. AW Toga, PM Thompson: **Maps of the brain.** *Anat Rec* 2001, **265**:37-53.
66. J Mazziotta, A Toga, A Evans, P Fox, J Lancaster, K Zilles, R Woods, T Paus, G Simpson, B Pike, et al: **A four-dimensional probabilistic atlas of the human brain.** *J Am Med Inform Assoc* 2001, **8**:401-30.
67. J Mazziotta, A Toga, A Evans, P Fox, J Lancaster, K Zilles, R Woods, T Paus, G Simpson, B Pike, et al: **A probabilistic atlas and reference system for the human brain: International Consortium for Brain Mapping (ICBM).** *Philos Trans R Soc Lond B Biol Sci* 2001, **356**:1293-322.
68. PM Thompson, TD Cannon, KL Narr, T van Erp, VP Poutanen, M Huttunen, J Lonnqvist, CG Standertskjold-Nordenstam, J Kaprio, M Khaledy, et al: **Genetic influences on brain structure.** *Nat Neurosci* 2001, **4**:1253-8.
69. AW Toga, PM Thompson: **New approaches in brain morphometry.** *Am J Geriatr Psychiatry* 2002, **10**:13-23.
70. AW Toga: **Neuroimage databases: the good, the bad and the ugly.** *Nat Rev Neurosci* 2002, **3**:302-9.
71. AW Toga: **Imaging databases and neuroscience.** *Neuroscientist* 2002, **8**:423-36.
72. N Pouratian, AF Cannestra, NA Martin, AW Toga: **Intraoperative optical intrinsic signal imaging: a clinical tool for functional brain mapping.** *Neurosurg Focus* 2002, **13**:e1.
73. M Guiou, S Sheth, M Nemoto, M Walker, N Pouratian, A Ba, AW Toga: **Cortical spreading depression produces long-term disruption of activity-related changes in cerebral blood volume and neurovascular coupling.** *J Biomed Opt* 2005, **10**:11004.
74. E Daurignac, A Toga, D Jones, H Aronen, D Hommer, T Jernigan, J Krystal, D Mathalon: **Applications of morphometric and diffusion tensor magnetic resonance imaging to the study of brain abnormalities in the alcoholism spectrum.** *Alcohol Clin Exp Res* 2005, **29**:159-166.
75. MS Mega, ID Dinov, JC Mazziotta, M Manese, PM Thompson, C Lindshield, J Moussai, N Tran, K Olsen, CI Zoumalan, et al: **Automated brain tissue assessment in the elderly and demented population: construction and validation of a sub-volume probabilistic brain atlas.** *Neuroimage* 2005, **26**:1009-18.
76. C Fennema-Notestine, IB Ozyurt, CP Clark, S Morris, A Bischoff-Grethe, MW Bondi, TL Jernigan, B Fischl, F Segonne, DW Shattuck, et al: **Quantitative evaluation of automated skull-stripping methods applied to contemporary and legacy images: effects of diagnosis, bias correction, and slice location.** *Hum Brain Mapp* 2006, **27**:99-113.
77. P Kochunov, JF Mangin, T Coyle, J Lancaster, P Thompson, D Riviere, Y Cointepas, J Regis, A Schlosser, DR Royall, et al: **Age-related morphology trends of cortical sulci.** *Hum Brain Mapp* 2005, **26**:210-20.
78. AW Toga: **Computational biology for visualization of brain structure.** *Anat Embryol (Berl)* 2005, **210**:433-8.

## REFERENCES

79. AW Toga, EM Santori: **3D spatial relationships of histochemical activity in the rat superior colliculus.** *Eur J Morphol* 1995, **33**:71-9.
80. AW Toga, EM Santori, R Hazani, K Ambach: **A 3D digital map of rat brain.** *Brain Res Bull* 1995, **38**:77-85.
81. K Ikezaki, KL Black, EM Santori, ML Smith, DP Becker, BA Payne, AW Toga: **Three-dimensional comparison of peripheral benzodiazepine binding and histological findings in rat brain tumor.** *Neurosurgery* 1990, **27**:78-82.
82. EF Lee, RE Jacobs, I Dinov, A Leow, AW Toga: **Standard atlas space for C57BL/6J neonatal mouse brain.** *Anat Embryol (Berl)* 2005, **210**:245-63.
83. A MacKenzie-Graham, ES Jones, DW Shattuck, ID Dinov, M Bota, AW Toga: **The informatics of a C57BL/6J mouse brain atlas.** *Neuroinformatics* 2003, **1**:397-410.
84. A MacKenzie-Graham, EF Lee, ID Dinov, M Bota, DW Shattuck, S Ruffins, H Yuan, F Konstantinidis, A Pitiot, Y Ding, et al: **A multimodal, multidimensional atlas of the C57BL/6J mouse brain.** *J Anat* 2004, **204**:93-102.
85. K Rein, M Zockler, M Heisenberg: **A quantitative three-dimensional model of the Drosophila optic lobes.** *Curr Biol* 1999, **9**:93-6.
86. K Rein, M Zockler, MT Mader, C Grubel, M Heisenberg: **The Drosophila standard brain.** *Curr Biol* 2002, **12**:227-31.
87. R Brandt, T Rohlfing, J Rybak, S Krofczik, A Maye, M Westerhoff, HC Hege, R Menzel: **A threedimensional average-shape atlas of the honeybee brain.** *Journal of Comparative Neurology* 2005, **(in press)**.
88. T Rohlfing, R Brandt, R Menzel, CR Maurer, Jr.: **Evaluation of atlas selection strategies for atlas-based image segmentation with application to confocal microscopy images of bee brains.** *Neuroimage* 2004, **21**:1428-42.
89. A Maye, TH Wenckebach, HC Hege: **Visualization, Reconstruction, and Integration of Neuronal Structures in Digital Brain Atlases.** *International Journal of Neuroscience* 2006, **116**:431-459.
90. **Amira 3.1 User's Guide and Reference Manual.** Berlin: Konrad-Zuse-Zentrum für Informatik Berlin (ZIB); 1999.
91. PJ Besl, ND McKay: **A Method for Registration of 3-D Shapes.** *IEEE Transactions on Pattern Analysis and Machine Intelligence* 1992, **14**:238 - 256.
92. NJ Strausfeld: **Atlas of an Insect Brain:** Springer-Verlag; 1976.
93. K Ito: **Images of the Drosophila brain:** [http://jfly.iam.u-tokyo.ac.jp/html/figures/Brain\\_K\\_Ito/brain\\_k\\_ito.html](http://jfly.iam.u-tokyo.ac.jp/html/figures/Brain_K_Ito/brain_k_ito.html); 1994.
94. JD Armstrong, K Kaiser, A Muller, KF Fischbach, N Merchant, NJ Strausfeld: **Flybrain, an on-line atlas and database of the Drosophila nervous system.** *Neuron* 1995, **15**:17-20.
95. H Otsuna, K Ito: **Systematic analysis of the visual projection neurons of Drosophila melanogaster. I. Lobula-specific pathways.** *J Comp Neurol* 2006, **497**:928-58.
96. A Guo, L Li, SZ Xia, CH Feng, R Wolf, M Heisenberg: **Conditioned visual flight orientation in Drosophila: dependence on age, practice, and diet.** *Learn Mem* 1996, **3**:49-59.
97. T Lee, L Luo: **Mosaic Analysis with a Repressible Cell Marker for Studies of Gene Function in Neuronal Morphogenesis.** *Neuron* 1999, **22**:451-461.
98. Bloomington Drosophila Stock Center: **Personal communication to FlyBase available from** <http://flybase.bio.indiana.edu/.bin/fbpcq.html?FBF0104719>. 1998.9.14.

## REFERENCES

99. E Spana: **Personal communication to FlyBase available from <http://flybase.bio.indiana.edu/.bin/fbpcq.html?FBrf0111645>.** 1999.9.27.
100. AH Brand, N Perrimon: **Raf acts downstream of the EGF receptor to determine dorsoventral polarity during Drosophila oogenesis.** *Genes Dev.* 1994, **8**:629--639.
101. A Hidalgo, J Urban, A Brand: **Targeted ablation of glia disrupts axon tract formation in the Drosophila CNS.** *Development* 1995, **121**:3703-3712.
102. Y Zhang, K Broadie: **Personal communication to FlyBase available from <http://flybase.bio.indiana.edu/.bin/fbpcq.html?FBrf0157297>.** 2003.2.
103. M Schwaerzel, M Heisenberg, T Zars: **Extinction antagonizes olfactory memory at the subcellular level.** *Neuron* 2002, **35**:951-60.
104. JB Connolly, IJ Roberts, JD Armstrong, K Kaiser, M Forte, T Tully, CJ O'Kane: **Associative learning disrupted by impaired Gs signaling in Drosophila mushroom bodies.** *Science* 1996, **274**:2104-7.
105. RA Schulz, C Chromey, MF Lu, B Zhao, EN Olson: **Expression of the D-MEF2 transcription factor in the Drosophila brain suggests a role in neuronal cell differentiation.** *Oncogene* 1996, **12**:1827--1831.
106. H Pfister: **Etablierung und Characterisierung Pilzkörperspezifischer GAL4-enhancer-trap-Linien in Drosophila melanogaster.** In: *Book Etablierung und Characterisierung Pilzkörperspezifischer GAL4-enhancer-trap-Linien in Drosophila melanogaster.* (Editor ed.^eds.). City: Lehrstuhl für Genetik und Neurobiologie; 1997.
107. L Manseau, A Baradaran, D Brower, A Budhu, F Elefant, H Phan, AV Philp, M Yang, D Glover, K Kaiser, et al: **GAL4 enhancer traps expressed in the embryo, larval brain, imaginal discs, and ovary of Drosophila.** *Dev Dyn* 1997, **209**:310-22.
108. KA Osborne, A Robichon, E Burgess, S Butland, RA Shaw, A Coulthard, HS Pereira, RJ Greenspan, MB Sokolowski: **Natural Behavior Polymorphism Due to a cGMP-Dependent Protein Kinase of Drosophila.** *Science* 1997, **277**:834-836.
109. AR Rodan, JA Kiger, Jr, U Heberlein: **Functional Dissection of Neuroanatomical Loci Regulating Ethanol Sensitivity in Drosophila.** *J. Neurosci.* 2002, **22**:9490-9501.
110. G Liu, H Seiler, A Wen, T Zars, K Ito, R Wolf, M Heisenberg, L Liu: **Distinct memory traces for two visual features in the Drosophila brain.** 2006, **439**:551-556.
111. M Tettamanti, JD Armstrong, K Endo, MY Yang, K Furukubo-Tokunaga, K Kaiser, H Reichert: **Early development of the Drosophila mushroom bodies, brain centres for associative learning and memory.** *Dev. Genes Evol.* 1997, **207**:242--252.
112. T Zars, R Wolf, R Davis, M Heisenberg: **Tissue-specific expression of a type I adenylyl cyclase rescues the rutabaga mutant memory defect: in search of the engram.** *Learning Memory* 2000, **7**:18--31.
113. JDA Susan C. P. Renn, Mingyao Yang, Zongsheng Wang, Xin An, Kim Kaiser, Paul H. Taghert,: **Genetic analysis of the *Drosophila* ellipsoid body neuropil: Organization and development of the central complex.** *Journal of Neurobiology* 1999, **41**:189-207.
114. JR Martin, T Raabe, M Heisenberg: **Central complex substructures are required for the maintenance of locomotor activity in Drosophila melanogaster.** *J Comp Physiol [A]* 1999, **185**:277-88.

## REFERENCES

115. RF Stocker, G Heimbeck, N Gendre, JS de Belle: **Neuroblast ablation in *Drosophila* P[GAL4] lines reveals origins of olfactory interneurons.** *J Neurobiol* 1997, **32**:443-56.
116. K Ito, R Okada, NK Tanaka, T Awasaki: **Cautionary observations on preparing and interpreting brain images using molecular biology-based staining techniques.** *Microsc Res Tech* 2003, **62**:170-86.
117. S Hayashi, K Ito, Y Sado, M Taniguchi, A Akimoto, H Takeuchi, T Aigaki, F Matsuzaki, H Nakagoshi, T Tanimura, et al: **GETDB, a database compiling expression patterns and molecular locations of a collection of Gal4 enhancer traps.** *Genesis* 2002, **34**:58-61.
118. SH Cole, GE Carney, CA McClung, SS Willard, BJ Taylor, J Hirsh: **Two Functional but Noncomplementing *Drosophila* Tyrosine Decarboxylase Genes: DISTINCT ROLES FOR NEURAL TYRAMINE AND OCTOPAMINE IN FEMALE FERTILITY**  
**10.1074/jbc.M414197200.** *J. Biol. Chem.* 2005, **280**:14948-14955.
119. AF Sören Diegelmann, Christian Leibold, Thomas Spall, Erich Buchner,: **Transgenic flies expressing the fluorescence calcium sensor cameleon 2.1 under UAS control.** *genesis* 2002, **34**:95-98.
120. KMC O'Dell, JD Armstrong, MY Yang, K Kaiser: **Functional dissection of the *Drosophila* mushroom bodies by selective feminization of genetically defined subcompartments.** *Neuron* 1995, **15**:55--61.
121. MY Yang, JD Armstrong, I Vilinsky, NJ Strausfeld, K Kaiser: **Subdivision of the *Drosophila* mushroom bodies by enhancer-trap expression patterns.** *Neuron* 1995, **15**:45--54.
122. JR Martin, R Ernst, M Heisenberg: **Mushroom bodies suppress locomotor activity in *Drosophila melanogaster*.** *Learn Mem* 1998, **5**:179-91.
123. ST Sweeney, K Broadie, J Keane, H Niemann, CJ O'Kane: **Targeted expression of tetanus toxin light chain in *Drosophila* specifically eliminates synaptic transmission and causes behavioral defects.** *Neuron* 1995, **14**:341-351.
124. T Zars, M Fischer, R Schulz, M Heisenberg: **Localization of a short-term memory in *Drosophila*.** *Science* 2000, **288**:672-5.
125. DS Manoli, M Foss, A Vilella, BJ Taylor, JC Hall, BS Baker: **Male-specific fruitless specifies the neural substrates of *Drosophila* courtship behaviour.** *Nature* 2005, **436**:395-400.
126. WJ Joiner, A Crocker, BH White, A Sehgal: **Sleep in *Drosophila* is regulated by adult mushroom bodies.** 2006, **441**:757-760.
127. M Kurusu, T Nagao, U Walldorf, S Flister, WJ Gehring, K Furukubo-Tokunaga: **Genetic control of development of the mushroom bodies, the associative learning centers in the *Drosophila* brain, by the *eyeless*, twin of *eyeless*, and *dachshund* genes**  
**10.1073/pnas.040564497.** *PNAS* 2000, **97**:2140-2144.
128. S Zhu, AS Chiang, T Lee: **Development of the *Drosophila* mushroom bodies: elaboration, remodeling and spatial organization of dendrites in the calyx.** *Development* 2003, **130**:2603--2610.
129. S Zhu, R Perez, M Pan, T Lee: **Requirement of Cul3 for axonal arborization and dendritic elaboration in *Drosophila* mushroom body neurons.** *J Neurosci* 2005, **25**:4189-97.
130. L Luo, T Lee, T Nardine, B Null, J Reuter: **Using the MARCM system to positively mark mosaic clones in *Drosophila*.** *D. I. S.* 1999, **82**:102-105.
131. RJ Watts, ED Hoopfer, L Luo: **Axon pruning during *Drosophila* metamorphosis: evidence for local degeneration and requirement of the ubiquitin-proteasome system.** *Neuron* 2003, **38**:871-85.
132. A Ramaekers, E Magnenat, EC Marin, N Gendre, GS Jefferis, L Luo, RF Stocker: **Glomerular maps without cellular redundancy at**

REFERENCES

- successive levels of the Drosophila larval olfactory circuit. *Curr Biol* 2005, **15**:982-92.**
133. CI Michel, R Kraft, LL Restifo: **Defective Neuronal Development in the Mushroom Bodies of Drosophila Fragile X Mental Retardation 1 Mutants**  
**10.1523/JNEUROSCI.1102-04.2004.** *J. Neurosci.* 2004, **24**:5798-5809.
134. H Gu, DK O'Dowd: **Cholinergic Synaptic Transmission in Adult Drosophila Kenyon Cells In Situ**  
**10.1523/JNEUROSCI.4109-05.2006.** *J. Neurosci.* 2006, **26**:265-272.
135. Y Adachi, B Hauck, J Clements, H Kawauchi, M Kurusu, Y Totani, Y Kang, T Eggert, U Walldorf, K Furukubo-Tokunaga, et al: **Conserved cis-regulatory modules mediate complex neural expression patterns of the eyeless gene in the Drosophila brain.** *Mech. Dev.* 2003, **120**:1113--1126.
136. SE McGuire, PT Le, RL Davis: **The role of Drosophila mushroom body signaling in olfactory memory.** *Science* 2001, **293**:1330--1333.
137. G Gu, J Yang, KA Mitchell, JE O'Tousa: **Drosophila ninaB and ninaD act outside of retina to produce rhodopsin chromophore.** *J. Biol. Chem.* 2004, **279**:18608--18613.
138. N Agrawal, J Pallos, N Slepko, BL Apostol, L Bodai, LW Chang, AS Chiang, LM Thompson, JL Marsh: **Identification of combinatorial drug regimens for treatment of Huntington's disease using Drosophila.** *Proc Natl Acad Sci U S A* 2005, **102**:3777-81.
139. T Sakai, T Kitamoto: **Differential roles of two major brain structures, mushroom bodies and central complex, for Drosophila male courtship behavior.** *J Neurobiol* 2006, **66**:821-34.
140. TL Yan Li, Yueqing Peng, Chunyan Yuan, Aike Guo,: **Specific functions of <I>Drosophila</I> amyloid precursor-like protein in the development of nervous system and nonneural tissues.** *Journal of Neurobiology* 2004, **61**:343-358.
141. MT Mader: **Analyse von Expressionsmustern in den Pilzkörnern von Drosophila melanogaster.**; 2001. Diploma thesis.
142. G Isabel, A Pascual, T Preat: **Exclusive Consolidated Memory Phases in Drosophila**  
**10.1126/science.1094932.** *Science* 2004, **304**:1024-1027.
143. A Baier, B Wittek, B Brembs: **Drosophila as a new model organism for the neurobiology of aggression?** *J. exp. Biol.* 2002, **205**:1233--1240.
144. M Hammer, R Menzel: **Multiple Sites of Associative Odor Learning as Revealed by Local Brain Microinjections of Octopamine in Honeybees.** *Learn. Mem.* 1998, **5**:146-156.
145. RF Stocker: **The organization of the chemosensory system in Drosophila melanogaster: a review.** *Cell Tissue Res* 1994, **275**:3-26.
146. GSXE Jefferis, EC Marin, RF Stocker, L Luo: **Target neuron prespecification in the olfactory map of Drosophila.** 2001, **414**:204-208.
147. AM Wong, JW Wang, R Axel: **Spatial Representation of the Glomerular Map in the Drosophila Protocerebrum.** *Cell* 2002, **109**:229-241.
148. K Yasuyama, IA Meinertzhagen, FW Schurmann: **Synaptic organization of the mushroom body calyx in Drosophila melanogaster.** *J Comp Neurol* 2002, **445**:211-26.
149. Y Ye, W Xi, Y Peng, Y Wang, A Guo: **Long-term but not short-term blockade of dopamine release in Drosophila impairs orientation during flight in a visual attention paradigm**  
**doi:10.1111/j.1460-9568.2004.03575.x.** *European Journal of Neuroscience* 2004, **20**:1001-1007.

## REFERENCES

150. GS Jefferis, EC Marin, RJ Watts, L Luo: **Development of neuronal connectivity in *Drosophila* antennal lobes and mushroom bodies.** *Curr. Opin. Neurobiol.* 2002, **12**:80--86.
151. EC Marin, RJ Watts, NK Tanaka, K Ito, L Luo: **Developmentally programmed remodeling of the *Drosophila* olfactory circuit.** *Development* 2005, **132**:725-37.
152. LM Masuda-Nakagawa, NK Tanaka, CJ O'Kane: **Stereotypic and random patterns of connectivity in the larval mushroom body calyx of *Drosophila***  
**10.1073/pnas.0509643102.** *PNAS* 2005, **102**:19027-19032.
153. D Berdnik, T Chihara, A Couto, L Luo: **Wiring Stability of the Adult *Drosophila* Olfactory Circuit after Lesion**  
**10.1523/JNEUROSCI.4941-05.2006.** *J. Neurosci.* 2006, **26**:3367-3376.
154. NK Tanaka, T Awasaki, T Shimada, K Ito: **Integration of Chemosensory Pathways in the *Drosophila* Second-Order Olfactory Centers.** *Current Biology* 2004, **14**:449-457.
155. RI Wilson, GC Turner, G Laurent: **Transformation of Olfactory Representations in the *Drosophila* Antennal Lobe**  
**10.1126/science.1090782.** *Science* 2004, **303**:366-370.
156. JK Douglass, NJ Strausfeld: **Retinotopic pathways providing motion-selective information to the lobula from peripheral elementary motion-detecting circuits.** *J Comp Neurol* 2003, **457**:326-44.
157. I Sinakevitch, JK Douglass, G Scholtz, R Loesel, NJ Strausfeld: **Conserved and convergent organization in the optic lobes of insects and isopods, with reference to other crustacean taxa.** *J Comp Neurol* 2003, **467**:150-72.
158. I Sinakevitch, NJ Strausfeld: **Chemical neuroanatomy of the fly's movement detection pathway.** *J Comp Neurol* 2004, **468**:6-23.
159. JK Douglass, NJ Strausfeld: **Anatomical organization of retinotopic motion-sensitive pathways in the optic lobes of flies.** *Microsc Res Tech* 2003, **62**:132-50.
160. JK Douglass, NJ Strausfeld: **Optic flow representation in the optic lobes of Diptera: modeling innervation matrices onto collators and their evolutionary implications.** *J Comp Physiol [A]* 2000, **186**:799-811.
161. F Tejedor, XR Zhu, E Kaltenbach, A Ackermann, A Baumann, I Canal, M Heisenberg, KF Fischbach, O Pongs: **minibrain: a new protein kinase family involved in postembryonic neurogenesis in *Drosophila*.** *Neuron* 1995, **14**:287-301.
162. K Kaphingst, S Kunes: **Pattern formation in the visual centers of the *Drosophila* brain: wingless acts via decapentaplegic to specify the dorsoventral axis.** *Cell* 1994, **78**:437-48.
163. Z Huang, S Kunes: **Hedgehog, transmitted along retinal axons, triggers neurogenesis in the developing visual centers of the *Drosophila* brain.** *Cell* 1996, **86**:411-22.
164. DT Champlin, JW Truman: **Ecdysteroid coordinates optic lobe neurogenesis via a nitric oxide signaling pathway.** *Development* 2000, **127**:3543-51.
165. J Haag, M Egelhaaf, A Borst: **Dendritic integration of motion information in visual interneurons of the blowfly.** *Neurosci Lett* 1992, **140**:173-6.
166. J Haag, A Vermeulen, A Borst: **The intrinsic electrophysiological characteristics of fly lobula plate tangential cells: III. Visual response properties.** *J Comput Neurosci* 1999, **7**:213-34.
167. J Haag, F Theunissen, A Borst: **The intrinsic electrophysiological characteristics of fly lobula plate tangential cells: II. Active membrane properties.** *J Comput Neurosci* 1997, **4**:349-69.

## REFERENCES

168. J Haag, A Borst: **Neural mechanism underlying complex receptive field properties of motion-sensitive interneurons.** *Nat Neurosci* 2004, **7**:628-34.
169. K Basler, G Struhl: **Compartment boundaries and the control of Drosophila limb pattern by hedgehog protein.** *Nature* 1994, **368**:208-14.
170. S Schmitt, JF Evers, C Duch, M Scholz, K Obermayer: **New methods for the computer-assisted 3-D reconstruction of neurons from confocal image stacks.** *Neuroimage* 2004, **23**:1283-98.
171. JF Evers, S Schmitt, M Sibila, C Duch: **Progress in functional neuroanatomy: precise automatic geometric reconstruction of neuronal morphology from confocal image stacks.** *J Neurophysiol* 2005, **93**:2331-42.
172. T Rohlfing, DB Russakoff, CR Maurer, Jr.: **Performance-based classifier combination in atlas-based image segmentation using expectation-maximization parameter estimation.** *IEEE Trans Med Imaging* 2004, **23**:983-94.
173. T Rohlfing, DB Russakoff, CR Maurer: **Expectation maximization strategies for multi-atlas multi-label segmentation.** *Inf Process Med Imaging* 2003, **18**:210-21.
174. J Schindelin: **The standard brain of Drosophila melanogaster and its automatic segmentation.** Würzburg: Julius-Maximilians Universität; 2005. PhD.



## CURRICULUM VITAE

### **Arnim Jenett**

Department of Genetics and Neurobiology  
University of Wuerzburg  
Am Hubland  
D-97074 Wuerzburg  
Germany

Phone: +49 931 888 4466

Fax: +49 931 888 4465

E-mail: [arnim.jenett@biozentrum.uni-wuerzburg.de](mailto:arnim.jenett@biozentrum.uni-wuerzburg.de)

#### **Graduate studies:**

2002 -2007: PhD-studies in Biology, Julius-Maxmilians-Universität, Würzburg, Germany "The Virtual Insect Brain Protocol, development and application of software for the standardization of neuroanatomy"

#### **Undergraduate studies:**

2002 - 2003: Diploma in Neurobiology at the Free University, Berlin, Germany (Neurobiology, Zoology, Human biology, Biopsychology)  
Diploma thesis: "Analyse der Ontogenese oktopaminerger Strukturen in der olfaktorischen Bahn der Honigbiene *Apis mellifera*"

1996 - 2001: Intermediate examination(Vordiplom) in Biology at the Free University, Berlin, Germany

1996: Studies in medical science, Medical University, Lübeck, Germany

1994 - 1996: Studies in engineering, University of Applied Science, Lübeck, Germany

#### **Military Service:**

2000: Promotion to Feldwebel d.R. (Senior Non-Commisioned Officer)

1999 - 2006: Reservist at the RK01 "Alt Berlin", Berlin, Germany

1993 - 1994: Basic military service at the medical service of the Deutsche Bundeswehr. Attendee of the international 4 days march, Nijmegen, Netherlands

#### **Education:**

1989-1993: High school: (Gymnasium) Evangelische Landesschule zur Pforte, Meinerzhagen, Germany

1989: High school: Pascal-Gymnasium, Münster, Germany

1988: High school: Gymnasium Athenaeum, Stade, Germany

1986 - 1987: High school: Realschule Camper Höhe, Stade, Germany

## CURRICULUM VITAE

1979 - 1983: Elementary schools, Stade, Germany

### Teaching experience:

2002 - 2006: Supervisor of practical courses for neurobiology to undergraduates, Julius-Maximilians-Universität, Würzburg, Germany

2001 - 2003: Tutor for neurobiology to undergraduates, Free University, Berlin

### Working experience:

1995: Practical courses in metal construction in preparation for studies in engineering.

2000: Computer aided reconstruction of the brain of the honeybee *Apis mellifera*

### Scientific visits:

July 2006: Lab talk at the Kubo Lab, Department of Biological Sciences, Graduate School of Science, The University of Tokyo

July 2006: Lab talk at the Sasaki Lab, Division of Applied Entomology and Zoology, Tamagawa University

July 2006: Lab talk at the Furukubo-Tokunaga Lab, Institute of Biological Sciences, University of Tsukuba

July 2006: Lab talk at the Mizunami Lab, Graduate School of Life Sciences, Tohoku University, Sendai

July 2006: Lab talk at the Yamamoto Lab, Tohoku University Graduate School of Life Sciences, Sendai

Aug 2006: Lab talk at the Kanzaki Lab, Intelligent Cooperative Systems, Research Center for Advanced Science and Technology, The University of Tokyo

June -Aug 2006: Lab visit at the Ito Lab, Institute of Molecular and Cellular Biosciences, Center of Bioinformatics, University of Tokyo

Oct 2004: Lab talk at the Lou Lab, HHMI Dept. of Biological Science, Stanford University.

Oct 2004: Lab talk at the Hartenstein Lab, UCLA, Los Angeles.

### Publications:

Giurfa M, Zhang S, Jenett A, Menzel R, Srinivasan MV (2001) The concepts of 'sameness' and 'difference' in an insect. *Nature*, 410(6831):930-3

Jenett A, Schindelin J, Heisenberg M: The Virtual Insect Brain Protocol: creating and comparing standardized neuroanatomy. *BMC Bioinformatics* 2006, 7:544.

### Abstracts:

Jenett A., Schindelin J., Shinomiya K., Heisenberg M. (2006) The Virtual Insect Brain Protocol: A software tool for the creation of standardized neuroanatomy. The 11th European Symposium on *Drosophila* Neurobiology - Neurofly, Leuven (2.-6.9.2006) (poster)

Jenett A., Schindelin J., Heisenberg M. (2006) The Virtual Insect Brain Protocol: A software tool for the creation of standardized neuroanatomy. Poster session of the JSPS summer program, SOKENDAI, Hayama (16.6.2006) (poster)

## CURRICULUM VITAE

- Jenett A., Schindelin J., Heisenberg M. (2005) The Standard Protocol: Towards a genetic atlas of the *Drosophila* brain. Proceedings of the 30th Göttingen Neurobiology Conference and the 6th Meeting of the German Neuroscience Society 2005 (17.-20.2.2005) (poster)
- Jenett A., Schindelin J., Heisenberg M. (2004) The standard brain protocol: towards a genetic atlas of the brain. The 10th European Symposium on *Drosophila* Neurobiology - Neurofly, Neuchatel (4.-8.9.2004) (poster)
- Jenett A., Schindelin J., Grübel K., Heisenberg M. (2003) The Virtual Brain Project: Comparison of expression patterns of different reporter genes driven by the same Gal4-enhancer trap line. Proceedings of the 29th Göttingen Neurobiology Conference and the 5th Meeting of the German Neuroscience Society 2003 (12.-15.6.2003) ISBN 3-13-137351-2
- Jenett A., Malun D. (2003) Immunoreactivity against octopamine in the pupal and adult brain of the honeybee, *Apis mellifera* Proceedings of the 29th Göttingen. Neurobiology Conference and the 5th Meeting of the German Neuroscience Society 2003 (12.-15.6.2003) (poster) ISBN 3-13-137351-2
- Jenett A., Schindelin J., Heisenberg M. (2002) Detailed 3D-reconstruction and standardisation of the *Drosophila* brain by insertion of multiple Gal4 expression patterns in the standard brain atlas with amira. Workshop on Neuroinformatics in Model Organisms, Edinburgh (16.-20.9.2002) (oral presentation)
- Jenett A., Rybak J., Schröter U., Brandt R., Malun D. (2001) Octopamine-like immunoreactivity in the pupal and adult honeybee brain. Proceedings of the 2001 Berlin Meeting of the European Section of IUSI (25.-29.9.2001) (poster)
- Giurfa M., Jenett A., Bönisch C., Wiley C., Menzel R. (2001) "Sameness" and "difference" in honey bees. 43. Tagung experimentell arbeitender Psychologen 2001 (9.-11.4.2001) (poster)

### **Skills:**

Basal *Drosophila* genetics

Behavioral paradigms

Comparative neuroanatomy

Basal electron microscopy (SEM and TEM)

Confocal microscopy

Software: Microsoft Office, Corel, Paint Shop Pro, amira

Programming: tcl, html, php, bash

### **Extra-curricular activities:**

1996 - 1999: Member of the Turnerschaft Berlin im Coburger Convent (students fraternity), 3 semesters member of executive board.

### **Interests:**

Photography, biking, hiking, traveling, long distance running, chorusing, various artistic works

### **Languages:**

German, English, French (passive)



## DANKSAGUNGEN

Mein erster Dank gilt dem Mann mit der Idee: meinem Betreuer, Prof. Martin Heisenberg, ohne den es diese Arbeit nicht gegeben hätte. Auch wenn - oder vielleicht gerade weil - wir nicht immer einer Meinung waren, habe ich viel durch Sie gelernt. Dafür bin ich Ihnen sehr dankbar. Hoffentlich lässt sich diese Zusammenarbeit auch in Zukunft fortführen.

Herzlichen Dank auch an Johannes E. Schindelin, der mich Geduld und das Programmieren lehrte. Wenn ich nicht Dich als Kollegen gehabt hätte; ich könnt bis heut nicht programmieren. Damit sicherst Du meine Zukunft. Herzlichen Dank dafür.

Tief stehe ich in der Schuld von Conny Grübel, die immer mitgedacht und so manches Malheur verhindert hat. Vielen herzlichen Dank für Deine Umsicht, Deine Geduld und Ausdauer. Jeder, der mit Dir arbeiten darf, kann sich glücklich schätzen.

Auch den anderen Kollegen und Freunden am Lehrstuhl sei herzlich gedankt dafür, dass sie mir immer wieder gezeigt haben, dass man auch reichlich Spaß bei der Arbeit haben kann, wenn ich das mal wieder vergessen hatte. Danke Euch, Ihr ward so manches mal wahre Lebensretter. Ich wünsche Euch für die Zukunft stets viele so nette Leute um Euch, wie Ihr sie mir ward.

Sehr zu Dank verpflichtet bin ich all meinen Gastgebern, mich auf meinen Vortragsreisen stets zuvorkommend aufgenommen haben. Die Einblicke in die fremden Labors und die positive Resonanz sind mir während der alltäglichen Arbeit zu einer nicht zu unterschätzenden Motivationsquelle geworden.

Zuletzt aber dafür umso inniger möchte ich mich bei meinen Eltern, Geschwistern und Freunden bedanken, weil sie mich zu dem Menschen gemacht haben, der ich heute bin. Aus so manchem Alptraum ward ihr es, die mich wieder geweckt, getröstet und wieder auf die Beine gestellt haben. Ohne Euer Verständnis und Euren Zuspruch hätte ich es wohl nicht geschafft bis hierher zu kommen. Unendlich vielen Dank für Eure Unterstützung.